EVALUATION OF PAVEMENT SKID RESISTANCE

USING COMPUTATIONAL INTELLIGENCE

By

YOU ZHAN

Bachelor of Surveying and Mapping Engineering
Southwest Jiaotong University
Chengdu, China
2012

Master of Civil Engineering
Southwest Jiaotong University
Chengdu, China
2014

Submitted to the Faculty of the
Graduate College of the
Oklahoma State University
in partial fulfillment of
the requirements for
the Degree of
DOCTOR OF PHILOSOPHY
August, 2018

EVALUATION OF PAVEMENT SKID RESISTANCE

USING COMPUTATIONAL INTELLIGENCE

Dissertation Approved:

Dissertation Adviser Dr. Qiang Joshua Li

Committee Member Dr. Kelvin C. P. Wang

Committee Member Dr. Stephen A. Cross

Outside Committee Member Dr. James K. Good

ACKNOWLEDGEMENTS

First, I would like to express my deepest appreciation to my supervisor Dr. Qiang (Joshua) Li for the continuous support of my Ph.D. study: I would not start my research and achieve these results without his persistent help and guidance. He always has the attitude to help me in all my research including writing of this dissertation. Thanks for Dr. Kelvin Wang, who brings me to the Oklahoma State University (OSU) and offers me great opportunities to learn advanced computational technology in transportation. Their unlimited passion and rigorous attitude on researches have motivated me towards future achievements in my whole career.

I would like to thank the rest of my dissertation committee members Dr. James K. Good and Dr. Stephen A. Cross for their patient instructions, insightful comments, and the valuable questions which help me widen my perspectives in my dissertation. Thanks them for inspiring me with the systematic knowledge lectured at their classes.

Special appreciation belongs to Guangwei Yang, Justin Thweatt, Allen Zhang, Yue Fei, Yang Liu, Yi Peng, Dr. Cheng Chen, Wenying Yu and Yao Zhou in general. Thanks for their advices and helps with my study and work in the past four years.

Thanks also go to the Chinese Scholarship Council (CSC), the Southwest Jiaotong University (SWJTU) and Dr. Yanjun Qiu who is my advisor in SWJTU and a visionary and charismatic leader both administratively and academically. Dr. Qiu and SWJTU's recommendation and CSC's financial support made the four years' life in OSU a reality.

I sincerely thank my parents and my parents-in-law for their completely understanding and supporting in every bit of our life. I appreciate the love and help from them that accompanied us to go through the tough time.

I also dedicate this Ph.D. dissertation to my newborn daughter, Olive Yuehan Zhan, who is going to be the pride and joy of my life. I love you more than anything and your coming inspires daddy to move forward during the last period of Ph.D. studies.

Last but not the least, I don’t know how to begin with saying thank you to my soul mate, my dearest wife and my best friend, Lin Han. I love you for everything, for being so understanding and for putting up with me through the toughest moments of my life. Your presence is the best thing that has ever happened to me. I love you sweet heart and this dissertation is for you.

Name: YOU ZHAN

Date of Degree: JUNE, 2018

Title of Study: EVALUATION OF PAVEMENT SKID RESISTANCE USING COMPUTATIONAL INTELLIGENCE

Major Field: Civil Engineering

ABSTRACT: Pavement micro-texture is affected by the aggregate characteristics contained within the surface. It is long desired to develop friction prediction models using pavement surface and aggregate textural properties. However, the development of such models has proven to be challenging because of two reasons: (1) The acquiring of complete and high quality pavement surface data for friction studies remains difficult. (2) No consistent and reliable methodologies and models have been developed for friction prediction and evaluation.

The objective of this dissertation is to investigate the most influencing factors for pavement skid resistance, and develop reliable and consistent friction prediction models based on aggregate physical properties and pavement surface texture characteristics from three perspectives. The state-of-the-art 3D laser imaging technology, high speed texture profiler, and the continuous friction measurement equipment (CFME) - Grip Tester, are used in parallel in the field to collect 1-mm 3D pavement surface data, macro-texture profiles and pavement friction data respectively at highway speed for selected testing locations, while the newly developed portable ultra-high resolution 3D texture scanner (LS-40) is utilized in the laboratory to acquire both macro- and micro-texture characteristics of pavement surfaces, and the Aggregate Image Measurement System (AIMS) to analyze surface characteristics of aggregates before and after the Micro-Deval polishing process.

Firstly, this study predicts pavement friction as a function of pavement surface and aggregate texture properties. Secondly, panel data analysis (PDA), which is able to investigate the differences of cross-sectional information, but also the time-series changes over time, is conducted to evaluate pavement skid resistance performance and identify the most influencing factors.Finally, inspired by the big success of deep learning in the field of image recognition and computer vision, a novel Deep Residual Network (ResNets) tailored for pavement friction prediction, named Friction-ResNets, is developed using pavement surface texture profiles as the inputs.

This dissertation developed several novel friction prediction models that could assist in selecting the most effective PM treatments, and proper aggregates with desired texture characteristics for optimized skid resistance. This study also demonstrates the feasibility of replacing the contact based method for pavement friction evaluation with non-contact texture measurements.

ILLUSTRATION OF PARAMETERS		
Notation	**Parameter**	**Unit**
FN	Friction Number	-
MPD	Mean Profile Depth	inch
T_{etp}	Entropy	-
T_{eng}	Energy	0-1
T_{hgt}	Homogeneity	0-1
S_{al}	Autocorrelation length	mm
S_{tr}	Texture aspect ratio	0-1
S_{td}	Texture direction	0 º- 180 º
S_{pd}	Peak density	1/mm^2
S_{pc}	Peak curvature	1/mm
S_{5p}	5 point peak height	mm
S_{5v}	5 point valley height	mm
S_{10z}	10 point height	mm
S_{da}	Dales area	mm^2
S_{ha}	Hills area	mm^2
S_{dv}	Dales volume	mm^3
S_{hv}	Hills volume	mm^3
S_p	Maximum peak height	mm
S_v	Maximum pit height	mm
S_z	Maximum height of the surface	mm
S_a	Arithmetical mean height of the surface	mm
S_q	Root mean square height of the surface	mm
S_{sk}	Skewness of height distribution	-
S_{ku}	Kurtosis of height distribution	-
S_{mr}	Areal material ratio	%
S_{mc}	Inverse areal material ratio	mm
S_{xp}	Peak extreme height	mm
V_v	Void volume	mm ³/mm ²
V_m	Material volume	mm ³/mm ²
V_{mp}	Peak material volume	mm ³/mm ²
V_{mc}	Core material volume	mm ³/mm ²
V_{vc}	Core void volume	mm ³/mm ²
V_{vv}	Dales void volume	mm ³/mm ²
AAT	Annual Average Temperature	deg C
AAP	Annual Average Precipitation	mm
AAH	Annual Average Humidity	%
AAFI	Annual Average Freeze Index	deg C deg days
AADT	Annual Average Daily Traffic	-
AADTT	Annual Average Daily Truck Traffic	-
ESAL	18-Kip Equivalent Single Axel Load	-
IF	Pavement Initial Friction Value	-
LCWP	Length of Longitudinal Cracking within Wheel Path	m
LCNWP	Length of Longitudinal Cracking outside of Wheel Path	m
IRI	International Roughness Index (IRI)	m/km
ADC	Average FWD Deflection (9-kip) for the Center Sensor	microns
ADF	Average FWD Deflection (9-kip) for the Farthest Sensor	microns
NMAS	Nominal Maximum Aggregate Size	mm
MD	Micro Deval Loss	% (avg)

TABLE OF CONTENTS

LIST OF TABLES

LIST OF FIGURES

Chapter 1 INTRODUCTION

1.1 Background

"Pavement Preservation (When, Where, and How)" has been selected as one of the highlights of the 2017-2018 Every Day Count Initiate (EDC-4) by Federal Highway Administration (FHWA) for wide implementation in state highway agencies. Even though preventive maintenance (PM) treatments have been employed by many highway agencies to restore surface properties of pavements and retard future deterioration, few has included pavement frictional properties into the pavement management systems (PMS) decision making process.

Sufficient friction (skid resistance) between tire and pavement plays a crucial role to reduce traffic accidents and provide safe and efficient driving environments for vehicles. However, pavement friction performance deteriorates with time under various factors such as climate conditions and traffic loading. Therefore, continuous monitoring of pavement friction and understanding the long-term friction degradation is of great significance for the development of effective practices to improve pavement friction performance over total service life. Field friction of pavement surface is generally measured by the interplay force between a locked tire and pavement surface (Roe et al. 1998). There are a wide range of devices and measurements for measuring pavement friction in the field: Grip tester, locked wheel trailer, Mu-meter, Side-Force Coefficient Road Inventory Machine, Variable-slip devices etc. (ASTM E274 2011, ASTM E670 2009, ASTM E1859 2015).

Pavement–tire friction is the result of a complex interaction between pavement surfaces and vehicle tires composing of two principal frictional force components - hysteresis and adhesion (Hall et al. 2009). As shown in Figure 1.1, the hysteresis force developed within the tire is most responsive to the macro-level asperities formed in the surface via mix design and/or construction techniques. Adhesion force is primarily developed at the pavement–tire interface, and is most responsive to the micro-level asperities of the aggregate particles contained on the pavement surface (Moaveni et al. 2014). Micro-texture of aggregates is mainly dependent on their surface characteristics, such as angularity, surface texture and aggregate shape. Pavement macro-texture is generally evaluated in terms of mean texture depth (MTD) or mean profile depth (MPD) via sand patch (ASTM E965-15 2015), circular track meter (ASTM E2157-15 2015), or high speed profiler measurements (ASTM E950 2018), while micro-texture can thus far only be characterized in the laboratory using high resolution devices and based on imaging analysis (Dunford et al. 2012, Bessa et al. 2014, Nataadmadja et al. 2012).

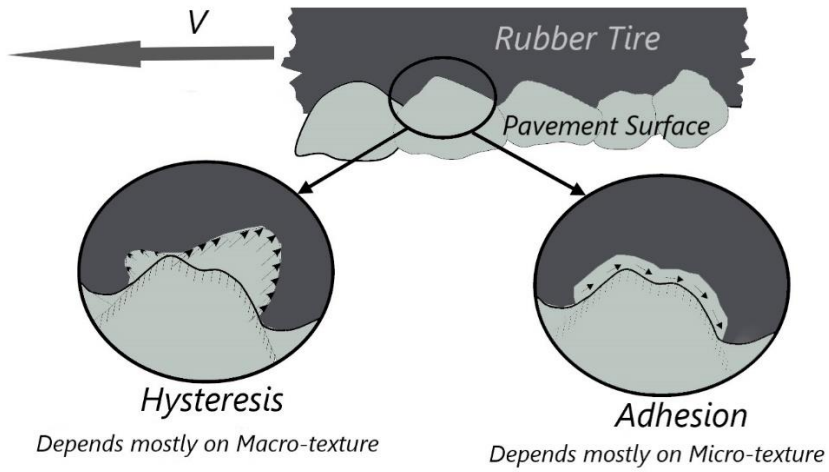

Figure 1.1. Key Mechanisms of Pavement-Tire Friction (Hall et al. 2009).

Meanwhile, aggregate is the main component of many treatments (> 90%). The aggregate characteristics of pavement surface are directly related to aggregate particles' polishing and abrasion resistance, therefore affecting pavement friction. Mineral aggregates with high resistance to polishing and abrasion are considered to be of high quality because they provide sufficient texture for pavement skid resistance. The processes of polishing and abrasion during production operations and transportation services can result in a change of properties when compared with the ones assumed in the initial mixture design process. Therefore, the aggregate characteristics in the field would be different if compared with those originally designed and expected in the laboratory (Mahmoud, 2005). In addition, the aggregate characteristics will also deteriorate over time under traffic loading and climatic impacts.

1.2 Problem Statement

As mentioned before, skid resistance of pavement surfaces is a very important indicator for road safety. Pavement friction has a serious effect on the accidents occurrence, and insufficient friction could be a determining factor for fatal collision (Mataei et al. 2016). Therefore, it is very considerable to find a proper method for measuring or evaluating the frictional properties of the pavement surface in the field. Most existing friction testing instruments comprised of applying a standard test tire to the pavement surface with a controlled wheel slip. However, these methods either waste tires or disturbs the traffic flows during the tests. It is not very practical and economical to continually monitor road surface using these instruments because generally a truck carrying a large water tank is needed to wet the surface with a defined water layer (Kummer and Meyer 1963). Furthermore, such methods are sensitive to testing speed, water film depth, ambient temperature, pavement surface texture, angle of test wheel, and viscoelastic properties of asphalt mix (Saito et al. 1996, Jayawickrama and Thomas 1998, Henry 2000, Hall et al. 2009, Bijsterveld and Val 2016). As a result, acquiring precise field friction data with high reproducibility and repeatability remains a challenges for decades. It is long desired to develop non-contact

measurements to predict pavement surface friction precisely and consistently. However, the development of such models has proven to be challenging. Based on extensive literature review, at least four problems have not been fully addressed and understood.

(1) Methodology to characterize aggregate surface properties: There are a variety of traditional approaches to characterizing aggregate surface properties based on different mechanisms to quantify the relative durability of an aggregate subject to traffic loadings. Tests most commonly used in the highway community include Micro-Deval, Los Angeles (LA) Abrasion, and the Sodium Sulfate Soundness tests, which provide insight about the quality of aggregates used for highway construction. However, the repeatability and validity of these tests have been questioned by many researchers (Wu et al. 1998, Tarefder et al. 2003, Brandes and Robinson 2006, Kline et al. 2007). As a result, several state-of-the-art technologies have been investigated for aggregate surface characterization, such as Aggregate Image Measurement System (AIMS) (Masad 2003). However, these systems were mostly developed in 1990s with more than 20-year old hardware and software techniques and could have various limitations (Pradhan 2016, Maerz 1998, Florková and Jambor 2017). Some systems only allow texture evaluation of particles based on two-dimensional (2D) parameters.

(2) Relationship between pavement friction and aggregate characteristics: Aggregates constitute roughly 95% (volume wise) of HMA mixes, and their properties have a significant impact on the performance of the mix and the pavement constructed using the mix. Various studies correlated pavement friction with aggregate characteristics (Davis 2001, Shah et al. 2010, Kangkhajitre and Kanitpong 2011, Sengoz 2014). However, most of the previous studies relied on traditional aggregate properties in terms of aggregate shape, texture, and angularity, or other 2D indicators, failing to correlate pavement

friction to proper aggregate characteristics. Knowledge gasps still remain in understanding the relationship between pavement friction and aggregate characteristics.

(3) Instruments to acquire complete and high quality pavement surface data: The development of friction prediction models has proven to be challenging because the acquiring of complete and quality pavement surface data for friction studies remains difficult. Pavement skid resistance as an area of study has suffered from inadequate and poor quality pavement surface data. Many state highway agencies have collected pavement surface data for years through manual, automated, or semi-automated means. However, such data sets are of poor quality due to problems associated with consistency, repeatability, and accuracy of collected data and subsequent analyses. Therefore, a new automated technology that can capture realistic pavement surface characteristics in the digital domain at sufficiently high resolution, or actual surface models of pavements is critically needed for the next-generation friction model development.

(4) Development of robust friction models: Many research efforts have been conducted to identify the most influential factors and develop friction deterioration models using linear regression (Jayawickrama and Thomas 1998, Bazlamit and Reza 2005, Neaylon 2009, Fuentes et al. 2010, Wang et al. 2013, Kotek and Florkova 2014, Kanafi et al. 2014). For long term performance monitoring, pavement performance data including friction are generally observed multiple times at a specific interval for many pavement sections. Most existing models, which have been estimated using only cross-sectional (considering multiple individual pavement sites) or time-series (considering multiple observations on one site) friction data, fail to incorporate all these influencing factors into a friction prediction model appropriately. In recent years, machine-learning (ML) technology has been widely used in the area of image recognition, automatic speech recognition, website searching etc. with great success. Limited number of research was also found to estimate pavement friction using ML technologies (Najafi et al. 2016, Marcelino et al. 2017,

Panahandeh and Mohammadiha 2017). However, traditional ML techniques had limitations to process natural data in its raw form, requiring domain experts to pre-process the input data and develop customized feature extractor(s) to transform the raw data into feature vectors on a case-by-case scenario (LeCun et al. 2015). On the other hand, the emerging deep learning (DL) neural networks and multiple levels of representation "allows a machine to be fed with raw data and to automatically discover the representations needed for detection or classification" (LeCun et al. 2015). In particular, deep convolutional neural networks (CNN) has led to many breakthroughs for image classification and recognition (Krizhevsky et al. 2012, Zeiler and Fergus 2014, Russakovsky et al. 2014, Srivastava et al. 2015, Szegedy et al. 2015). However, it was also found that deeper neural networks were much more difficult to train than expected: "With the network depth increasing, a degradation problem has been exposed, and adding more layers to a suitably deep model leads to higher training error" (He et al. 2016).

1.3 Objectives

The objective of this research is to investigate the influencing factors for pavement skid resistance evaluation, and develop reliable and consistent friction prediction models based on physical aggregate properties and pavement surface texture measurements from both laboratory and field testing. The state-of-the-art 3D laser imaging technology, High speed Profiler, and Grip Tester are used in parallel to collect 1-mm 3D pavement surface data, macro-texture data and continuous friction measurements respectively at highway speed in predefined field testing locations, while the newly developed laser triangulation based portable ultra-high resolution 3D scanner (LS-40) and Aggregate Image Measurement System (AIMS) are utilized in the laboratory to analyze the surface characteristics of aggregates. The testing beds in this study include the 255 LTPP SPS-3 testing sections at a national scale, 45 pavement sites under six major PM treatments and seven

typical types of aggregates in Oklahoma, 49 High Friction Surface Treatment (HFST) sites with comprehensive types of abutting pavement sections in 12 states.

Specifically, it includes the following sub-objectives:

(1) To study the aggregate properties for better skid resistance characterization. A wide range of 3D aggregate and pavement surface texture parameters at both macro- and micro-scales are calculated from a 3D laser triangulation-based surface measurement and analysis device (LS-40 Portable 3D Surface Analyzer), to identify their correlations to pavement friction, and then develop friction prediction models based on the most influential aggregate and pavement surface texture parameters.

(2) To identify the most influential factors on pavement friction. Panel data analysis (PDA), which has been successfully used in economic, social and behavioral science areas, is applied for friction panel model development in this study. This method blends cross-sectional information reflected in the differences between pavement testing sites, and the time-series information reflected in the changes within those sites over time, allowing researchers to construct and test realistic behavioral models that cannot be identified using only cross-sectional or time-series data (Washington et al. 2011).

(3) To use non-contact high speed texture measurement to predict pavement friction. A deep residual network tailored for friction prediction is proposed in this paper. This model is called Friction-ResNets. Friction-ResNets has the ability to learn and extract the textural features and classification boundaries automatically from raw input data, which could be used for friction prediction directly. Furthermore, the “convolutional group” and “skipped connection” designed in this network perfectly solves the problem of “degradation”, and increase the prediction accuracy by adding eleven convolution layers.

1.4 Organization of Dissertation

This dissertation is organized in the following way:

Chapter 2 conducts comprehensive literature review on pavement skid resistance and measurement, pavement surface texture and measurement, aggregate properties and characterization, relationship between friction and texture, relationship between friction and aggregate characteristics, and friction model development.

Chapter 3 evaluates pavement skid resistance as a function of pavement surface and aggregate texture properties. Multivariate analysis is performed to examine the relationship between pavement skid resistance, and surface and aggregate texture properties.

Chapter 4 develops pavement friction panel models for major preventive maintenance treatments. Panel data analysis (PDA), which is able to investigate the differences of cross-sectional information, but also the time-series changes over time, is conducted to identify the most significant influencing factors for pavement friction prediction model development.

Chapter 5 proposes a novel Friction-ResNets based on deep residual learning for pavement friction prediction using non-contact surface texture data. To the best of authors' knowledge, this work is the first one to exploit a real "deep" ResNets to predict pavement friction.

Chapter 6 lists the conclusions and recommendations for future work.

Chapter 2 LITERATURE REVIEW

2.1 Pavement Skid Resistance and Measurement

2.1.1 Mechanism of Pavement-Tire Skid Resistance

Kummer and Meyer (1967) illustrated the mechanism of rubber-pavement friction. As shown in Figure 2.1, friction force F is the sum of adhesion force F_a, and hysteresis force F_h. Hence:

$$F = F_a + F_h \tag{2.1}$$

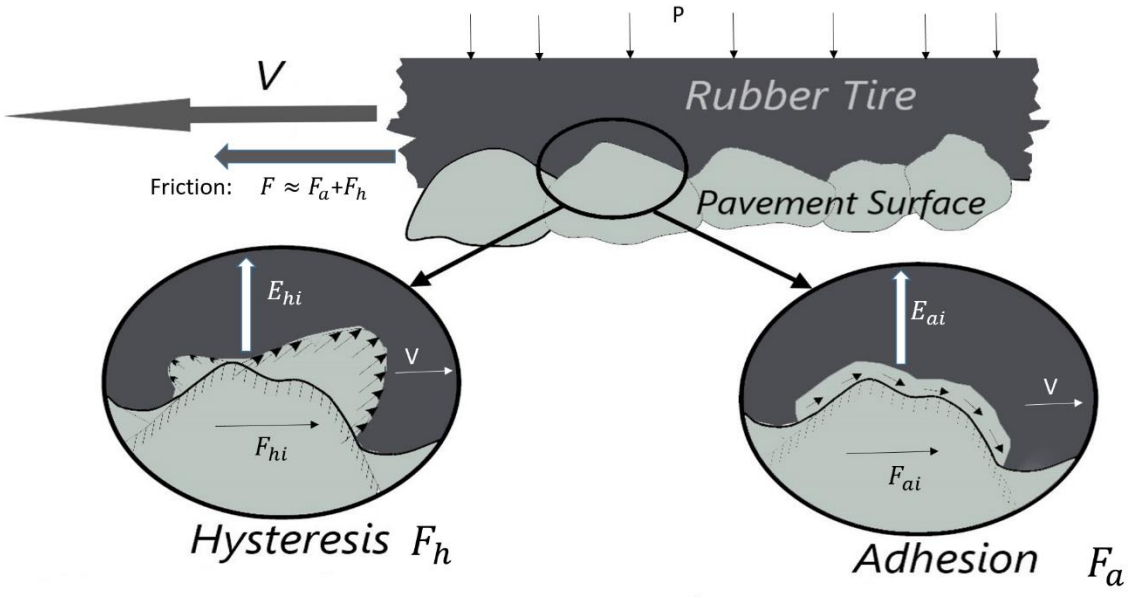

Figure 2.1. Mechanism of rubber-tire friction

The enlarged circles of Figure 2.1 demonstrate the corresponding mechanisms. The adhesion is considered to be the interface shear strength, *s*, and contact area, A_i, of the rubber with a single mineral particle. Thus, adhesion force:

$$F_a = s\sum_1^N A_i = sA \tag{2.2}$$

in which, *A* in the actual contact area.

The hysteresis component is caused by damping loss within the rubber when the latter is "flowing" over and around the mineral particle. The damping possessed by the rubber opposes the displacement of the rubber upstream of the obstacle, as well as the downstream recovery, producing unsymmetrical pressure distribution shown. The hysteresis component may be found by integrating the pressure over the "wetted" area and by resolving the resulting force into a vertical component and a horizontal component which opposes the sliding. It may be expressed in terms of the energy, E_{hi}, for each deforming particle dissipated per unit sliding length, *b*, Hence, for the entire rubber block

$$F_h = \frac{1}{b}\sum_1^N E_{hi} = \frac{1}{b}E_h \tag{2.3}$$

in which E_h is the lumped energy dissipated within the rubber due to deformation produced by N particles.

It is customary to present the measured friction force as a dimensionless "coefficient". Dividing equation 2.1 by the load *L*,

$$f = f_a + f_h \tag{2.4}$$

In which, friction coefficient *f* is the sum of adhesion coefficient f_a, and hysteresis coefficient f_h.

If load *L* is equal to:

$$L = A_n p \tag{2.5}$$

in which, A_n is the geometric area of rubber block subjected to pressure p, combining Equation 2.2 and 2.5 gives for the adhesion coefficient:

$$f_a = \frac{A}{A_n}\frac{s}{p} \tag{2.6}$$

Also, Equation 2.3 and 2.5 gives for the hysteresis coefficient:

$$f_h = \frac{E_h}{bpA_n} \tag{2.7}$$

Or,

$$f_h = \frac{QD}{bpA_n} \tag{2.8}$$

Since, Q is the volume of rubber participating in the deformation and D is the energy dissipated per unit volume of rubber due to damping.

$$E_h = QD \tag{2.9}$$

Figure 2.2 illustrate the sliding speed and pressure dependence of the adhesion coefficient. Figure 2.3 demonstrate the typical hysteresis coefficient-speed curves for a low-damping natural rubber, a medium-damping styrene-butadiene rubber, and a high-damping butyl rubber.

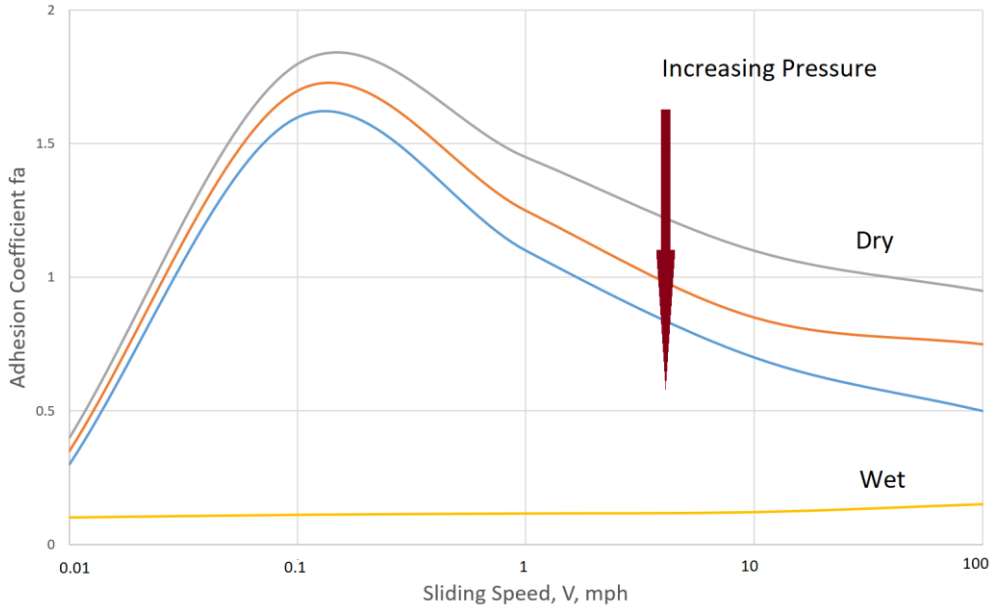

Figure 2.2. Adhesion (Kummer and Meyer 1967)

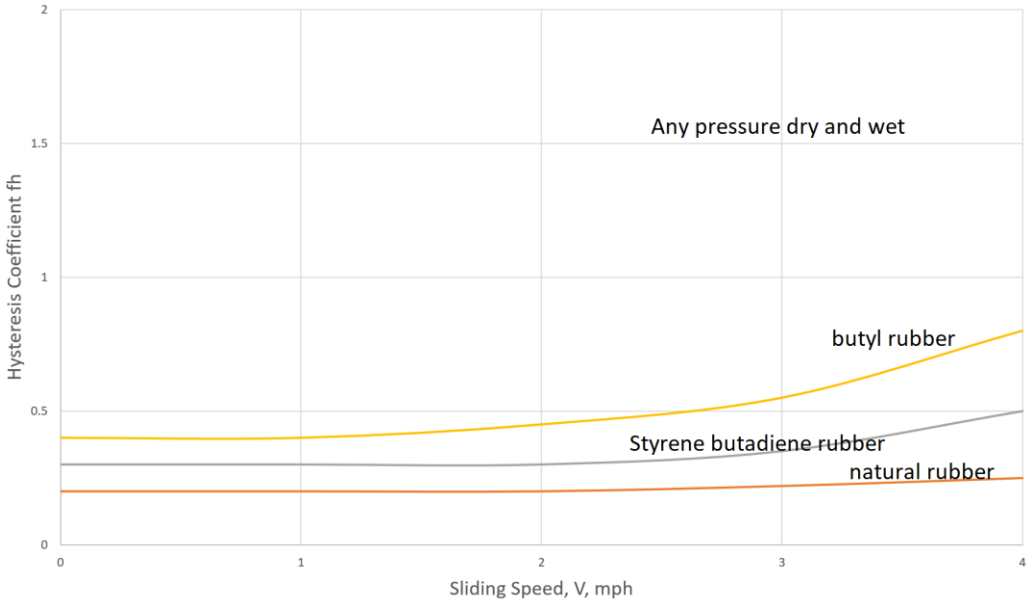

Figure 2.3. Hysteresis (Kummer and Meyer 1967)

2.1.2 Pavement Skid Resistance Measurements

Pavement skid resistance can be measured both in the laboratory and in the field using a wide range of devices. British Pendulum Tester (BPT) and Wehner-Schulze machine are two typical devices used in the lab for friction testing.

The British Pendulum Tester (BPT) is a dynamic pendulum impact-type tester used to measure the energy loss when a rubber slider edge is propelled over a test surface. Asi (2007) used BPT to evaluate friction performance of different pavement mixes considering different aggregates, different binder contents along with different mixture design procedures. Steven (2009) developed a temperature adjustment equation for the BPT and evaluated the influence of temperature, different instruments, operators and levels of slider pad wear. ASTM E303-93 (2013) illustrates the procedure for measuring surface friction properties using the BPT.

Wehner-Schulze machine has been widely used in polishing and measuring skid resistance and macro- or micro-texture profile of aggregate or pavement mix specimen. Kane et al. (2010) utilized Wehner-Schulze machine to simulate the polishing process and measure friction on pavement specimen in lab. Ueckermann et al. (2015) applied Wehner-Schulze machine in lab and proposed rubber friction prediction model using texture data. Wehner-Schulze machine was also used to predict pavement or aggregate friction in other studies (Do et al. 2009, Chen and Wang 2011, Dunford 2013, Friel et al. 2013).

Field friction of pavement surface is generally measured by the interplay force between a locked rubber tire and pavement surface (Roe et al. 1998). There are a number of devices and measurements for measuring pavement friction in the field: Dynamic Friction Tester (DFT) (ASTM E1911-09a 2009) used torque, which is monitored continuously as the disk rotational velocity reduces due to the friction between the sliders and the test surface, to calculate the friction coefficient at different speeds. Another method testing side force friction on paved

surface is pulling the Mu-Meter (ASTM E670-09 2009) over a pavement surface at a constant speed while the test wheels are under a constant static load. The Locked-Wheel Skid Trailer (ASTM E274-11 2011) measures the steady-state friction force on a locked test wheel as it is dragged under constant load and at constant speed (typically 40 mph) over a wet pavement surface. Grip Tester is a continuously friction measurement equipment (CFME) that follows the ASTM E274 - 11 (2011) "Standard Test Method for Skid Resistance of Paved Surfaces Using a Full-Scale Tire". The Grip Tester measures the longitudinal friction along the wheel path operating around the critical slip of an ABS at highway speed equipped with an Automatic Water Delivery System (AWS). The testing speed for this study is 40 mph with a constant water film thickness of 0.25 mm.

2.2 Factors Affecting Pavement Friction

Many research efforts have been conducted to evaluate the most influential factors on surface friction. Jayawickrama and Thomas (1998) used both linear and non-linear regression models to determine the significance of seasonal variation on pavement friction in Texas. Kokkalis and Panagouli (1998) investigated the impacts of pavement texture to skid resistance under wetting condition. Cenek (2004) investigated the sensitivity of skid resistance of chip seal surfaces to aggregate and texture characteristics under different traffic loading. Bazlamit and Reza (2005) evaluated the effects of temperature on friction for various asphalt pavements in Ohio. Asi (2007) evaluated the pavement friction performance of different asphalt concrete mixes, including mix with 30% slag, Superpave, Stone mastic asphalt (SMA), and Marshall Mixes. Using friction data of eight different surface textures obtained from 197 Long Term Pavement Performance (LTPP) sections, Ahammed & Tighe (2008) found that tined or grooved surfaces maintained consistently higher friction over time. Neaylon (2009) found that harder and more durable aggregates could retain higher friction values longer, contributing to adequate pavement safety and longer service life. Ahammed & Tighe (2012) instated that aggregate quality is the predominant factor for asphalt pavement surface friction. Based on long-term monitoring of friction coefficients on different asphalt pavement surfaces, Kotek & Florkova (2014) found direct characteristics includes age of wearing course, traffic volume, and climate of section, other factors such as speed, temperature, tire pressure, type of road surface could affect pavement friction. Li et al. (2016) found average temperature and installation age significantly affect the skid resistance based on extensive data collection on HFST sites.

Particularly, preventive maintenance treatments have been employed by many highway agencies to restore pavement friction and retard future deterioration. The effectiveness of different pavement preservation treatments has been studied in the past decades. Prapaitrakul et al. (2005) investigated the effectiveness of fog seal, while Li et al. (2012) evaluated the long-term friction

performance for chip seal, fog-chip, rejuvenating seal, microsurfacing, ultrathin bonded wearing course (UBWC), thin overlay. Lu (2006) indicated fog seals introduced initial reduction of pavement friction due to the presence of binder coating the exposed aggregate surfaces, and it exhibited similar skid resistance comparing with untreated surface during the service life. Kowalski et al. (2009) performed long-term monitoring of friction and texture properties on dense-graded asphalt (DGA), stone matrix asphalt (SMA) and porous friction course (PFC), and identified comparable frictional performance on SMA and PFC than that on DGA. Watson et al. (2011) also demonstrated chip seal had better friction performance measured by locked wheel trailer using ribbed/smooth tire, and fine, dense graded mixtures displayed the greatest variability in the difference between ribbed and smooth tire followed by the coarse DGA. Putman (2012) also claimed that OGFC could provide higher skid resistance than HMA and reduce accident probability. Wang et al. (2013) studied the effectiveness of four types of preservation treatments on skid resistance of pavement and developed long-term friction deterioration models using Specific Pavement Studies (SPS) data from the Long Term Pavement Performance (LTPP) program.

Izeppi et al. (2010) did a study on field performance of High Friction Surfaces (HFS) by evaluating long term variation of pavement friction number and benefit-cost analysis of HFS, and concluded HFS can provide significant increase on surface skid resistance with a positive economic benefit. Li et al. (2016) studied the effectiveness of high friction surface treatment (HFST) in improving pavement friction. The effectiveness of HFS in improving pavement skid resistance and reducing crashes at horizontal curves also had been demonstrated through other relevant projects (Bledsoe 2015; Moravec 2013; and Bischoff 2008).

2.3. Relationship between Skid Resistance and Aggregate Properties

It is widely acknowledged that pavement skid resistance is related to pavement surface's micro-texture and macro-texture. Micro-texture is mainly dependent on aggregate characteristics, such as angularity, surface texture and aggregate shape, while macro-texture is a function of asphalt mix properties, compaction method, and aggregate gradation. Microtexture of aggregates or pavement coring samples can be characterized in the laboratory using high resolution devices based on imaging analysis (Bessa et al. 2014).

Mineral aggregates with high resistance to polishing and abrasion are considered to be of high quality because they provide sufficient micro-texture for pavement skid resistance. According to the United States Department of Transportation (USDOT), there are approximately 8.6 million lane miles of pavement in the nation, most of which were constructed with natural aggregates from the most economical (closest) locations. Considering the distribution of aggregate quality, 21 states have areas where the aggregates are either soft or medium soft, commonly limestone (NSP 2010). Even in areas that have higher quality aggregate, accelerated surface deterioration still occurs due to frequent exposure to studded tires and snowplows (Komas 2011). Lack of high quality aggregates increases the risk of highway crashes and transportation maintenance costs.

In the past decades, many research efforts have been conducted to evaluate the effectiveness of aggregate properties on pavement performance, identifying factors affecting pavement texture and friction. Aggregate properties in Superpave method are grouped into consensus aggregate properties, source properties and gradation limits. Coarse aggregate angularity, flat and elongated particles, fine aggregate angularity, and sand equivalent are consensus properties to ensure sufficient aggregate quality to provide satisfactory HMA performance for the design traffic level. Los Angeles (LA) abrasion, sulfate soundness and deleterious materials are source properties that are generally set by local agencies for locally available materials. The gradation limits include definitions for nominal maximum and maximum aggregate size and control points for various

nominal maximum aggregate sizes. Since mineral aggregates make up 80% to 90% of the total volume or 94% to 95% of the mass of hot mix asphalt (HMA), it is important to maximize the quality of the mineral aggregates to ensure proper pavement performance, such as skid resistance of pavement surface. Prowell et al. (2005) and Masad (2007) grouped aggregate characteristics that have significant effect on performance of HMA mixes into three independent scales: shape, angularity and texture. Hall et al. (2009) found that the mineralogical and petrographic properties (aggregate composition/structure and mineral hardness), physical and geometrical properties (angularity, shape, and texture), mechanical properties (abrasion/wear resistance and polish characteristics), and durability properties (soundness) could influence short- and long-term texture performance. In order to investigate the relationship between the shape characteristics of aggregate and the pavement surface properties, Sengoz et al. (2014) found basalt type aggregates display higher friction values compared to limestone aggregates. Moaveni et al. (2014) found that aggregate polishing and degradation resulted in accelerating the surface deterioration and increasing remediation frequency. National Center for Asphalt Technology (NCAT 2017) found that aggregates initially characterized by a high level of angularity or texture might fail to maintain a sufficient level of friction due to polishing under traffic.

In addition, several state-of-the-art non-contact optical methods have been investigated and successfully implemented for aggregate surface characterization and friction performance evaluation. Masad et al. (1999) used digital image analysis to characterize the aggregate properties of pavement. Chen et al. (2006) using laser profiler to measure the contour of the aggregate surface with high precision. Arambula et al. (2013) concluded aggregates with higher soundness value and polishing resistance exhibited higher friction numbers than SAC-B. Ueckermann et al. (2015) measured pavement macro- and micro-texture using an optical testing system and developed a rubber friction model to predict surface skid resistance.

2.4. Relationship between Skid Resistance and Texture

As mentioned in preceding section, pavement friction is related to pavement surface's texture. Micro-texture is mainly dependent on adhesion force, while macro-texture relies on hysteresis force, which can be evaluated in terms of mean texture depth (MTD) or mean profile depth (MPD) via sand patch, circular track meter, or high speed profiler testing (ASTM E965-15 2015, ASTM E2157-15 2015, ASTM E950 2018). The hysteresis force is highly related to the macro-texture with wavelengths from 0.5 mm to 50 mm, which can be continuously tested in the field using laser-based devices at highway speeds. Macro-texture is an essential component to maintain sufficient friction when the vehicle is moving at a medium or higher speed on highways (Flintsch et al. 2003, Flintsch et al. 2005, Bitelli et al. 2012, Kargah-Ostadi and Howard 2015).

Comparing to direct contact measurements of skid resistance, pavement texture measurement is generally contactless based which overcomes many of the limitations. Therefore, during the past years, various studies has been conducted to study the relationship between friction and pavement texture properties. Meegoda and Gao (2015) developed the correlation between skid resistance and pavement surface macro-texture (MPD) with satisfactory accuracy. Izeppi et al. (2010), however, concluded no consistent relationships between pavement friction and texture based on the widely used traditional texture indicators, such as MPD and MTD. Kargah-Ostadi and Howard (2015) also found that the correlation between MPD and friction appeared to be significantly stronger only at higher speeds of friction testing. Because of the lack of correlation between MPD and friction, Kane at al. (2015) developed texture parameters using Hilbert-Huang transform, and correlated the developed parameters to pavement friction. Yang et al. (2017) implements discrete wavelet transform to decompose pavement surface macro-texture profile data into multi-scale characteristics and investigate their suitability for pavement friction prediction.

2.5. Methodology to Develop Non-Contact Friction Prediction Model

Substantial efforts have been put into researches in the non-contact prediction of pavement friction. Various linear regression models have been developed and evaluated in the past decades. Burchett (1978) utilized traditional regression analysis to evaluate the seasonal variations of pavement skid resistance. Fuentes et al. (2010) investigated the effect of pavement roughness on skid resistance using regression analysis and analysis of variance (ANOVA). Rezaei et al. (2011) developed traditional statistical skid resistance prediction models based on measurable quantities such as aggregate characteristics, aggregate gradation, and traffic. Kanafi (2014) studied the macro- and micro-texture variations on pavement friction and developed prediction models.

Experiment-based and model-based friction estimation methods have shown their advantage with reasonable accuracy and repeatability using data collected in vehicle or tire via optical sensor, acoustic sensor, tire tread sensor, or camera (Khaleghian et al. 2017). Kane et al. (2014) utilized 'Hilbert–Huang transform' (HHT) to investigate the pavement friction–texture relationship. Yang et al. (2017) implements discrete wavelet transform to analyze pavement profile data and investigate their suitability for friction prediction model development. Furthermore, various analytical models based on traditional signal processing techniques, such as fractal analysis, power spectral analysis, and novel parameters, have been developed to explore unconventional parameters for the characterization of texture properties and the relationship between pavement texture and pavement friction (Villani et al. 2014, Hartikainen et al. 2014, and Li et al. 2017).

Machine-learning (ML) technology has powered a plenty facets of modern society. ML technology has been used in the area of image recognition, automatic speech recognition, website searching etc. Some researchers used ML technology to estimate pavement friction in recent two years (Najafi et al. 2016, Marcelino et al. 2017, Panahandeh and Mohammadiha 2017).

2.6 Summary and Recommendations

In a summary, skid resistance can be directly measured using several types of friction instruments, which can be summarized in terms of spot measurement versus continuous measurement. Wehner-Schulze machine, British Pendulum Tester (BPT) and dynamic friction tester (DFT) are typical spot measurements. Spot measurements require lane closures in order to operate and are subject to operator bias when selecting test locations. Continuous measurements, such as Grip tester, locked wheel trailer, and Mu-meter, have been widely used by highway agencies for statewide friction management and project level pavement preservation. However, they all rely on the broad principle of sliding rubber over a road surface and measuring the reaction forces developed in some way. These contact methods have many limitations, such as consuming water and testing tires, only collecting data at limited areas on pavement surfaces with data variations, and interrupting traffic flows during testing. In addition, measurements based on contact methods are heavily depending on many factors during testing, such as water film depth, testing speed, pavement temperature, traffic wandering, testing tire wear, and pavement conditions. Comparing to direct contact measurements, non-contact measurements overcomes many of the limitations. Therefore, during the past years, there are tremendous researches on friction prediction and friction model development. However, none of the researches has been generally recognized and broadly applied.

For one reason, most of the previous studies characterized aggregate properties using traditional instruments with both hardware and software limitations, failing to correlate pavement friction to proper aggregate characteristics. With the rapid development of sensor technologies and computer algorithms during the past decade, more advanced and reliable instruments are becoming available. The most recent developments in 3D laser imaging technology, and computers have allowed the development of equipment to collect high resolution 3D image data for aggregate surface, such as 3D laser triangulation, stereo vision and LiDAR. A 3D laser

triangulation-based surface measurement and analysis device named LS-40 Portable 3D Surface Analyzer is will be used for 3D aggregate surface characterization in this study. The LS-40 Analyzer scans a 4'' by 4.5" area and produces a high resolution (0.01mm) digital surface structure with an intensity image and a surface depth related range image. The high-resolution image data obtained from LS-40 Analyzer make it possible to develop surface profiles and image-based methodologies to characterize aggregate surface properties in both 2D and 3D environments. A wide range of 3D aggregate and pavement surface texture parameters at both macro- and micro-scales will be developed, and their correlations to pavement friction will be identified.

Secondly, despite extensive studies have been conducted to identify the most influential factors and develop friction deterioration models using linear regression, knowledge gaps still remain in the understanding of the variations of pavement surface friction subject to potential influencing indicators, such as climate, the type of PM treatments, aggregate properties, age of treatment, traffic volume, pavement surface macro- and micro-texture, and other surface conditions. For one reason, no complete and high quality pavement surface data to facilitate the development of friction prediction models and further validation of relevant mechanistic models. More advanced and reliable instruments, which is capable of collecting high resolution three -dimensional (3D) image data for pavement surface should be applied. Furthermore, most existing models are primarily developed using either time-series (multiple time-series observations on one site) or cross-sectional (one collection on multiple pavement sites) friction data. Pavement friction performance deteriorates over time under three categories of influencing factors: climate, traffic loading and pavement surface conditions. For long-term performance monitoring, these factors are generally observed multiple times at a pre-designated interval for the network with many pavement sections. Traditional multiple regression modeling or time-series approaches fail to incorporate these influencing factors with both time-series and cross-sectional characteristics (Qi

et al. 2007, Washington et al. 2011, Li et al. 2017). More reliable linear regression methodology should be applied for friction model development.

Last but not the least, it is long desired to develop non-contact methods to predict pavement surface friction, such as using non-contact surface texture data to predict surface friction, which may supply or replace the existing contacting friction measurements. During the last years, various research has been conducted to study the relationship between friction and pavement texture properties. However, no consistent relationships between pavement texture and friction have been agreed regardless of extensive various efforts. With the rapid development of sensor technologies and computer algorithms during the past decade, it is possible to acquire precise field friction data with high reproducibility and repeatability using the exiting measurements to reflect the real profile of pavement surface. However, it seems hard to develop a powerful algorithm to predict friction consistently using pavement profile data. Machine-learning (ML) and deep learning technology have powered a plenty facets of modern society. They have been used in the area of image recognition, automatic speech recognition, website searching etc. Some researchers used ML technology to estimate pavement friction in recent two years. However, traditional ML techniques had limitations to process natural data in raw form. Deep-learning technology with deeper neural networks and multiple levels of representation allows a machine to be fed with raw data and to automatically discover the representations needed for detection. However, deeper neural networks are more difficult to train because of degradation problem. A specific deeper network should be tailored for friction prediction, which has the ability to learn and extract the textural features and classification boundaries automatically from raw input data, but also solve the problem of "degradation", increasing the prediction accuracy by adding more convolution layers.

Chapter 3 PAVEMENT SKID RESISTANCE AS A FUNCTION OF PAVEMENT SURFACE AND AGGREGATE TEXTURE PROPERTIES

Skid resistance depends on the macro- and micro-textural characteristics of pavement surface. Mean profile depth (MPD) is a widely used two-dimensional macro-texture indicator calculated from a single pavement surface profile, while pavement micro-texture is primarily affected by the characteristics of aggregates contained within the surface. With the development of non-contact three-dimensional (3D) measurement technologies and improvements in the computing and processing power of computers in recent decades, it is feasible and desirable to describe road surface texture in both macro- and micro-scales in three dimensions at ultra-high resolution. Investigating new 3D indexes and parameters not only promise a quantum leap in describing surface texture characteristics but also could provide in-depth understanding of the relationship between texture and friction for the purpose of surrogating existing contact based friction measurement methodologies

3.1 3D Aggregate Surface Characterization Parameters

Four categories of parameters have been used in 3D surface measurements and characterization: textural parameters, feature parameters, height parameters, and material ratio & volume parameters (Davis et al. 1979, Chen and Pavlidis 1979, ISO 2012, Leach 2012). For each category, various parameters are used for the characterization of 3D aggregates so as to correlate to pavement surface friction. These parameters are calculated with all the data points measured in

a 3D surface and according to the features that play a specific role in a particular function on a 3D aggregate image (Li et al. 2017).

3.1.1 Textural Parameters

The calculation of textural parameters is typically based on the Gray Level Co-Occurrence Matrices (GLCM) and autocorrelation function (ACF). GLCM has been widely used for texture-based feature extraction during the past decade (Smith et al. 2002, Mustafa et al. 2010, Yang et al. 2012, Artyushkova et al. 2015, Olaniyi et al. 2017), which is a statistical pattern recognition process to understand spatial relations among pixels within an image. This process quantitatively tabulate how often a combination of gray levels occurs in the image under analysis. The output of the GLCM function is the relative frequency *p (i,j)* matrix of two neighboring pixels with the fixed distance in the image.

$$p(i,j) = \frac{D_{l,\theta}(i,j)}{\sum_{i,j=1}^{L} D_{l,\theta}(i,j)} \tag{3.1}$$

D(i,j) represents the amount of occurrence of the pixel set with a gray level located at *i* and *j* in the target image, with a radius of *l* and direction of θ. *L* is scaling level of the gray level. Entropy (T_{etp}), energy (T_{eng}) and homogeneity (T_{hgt}) are three textural parameters calculated from GLCM in this study, which is shown and defined in Table 3.1. Entropy is a measure of the unavailability of a system's energy to perform work. The higher the textural entropy, the more heterogeneous the image is (Beyenal et al. 2004). Energy measures the regularity in patterns of pixels and is sensitive to the orientation of the pixel clusters and the similarity of their shapes. A smaller energy values mean frequent and repeated patterns of pixel clusters, while a higher energy means a more homogeneous image structure (Beyenal et al. 2004). Homogeneity measures the similarity of spatially close image structures: a higher homogeneity indicates a more homogeneous image structure (Beyenal et al. 2004).

In image processing, an auto-correlation function (ACF) is a measure of the matching ratio between an image rendered in different coordinates and the original image. The autocorrelation length (S_{al}), texture aspect ratio (S_{tr}) and texture direction (S_{td}) are three major textural parameters calculated from the ACF (Leach 2012). As shown in Table 3.1, S_{al} represents the horizontal distance in the direction in which the auto-correlation function decays the fastest (Michigan Metrology 2014). S_{tr} is a measure of uniformity of the surface texture, which is obtained by dividing the horizontal distance in the direction in which the ACF decays the fastest (equivalent to S_{al}) by the horizontal distance in the direction of the slowest ACF decay (Puccinelli J. et al. 2014). S_{td} is the angle with the largest angular spectrum, which represents the lay of the surface texture (Puccinelli J. et al. 2014).

Table 3.1. Textural Parameters

Parameter	Description	Unit or Range	Equation
T_{etp}	Entropy	-	$T_{etp} = -\sum_i \sum_j p(i,j) \log(p(i,j))$
T_{eng}	Energy	0-1	$T_{eng} = \sum_i \sum_j p(i,j)^2$
T_{hgt}	Homogeneity	0-1	$T_{hgt} = \sum_i \sum_j \frac{1}{1+(i-j)^2} p(i,j)$
S_{al}	Autocorrelation length	mm	$S_{al} = min\sqrt{t_x^2 + t_y^2}$
S_{tr}	Texture aspect ratio	0-1	$S_{tr} = \frac{r_{min}}{r_{max}}$
S_{td}	Texture direction	0 º- 180 º	Assessed from the Fourier spectrum of the surface

3.1.2 Feature Parameters

As shown in Table 3.2, there are nine specifically named feature parameters defined in the international standards (ISO/TS CD 25178-2): peak density (S_{pd}), the peak curvature (S_{pc}), significant height (S_{5p}, S_{5v}, and S_{10z}) and areal & volume (S_{da}, S_{ha}, S_{dv} and S_{hv}). The feature parameters are derived from the segmentation of a surface into motifs (dales and hills). A surface point higher than its surrounding area is called a peak, and the significant peaks on a surface are

segmented by inverting the surface and applying the watershed segmentation algorithm and the pruning of the change tree by a specified pruning factor (Leach 2012). In Table 3.2, *N* is number of peaks, z*(x,y)* is the height of pixel in mm at location *(x,y)* within a 3D image (Leach 2012). S_{5p} (S_{5v}) is the arithmetic mean height of the five highest (lowest) significant peaks (pits), and S_{10z} is the sum of S_{5p} and S_{5v}.

S_{pd} refers to the density of peaks, which is calculated by dividing the number of peaks by the unit area (ISO 2012). Since a large number of S_{pd} indicates more points of contact with objects, it can be used as an auxiliary parameter to analyze contact problems. S_{pc} represents the arithmetic mean curvature of the significant peaks on the surface (ISO 2012). The larger the value of S_{pc} is, the smaller the radius of curvature is, indicating that the peak is sharper and is likely to be easily worn out during a sliding contact (Leach 2012).

Table 3.2. Feature Parameters

Parameter	Description	Unit	Equation
S_{pd}	Peak density	1/mm^2	$S_{pd} = \frac{N}{Area}$
S_{pc}	Peak curvature	1/mm	$S_{pc} = \frac{1}{N} \iint_{Peak-Area} \left(\frac{\partial^2 z(x,y)}{\partial x^2}\right) + (\frac{\partial^2 z(x,y)}{\partial y^2})\, dx\, dy$
S_{5p}	5 point peak height	mm	Arithmetic mean height of the five highest significant peaks
S_{5v}	5 point valley height	mm	Arithmetic mean height of the five lowest significant peaks
S_{10z}	10 point height	mm	$S_{10z} = S_{5p} + S_{5v}$
S_{da}	Dales area	mm^2	Closed dales area calculated as the mean area of all individual motifs
S_{ha}	Hills area	mm^2	Closed hills area calculated as the mean area of all individual motifs
S_{dv}	Dales volume	mm^3	Closed dales volume calculated as the mean area of all individual motifs
S_{hv}	Hills volume	mm^3	Closed hills volume calculated as the mean area of all individual motifs

3.1.3 Height Parameters

Height parameters involve only the statistical distribution of height values along the *z* axis. The maximum height of the surface (S_p, S_v, and S_z), the arithmetic mean height (S_a), the root mean square height (S_q), the skewness (S_{sk}), and the Kurtosis (S_{ku}), are the typical height texture parameters. The definitions and description of height parameters are shown in Table 3.3, in which *A* is the aggregate sample area and z*(x,y)* is the height of pixel in mm at location *(x,y)* within a 3D image. Unusual conditions, such as a burr or sharp spike on a surface with poor materials, can be represented by the maximum height parameters. In addition, S_a is generally used to capture the roughness variation of 3D surfaces under polishing in laboratory (Dunford et al. 2012). A surface with a positive S_{sk} is likely to have poor lubricant retention because of the lack of deep valleys in which to retain lubricant traces. A spiky surface will have a high S_{ku} value while a bumpy surface will have a low S_{ku} value (Leach 2012).

Table 3.3. Height Parameters

Parameter	Description	Unit	Equation
S_p	Maximum peak height	mm	height of the highest point of the surface
S_v	Maximum pit height	mm	height of the lowest point of the surface
S_z	Maximum height of the surface	mm	sum of the absolute values of S_p and S_v
S_a	Arithmetical mean height of the surface	mm	$S_a = \frac{1}{A}\iint_A \lvert z(x,y)\rvert \, dx\, dy$
S_q	Root mean square height of the surface	mm	$S_q = \sqrt{\frac{1}{A}\iint_A z(x,y)\, dx\, dy}$
S_{sk}	Skewness of height distribution	-	$S_{sk} = \frac{1}{{S_q}^3}\frac{1}{A}\iint_A z^3(x,y)\, dx\, dy$
S_{ku}	Kurtosis of height distribution	-	$Sk_u = \frac{1}{{S_q}^4}\frac{1}{A}\iint_A z^4(x,y)\, dx\, dy$

3.1.4 Material Ratio & Volume Parameters

The height distribution can be represented as a histogram of the surface heights that quantifies the number of points on the surface that lie at a given height (Figure 3.1a). The material ratio curve is the cumulative curve of such distribution (Figure 3.1b). The material ratio (*mr)*, counting from the highest peak (where curve equals to 0%) to the lowest valley (where curve equals to 100%), could simulate wear of a 3D pavement surface providing a bearing surface for vehicle tires. Material Ratio Parameters can be calculated from the material ratio curve (Leach 2012). Areal material ratio (S_{mr}), inverse areal material ratio (S_{mc}) and peak extreme height (S_{xp}) are typical material ration parameters. As shown in Figure 3.1b, S_{mr} (c) is the ratio (p) of the material at a specified height c to the evaluation area expressed as a percentage. On the contrary, S_{mc} (p) evaluates the height value c corresponding to a material ratio p given as a parameter. The S_{xp} parameter is aimed at characterizing the upper part of the surface, from the mean plane to the highest peak without taking into account a small percentage of the highest peaks that may not be significant.

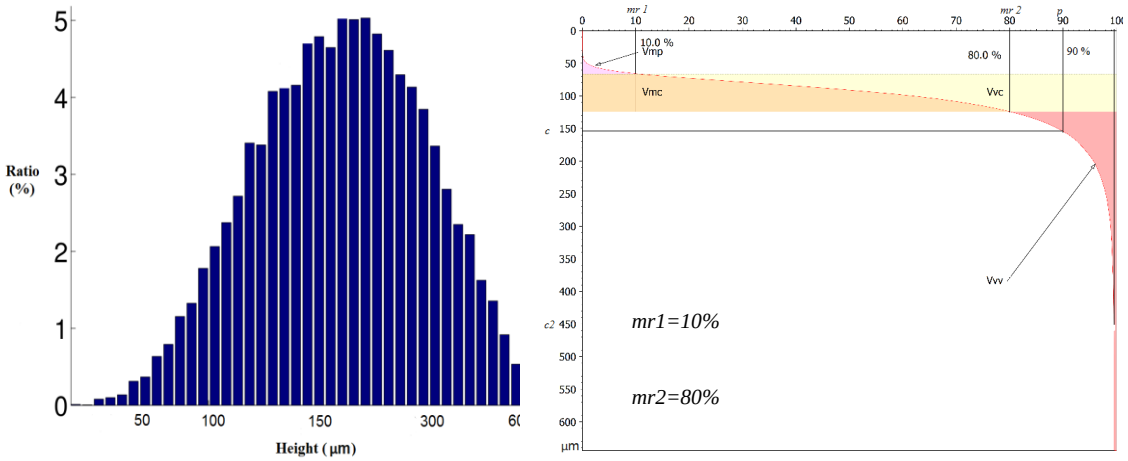

(a) Height Distribution (d) Material Ratio Curve

Figure 3.1. Calculation of Material Ratio & Volume Parameters

Volume Parameters can also be calculated from the material ratio curve (Leach 2012). Volume parameters used in this study include the void volume (V_v), the material volume (V_m), the peak

material volume (V_{mp}), the core material volume (V_{mc}), the core void volume (V_{vc}) and the dales void volume (V_{vv}). V_v (V_m) is calculated by integrating the volume enclosed above (below) the 3D texture image and below (above) the horizontal cutting plane at a height $h = S_{mc}(mr)$. In Figure 3.1b, V_{vc} (V_{mc}) is the area enclosed above (below) the areal material ratio curve and between the heights corresponding to *mr1* and *mr2*, and V_{vv} (V_{mp}) is the area enclosed above (below) the areal material ratio curve and between the height corresponding to *mr2* (*mr1*). The volume parameters can characterize wear and rolling properties during a running-in procedure (Deltombe et al. 2011). V_{mc} represents the part of the surface material which does not interact with another surface in contact, which can assist in understanding how much material is available for load support once the top levels of a surfaces are worn out (Adelle 2006).

The calculation of these parameters are provided in Table 3.4.

Table 3.4. Material Ratio & Volume Parameters

Parameter	Description	Unit	Equation
S_{mr}	Areal material ratio	%	Surface bearing area ratio
S_{mc}	Inverse areal material ratio	mm	Height of surface bearing area ratio
S_{xp}	Peak extreme height	mm	$S_{xp}(mr) = S_{mc}(2.5\%) - S_{mc}(50\%)$
V_v	Void volume	mm ^{3}/mm ^{2}	$V_v(mr) = k \iint_{mr}^{100\%} [S_{mc}(mr) - S_{mc}(q)]\, dq$
V_m	Material volume	mm ^{3}/mm ^{2}	$V_m(mr) = k \iint_{0}^{mr} [S_{mc}(q) - S_{mc}(mr)]\, dq$
V_{mp}	Peak material volume	mm ^{3}/mm ^{2}	$V_{mp} = V_m(mr1)$
V_{mc}	Core material volume	mm ^{3}/mm ^{2}	$V_{mc} = V_m(mr2) - V_m(mr1)$
V_{vc}	Core void volume	mm ^{3}/mm ^{2}	$V_{vc} = V_v(mr1) - V_v(mr2)$
V_{vv}	Dales void volume	mm ^{3}/mm ^{2}	$V_{vv} = V_v(mr2)$

3.2 Field Data Collection and Preliminary Analysis

3.2.1 Data Collection Testing Sites

Testing sites, as shown in Figure 3.2, are selected in Oklahoma considering the commonly-used aggregate sources, typical Oklahoma preventive maintenance (PM) treatments, different service lives and different traffic conditions. As shown in Table 3.5, among the twenty-two testing sites, six PM treatment types, eight aggregate sources are included. The aggregate sources and types for the testing sites are obtained from the Oklahoma Department of Transportation (ODOT) SiteManager® database. Two rounds of data collection were conducted in September 2016 and July 2017. It took approximately 5 days for each data collection round.

Table 3.5. Summary of data collection sites

Site ID	Treatment	Aggregate	Description
1	Chip seal	Limestone-Source 1	US-259
2	Micro-surface	Granite-Source 1	Lakeview in Stillwater
3	Resurface	Dolomite	SH-33
4		Dolomite	SH-33
5		Dolomite	SH-51
6		Dolomite	US-177
7		Granite-Source 1	US-77
8		Rhyolite	SH-51
9		Rhyolite	I-40
10		Rhyolite	US-77
11		Granite-Source 2	SH-9
12		Limestone-Source 2	US-64
13		Sandstone	US-270
14	UTBWC	Rhyolite	SH-270
15		Rhyolite	US-62
16	HFST	Mine Chat	SH-20-NB
17		Mine Chat	SH-20-SB
18	WMA	Rhyolite	SH-66
19		Rhyolite	SH-66
20		Rhyolite	SH-66
21		Rhyolite	SH-66
22		Rhyolite	SH-66

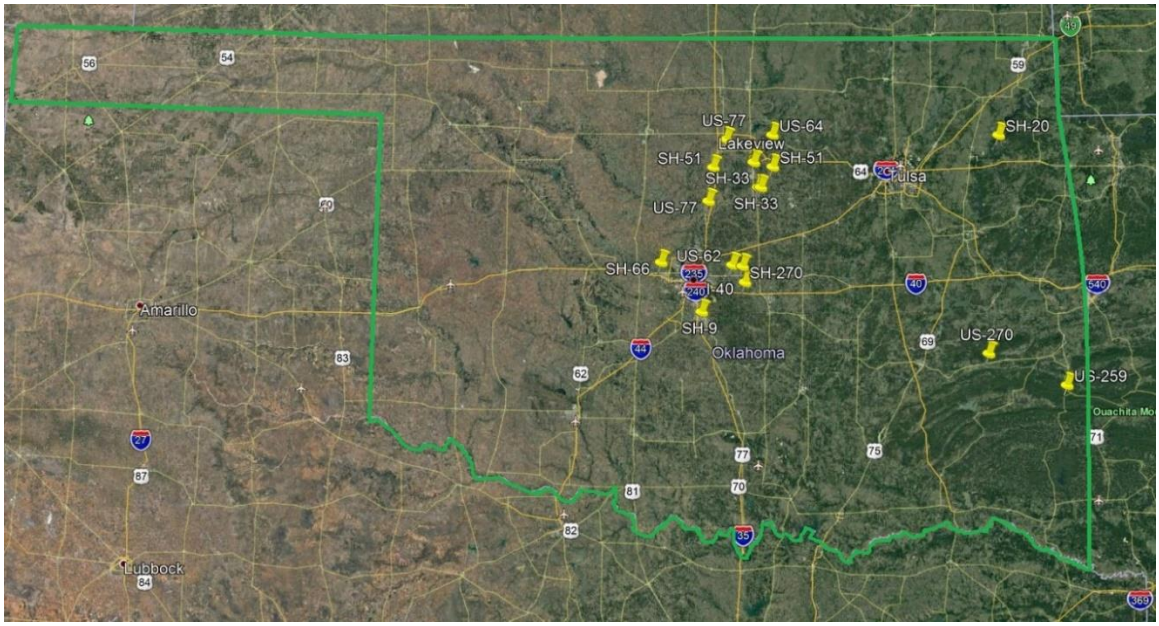

Figure 3.2. Maps of Data Collection Sites (Source: Google Earth)

3.2.2 Aggregate Sources

The aggregate materials used in this study are selected from a wide range of mineralogical properties and sampled from quarries in various geographical regions in the state of Oklahoma. The following eight sources of aggregate are identified and collected from quarries for lab testing.

- Granite (Source 1)
- Granite (Source 2)
- Limestone (Source 1)
- Limestone (Source 2)
- Dolomite
- Rhyolite
- Sandstone
- Mine Chat

3.2.3 Field Data Collection Instruments

Pavement friction and macro-texture data are continuously collected in parallel at the same predefined locations using Grip Tester (Figure 3.3) and AMES 8300 Survey Pro High Speed Profiler (Figure 3.4).

Grip Tester has been used in recent years by FHWA on many demonstration projects in United State. It is a continuously friction measurement equipment (CFME) that follows the ASTM E274 - 11 (2011) "Standard Test Method for Skid Resistance of Paved Surfaces Using a Full-Scale Tire". It is designed to measure the longitudinal friction along the wheel path operating around the critical slip of an ABS at highway speed across the entire stretch of a road with an Automatic Water Delivery System (AWS), which can provide greater detail about spatial variability and be an ideal option for project and network level friction management. The device has the capability to test at highway speeds (60 mph/100 km/h) as well as low speeds (20 mph / 32 km/h) using a constant water film thickness. In this dissertation, the collected data are recorded in 3.28-ft (1 m) intervals, with 40 mph testing speed and a constant water film thickness of 0.25 mm.

Figure 3.3. Grip Tester

AMES 8300 Survey Pro High Speed Profiler is designed to collect surface macro-texture data along with standard profile data at highway speeds, which meets the requirement of ASTM E950 (2018) Class 1 profiler specifications. Multiple texture indices such as Mean Profile Depth (MPD) can be calculated from the testing data. It is capable of collecting measurements at speeds between 25 and 65 mph with a resolution of 0.045 mm in vertical direction and 0.5 mm profile wavelength. Mean profile depth (MPD) is calculated from the collected longitudinal texture profiles at 3.28 feet interval in this study.

Figure 3.4. AMES 8300 High Speed Profiler

3.2.4 Preliminary Analysis Results

The average friction numbers and MPD values of two rounds of data collection events are presented in Figure 3.5 by Oklahoma common aggregate types. The testing sites with mine chat as the coarse aggregate produce the largest friction numbers along with MPD values, followed by sandstone and limestone. It is found that MPD values generally follow the same trend with friction numbers. However, the R-squared value of the linear regression friction prediction model with MPD as the only influencing factor is only 0.58. Several studies concluded that no rigorous relationship was found between MPD and friction performance (Izeppi et al. 2010, Yang et al. 2017).

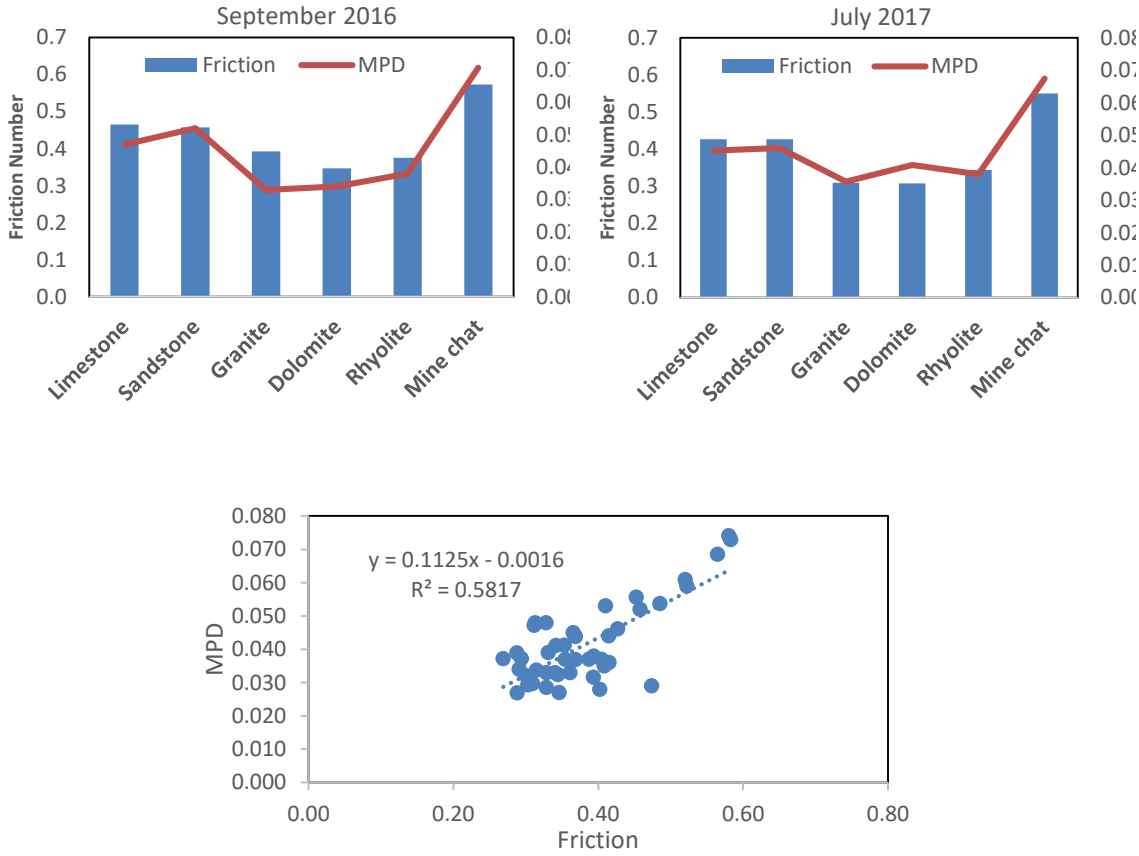

Figure 3.5. Friction and MPD Value Summary

3.3 Lab Testing of 3D Aggregates

Aggregate surface characteristics could significantly affect pavement skid resistance performance (Moaveni et al. 2014, Masad 2007). Although an aggregate might be initially characterized by a high level of surface properties and measure good friction values, it may not be suitable for a pavement surface layer if the aggregate cannot maintain a sufficient level of friction due to polishing under traffic. Most majority of the field testing sites in this study are more than 3 years in age. Therefore, Micro-Deval testing (AASHTO T 327) should be conducted to simulate field polishing and abrasion of aggregates due to traffic loading (Rezaei et al. 2009, Fowler and Rached 2012, Mahmoud and Masad 2007). Various aggregate properties after the Micro-Deval polishing process are tested in the laboratory using an ultra-high resolution 3D laser triangulation-based surface scanner, named LS-40 3D Surface Analyzer as shown in Figure 3.6.

As shown in Figure 3.6 (a), LS-40 scanner is able to scans a 4" by 4.5" areas and produces a high resolution (0.01mm) digital surface structure with a surface depth related range image (3D) and an intensity image (2D). The high-resolution image data obtained from this device make it possible to develop surface profiles and image-based methodologies to characterize aggregate surface properties in 3D environments, such as areal, volumetric and micro-texture of aggregate surface.

(a) LS-40 3D Surface Analyzer

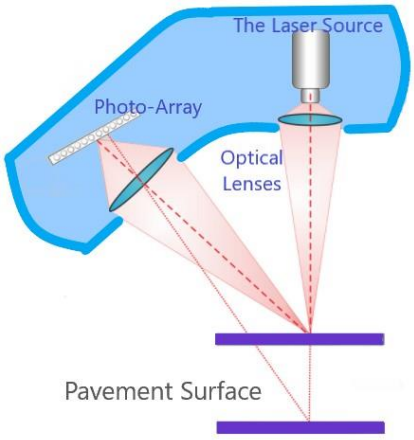

(d) Principle of Laser Triangulation
(Paulus et al. 2014)

Figure 3.6. Lab Testing Device

Three sets of samples (16 aggregate particles for each sample) for each aggregate type are scanned using the LS-40 scanner after the Micro-Deval polishing processes. Both 2D intensity and 3D range image data sets for the forty-eight aggregate particles of each aggregate source and type are acquired. One example set is shown in Figure 3.7.

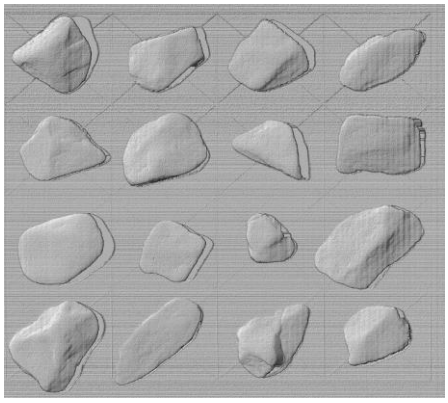

(a) Intensity Data

(d) Range Data

Figure 3.7. Examples 3D Aggregate Image (Sandstone)

Subsequently, the 3D Otsu thresholding approach is applied to segment 3D range images from each scan for further property extraction. Otsu is one of the popular histogram thresholding methods that utilizes the zeroth- and the first-order cumulative moments of the gray-level histogram (Otsu, 1979), and is extended to multi-threshold problems with optimal thresholding. Assuming an image $f(x, y)$ contains L gray levels and N pixels, $g(x, y)$ and $h(x, y)$ represent the

mean and the median of the gray values of the pixels in a $k \times k$ neighborhood regions centered with coordinate *(x, y)*. The 3D Otsu method takes the pixel's spatial information including the neighborhood median and mean into account, which can improve segmentation results and has better noise immunity compared to 1D or 2D Otsu (Sthitpattanapongsa and Srinark 2011).

$$\mathrm{g}(x,y) = \frac{1}{k^2}\sum_{i=-\frac{k}{2}}^{\frac{k}{2}}\sum_{j=-\frac{k}{2}}^{\frac{k}{2}} f(x+i, y+j)$$
$$\mathrm{h}(x,y) = med\{f(x+i, y+j): i = -\frac{k}{2}, \ldots, \frac{k}{2}; j = -\frac{k}{2}, \ldots, \frac{k}{2}\} \quad (1)$$

Example segmentation results are shown in Figure 3.8. Figure 3.8 (a) is the range image, with height information of each pixel in 3D. Figure 3.8(b) are the segmentation results, each aggregate is extracted from the sample set as shown in Figure 3.8(c). Figure 3.8(d) is the 3D rendering of each aggregate. The aggregate surface properties of the 16 particles are calculated for every sample set.

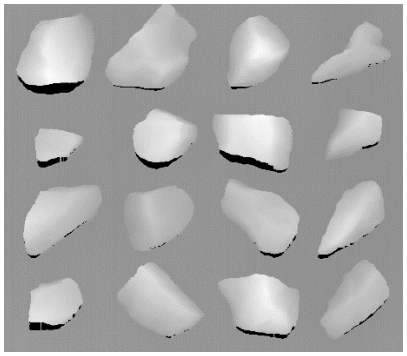

(a) Range Image

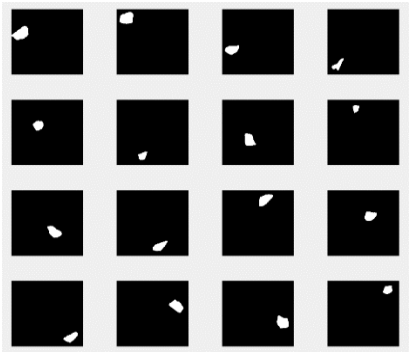

(b) Segmentation Results

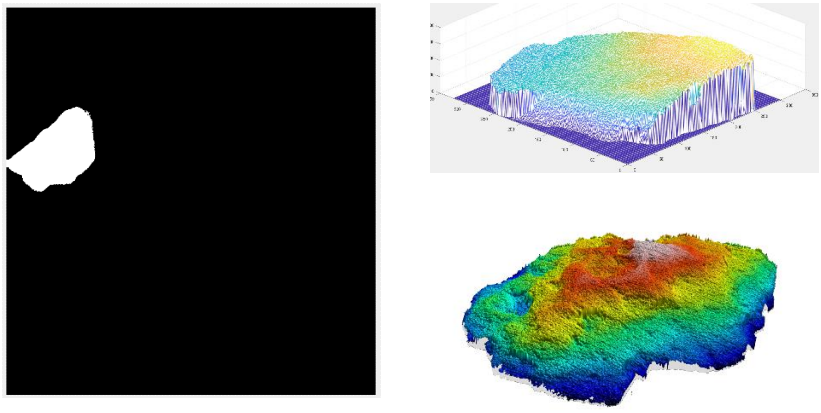

(c) Target Particle (d) Target Particle 3D Display

Figure 3.8. Image Segmentation Procedure

3.4 Selection of 3D Aggregate Parameters for Friction Model

As abovementioned, thirty-one 3D aggregate surface parameters are calculated for the four categories. In order to investigate the possible correlation among different parameters, the Pearson correlation coefficient matrix are computed within each category to exclude the parameters with strong correlations and remove their potential multi-collinearity during friction model development. A coefficient greater than 0.8 is generally described as strong, whereas a correlation less than 0.5 is generally described as weak correlation (Roberts et al. 2012).

The correlation coefficients within each category are summarized in Tables 3.6 to 3.9 for the 31 texture parameters specifically. There are several large correlation coefficients between those indicators, indicating these indicators are essentially describing the similar characteristics of the aggregates. If poor correlation is observed between two indicators, it indicates that they describe different aspects of the aggregate properties.

According to Table 3.6, entropy (T_{etp}) and texture aspect ratio (S_{tr}) are selected as the representatives of the textural parameters since both have poor correlation with other parameters. The rest of textural indicators are excluded since they are highly correlated to T_{etp} or $S_{tr.}$ Wear is found to be related to irreversible entropy generation within the Mechanically Affected Zone

(Abdel-Aal 2008), while texture isotropy, S_{tr}, of machined surface has significant influence on the wear process (Matuszewski et al. 2016).

Table 3.6. Pearson Correlation Matrix for Textural Parameters

	T_{etp}	T_{eng}	T_{hgt}	S_{al}	S_{tr}	S_{td}
$\boldsymbol{T_{etp}}$	1.00					
T_{eng}	**-0.96**	1.00				
T_{hgt}	**-0.96**	**0.94**	1.00			
S_{al}	**0.80**	**-0.63**	**-0.67**	1.00		
$\boldsymbol{S_{tr}}$	0.21	-0.30	-0.06	0.27	1.00	
S_{td}	-0.40	0.30	0.28	**-0.70**	**-0.58**	1.00

Similarly, as shown in Table 3.7, peak density (S_{pd}), peak curvature (S_{pc}), dale volume (S_{dv}) are kept to represent the feature parameters. Other research also finds that S_{pd} can be used in applications where contact is involved along with other parameters (Leach 2012), and to quantify aggregate micro-texture with respect to wear in the laboratory (Nataadmadja 2012). In addition, S_{pc} is able to quantify aggregate micro-texture with respect to the surface friction under wear condition (Nataadmadja 2012), while S_{dv} can be used to evaluate scuffing performance of metallic surfaces (Wojciechowski et al. 2017) and measure surface texture using optical methods (Pawlus et al. 2017).

Table 3.7. Pearson Correlation Matrix for Feature Parameters

	S_{pd}	S_{pc}	S_{dv}	S_{hv}	S_{da}	S_{ha}	S_{10z}	S_{5p}	S_{5v}
$\boldsymbol{S_{pd}}$	1.00								
$\boldsymbol{S_{pc}}$	0.40	1.00							
$\boldsymbol{S_{dv}}$	-0.18	0.11	1.00						
S_{hv}	-0.27	-0.41	**0.70**	1.00					
S_{da}	-0.38	0.07	**0.72**	**0.81**	1.00				
S_{ha}	-0.22	-0.37	**0.60**	**0.97**	**0.84**	1.00			
S_{10z}	0.09	**0.67**	0.47	0.21	0.66	0.33	1.00		
S_{5p}	**0.86**	0.31	-0.09	-0.13	-0.21	-0.04	0.25	1.00	
S_{5v}	-0.36	0.45	**0.52**	0.35	**0.81**	0.44	**0.87**	-0.24	1.00

Based on Table 3.8 and Table 3.9, only S_{sk} is selected for the height parameter and S_{mr} for material ratio & volume parameter. Based on past study, S_{sk} can be used to predict tribological behavior of contact surfaces and plan surface texturing (Sedlaček et al. 2016), while $S_{mr,}$ describes the contact area ratio that affects friction and lubrication directly.

Table 3.8. Pearson Correlation Matrix for Height Parameters

	S_{sk}	S_{ku}	S_a	S_p	S_q	S_v	S_z
$\boldsymbol{S_{sk}}$	1.00						
S_{ku}	**-0.96**	1.00					
S_a	**0.94**	**-0.92**	1.00				
S_p	**0.74**	**-0.63**	**0.83**	1.00			
S_q	**0.94**	**-0.92**	**1.00**	**0.84**	1.00		
S_v	**0.96**	**-0.92**	**0.93**	**0.71**	**0.93**	1.00	
S_z	**0.93**	**-0.86**	**0.96**	**0.90**	**0.96**	**0.95**	1.00

Table 3.9. Pearson Correlation Matrix for Material Ratio & Volume Parameters

	S_{mr}	S_{mc}	S_{xp}	V_{mc}	V_m	V_v	V_{mp}	V_{vc}	V_{vv}
$\boldsymbol{S_{mr}}$	1.00								
S_{mc}	**-0.77**	1.00							
S_{xp}	**-0.79**	**0.99**	1.00						
V_{mc}	**-0.78**	**1.00**	**1.00**	1.00					
V_m	**-0.67**	**0.86**	**0.87**	**0.86**	1.00				
V_v	**-0.77**	**1.00**	**0.99**	**1.00**	**0.86**	1.00			
V_{mp}	**-0.67**	**0.86**	**0.87**	**0.86**	**1.00**	**0.86**	1.00		
V_{vc}	**-0.76**	**1.00**	**0.99**	**1.00**	**0.86**	**1.00**	**0.86**	1.00	
V_{vv}	**-0.85**	**0.96**	**0.98**	**0.96**	**0.86**	**0.97**	**0.86**	**0.96**	1.00

3.5 Friction Prediction Model Development

Multivariate linear regression friction model is developed using the two years of field friction measurements, pavement surface and 3D aggregate texture parameters:

$$Friction\ Number = \varphi + \sum_1^8 \mathrm{K}_i * \mu_i \quad (2)$$

Where φ is the estimated intercept, while μ_i is the estimated coefficient for the corresponding parameter, and K_i represents the independent parameter, including:

- Pavement surface macro-texture: *MPD*
- Aggregate textural parameters: T_{etp}, S_{tr}
- Aggregate feature parameters: S_{pd}, S_{pc}, S_{dv}
- Aggregate height parameters: S_{sk}
- Aggregate material ratio & volume parameters: S_{mr}

The estimated regression coefficients and corresponding P-values of the multivariate model are summarized in Table 3.10. The adjusted R square of this model is 0.73, which is much larger than that if only MPD is considered. The statistical P-values of all the independent variables herein are smaller than 0.05, indicating their significances to pavement friction. In particular, the p-value of MPD is 0.04998, which is the largest for the independent variables, indicating that MPD is marginal significant at 95% confidence level and is the least influencing factor in the model. 3D Aggregate texture indicators, entropy (T_{etp}) and the peak curvature (S_{pc}), have the most significant influences on friction, whose P-values are smaller than 0.0001.

Based on the developed friction model, the predicted and actual observed friction numbers for all the testing sites are plotted in Figure 3.9. The predictions follow the actual measured friction number well with the R-squared values of 0.78.

Table 3.10. Friction Prediction Models

	Coefficients	*Standard Error*	*t Stat*	*P-value*	Significant level
Intercept	7.5363	1.7621	4.2769	0.00014	***
MPD	1.9723	0.9714	2.0303	0.04998	*
T_{etp}	-0.5246	0.1121	-4.6807	0.00004	****
S_{tr}	-8.6342	2.2734	-3.7979	0.00056	***
S_{pd}	-7.7719	2.0016	-3.8828	0.00044	***
S_{pc}	0.0040	0.0009	4.4543	0.00008	****
S_{dv}	-0.4512	0.2146	-2.1020	0.04282	*
S_{mr}	-270.7521	63.1482	-4.2876	0.00013	***
S_{sk}	-0.8860	0.4156	-2.1316	0.04014	*
				R Square	0.78
				Adjusted R Square	0.73
				Standard Error	0.04

Note: Significant levels: *P < .05, **P < .01, ***P < .001, ****P<.0001

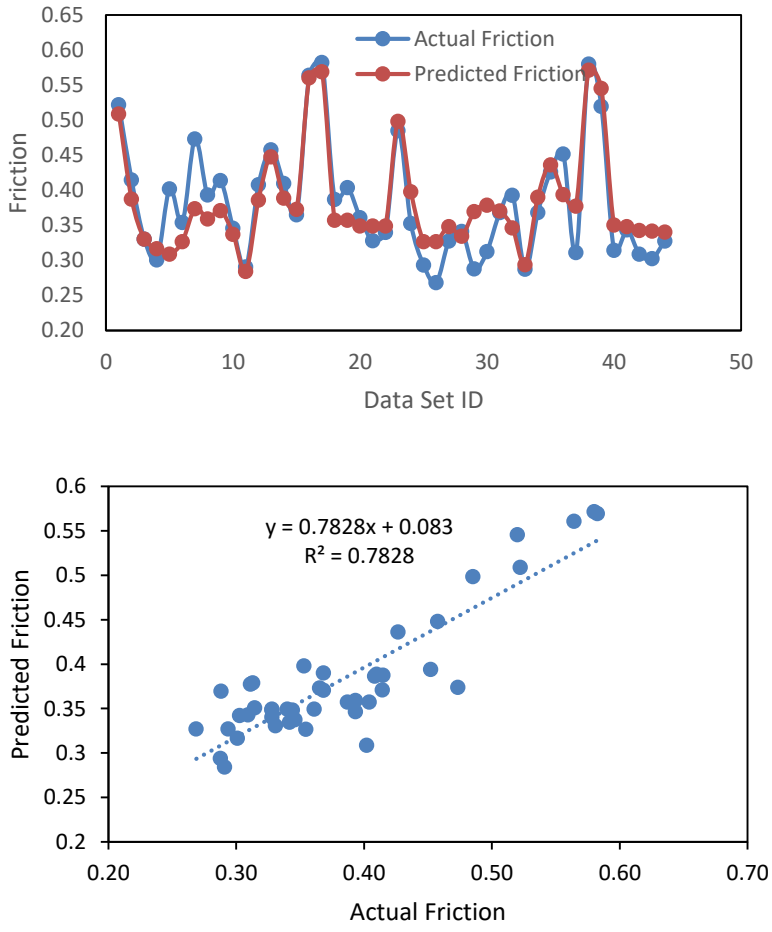

Figure 3.9. Friction Prediction Results

3.6 Summary

In this study, twenty-two pavement sites, constructed using six common types of preventive treatments and eight typical sources of aggregates in Oklahoma, are selected as the field test beds. Pavement skid resistance and surface macro-texture data are collected in parallel at highway speeds using a grip tester and a high speed texture profiler, while aggregate properties under 3D are measured using a portable ultra-high resolution 3D laser scanner. MPD values are calculated to represent surface macro-texture. Thirty-one 3D aggregate parameters in four categories (textural, feature, height, and material ratio & volume parameters) are investigated to characterize micro-texture attributes. The Pearson correlation coefficient matrix is computed within each category to exclude the parameters with strong correlations and remove their potential multi-collinearity during friction model development. Multivariate analysis is subsequently performed to examine the relationship between pavement skid resistance, and surface and aggregate texture properties. Eight texture parameters have showed statistical significance on pavement friction. Entropy (T_{etp} textural parameter) and peak curvature (S_{pc} feature based parameter) present the most significant influences on pavement friction, while MPD demonstrates the least impact. The developed model based on surface and aggregate texture properties can better predict pavement friction performance. The comprehensive analysis of texture properties could assist highway agencies understanding the appropriate characterization of aggregates and developing aggregate selection guideline for optimized skid resistance.

Chapter 4 PANEL DATA ANALYSIS OF SURFACE SKID RESISTANCE FOR VARIOUS PAVEMENT PREVENTIVE MAINTENANCE TREATMENTS

In this chapter, Panel Data Analysis (PDA) is used to investigate the effectiveness of various preservation treatments on pavement skid resistance and develop pavement friction panel models. The panel data used in this paper are firstly obtained from 255 SPS-3 testing sections in the LTPP database, which consists of multiple years of surface friction and relevant data for the four Preventive Maintenance (PM) treatments (thin overlay, slurry seal, crack seal, and chip seal) under various climate conditions, traffic levels and pavement performance. Then filed data collection are conducted from 45 pavement testing sites in Oklahoma with different traffic levels and pavement performance. These testing sites include six major preventive maintenance treatments and seven typical types of aggregates used in Oklahoma. The aggregate sources and types for these sites are obtained from the Oklahoma Department of Transportation (ODOT) SiteManager® database. From 2015 to 2017, multiple data collection events have been performed in the field to gather surface friction and relevant surface condition data (temperature, roughness, macro-texture, rutting).

Panel models, both fixed- and random-effects models, are developed and compared with the traditional ordinary regression models. Pavement friction performance for the preventive maintenance treatments is evaluated and the factors that significantly impact pavement skid resistance are identified.

4.1 Panel Data Analysis (PDA)

4.1.1 Panel Model

Panel Data Analysis (PDA), also known as pooled longitudinal or cross-sectional time-series analysis, are composed of a cross section of individual subjects, with many repetitive measurements over time for each individual (Lee and Kim, 2005). The main difference distinguishes panel model from cross-sectional regression model is that the panel model incorporates heterogeneity among subjects, allowing for subject-specific parameters. There are two major types of panel models: fixed-effect and random-effect. In the fixed-effects model, subject specific parameters are treated as fixed parameters to be estimated. Fixed-effects regression is the model to use when it is needed to control for omitted variables that differ between cases but are constant over time. However, in the random-effects model, these parameters are treated as random variables from an unknown population (Croissant and Millo, 2008). If it is reasonable enough to believe that some omitted variables may be constant over time but vary between cases, and others may be fixed between cases but vary over time, both types of variables can be contained by using random-effects models. Both fixed- and random-effects models are studied and compared in this research.

The equation of panel models is shown in the following:

$$y_{itj} = \alpha_i + x_{itj,1}\beta_1 + x_{itj,2}\beta_2 + x_{itj,3}\beta_3 + x_{itj,4}\beta_4 + x_{itj,5}\beta_5 + \varepsilon_{itj} \quad (1)$$

Where y_{itj} = pavement friction for the i^{th} PM treatments, t^{th} time period, j^{th} sites; i = PM treatments (i = 1,2, . . . ,5); t = time, year; j = each site, (j = 0, . . . , N_{it}); N_{it}= number of total sites for the i^{th} PM treatments, t^{th} time period; $x_{itj,1}$= climate variables; $x_{itj,2}$ = traffic variables; $x_{itj,3}$ = pavement age; $x_{itj,4}$ = pavement surface characteristics; $x_{itj,5}$ = structural adequacy variables or aggregate characteristics; ε_{itj}= error term for the i^{th} preventive treatments, t^{th} time period, j^{th} sites;

In the fixed-effects model, subject specific variable, α_i is supposed to be fixed as known parameters, and ε_{itj} is assumed to vary non-stochastically over i, or t. From that perspective, the fixed-effects model is analogous to a dummy variable model in one dimension. In the random-effects model, α_i is assumed to be a random variable, which is assumed to be independent and identically distributed (IID) with a mean zero and variance σ_ϵ^2, and ε_{itj} is assumed to vary stochastically over i, or t requiring special treatment of the error variance matrix (Hsiao, 1999).

4.1.2 Model Selection Criteria

Several types of alternative models can be used for the model development, including the Ordinary Least Square (OLS) model, fixed-effects panel model, and random-effects panel model. The process of selecting an appropriate model type is illustrated in Figure 4.1. F-test is performed to test the joint significance of the fixed-effects intercepts to compare the regular OLS model and fixed-effects model (Washington et al., 2011). The null hypothesis is that all of the fixed effect intercepts are zeros. If the null hypothesis is rejected, fixed-effects method is preferred and should be used.

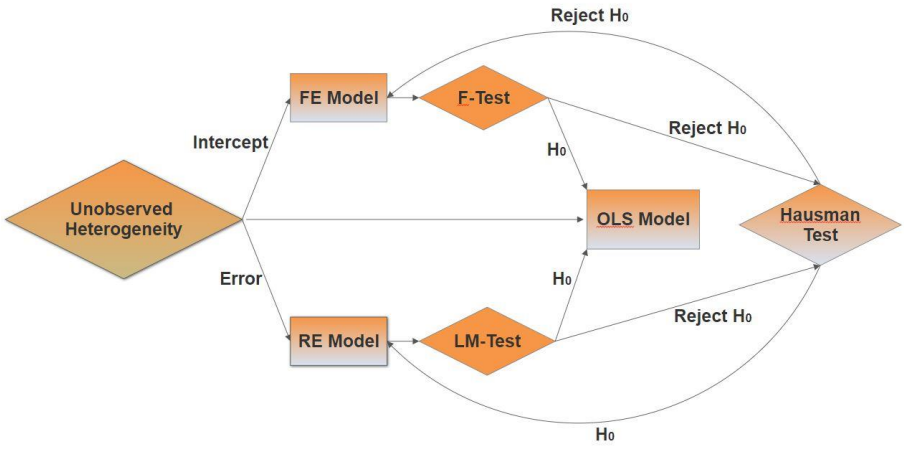

Figure 4.1. Panel Model Selection Criterion (Park 2011)

The random effects of panel data models can be examined using the Lagrange multiplier (LM) test (Breusch and Pagan 1980, Washington et al. 2011). LM test examines if individual (or time)

specific variance components equal to zeros. If the null hypothesis is rejected, significant random effects are presented in the panel data, indicating that the random-effects model can better deal with heterogeneity in the panel data than the OLS model.

In addition, Hausman test (Greene 2012) is conducted to differentiate the fixed and random effects within the panel models. This test evaluates the consistency of an estimator when compared to an alternative, less efficient estimator which is already known to be consistent. Consider the linear model $y = bx + e$, where y is the dependent variable and x is vector of repressors, b is a vector of coefficients and e is the error term. There are two estimators for b: b_0 and b_1. Under the null hypothesis, both of these estimators are consistent, but b_1 is efficient with the smallest asymptotic variance. If null hypothesis is rejected, it means that b_1 is inconsistent. In other words, random-effects model is preferred under the null hypothesis due to its higher efficiency, while under the alternative hypothesis fixed-effects model is at least consistent and thus preferred.

4.2 A Preliminary Case Study of PDA using LTPP SPS-3 Database

4.2.1 Data Sources

Firstly, a preliminary case study of PDA is conducted using the friction data in LTPP SPS-3 database. The LTPP program is a long term study of in-service pavements across the United States and Canada. The SPS-3 experiment was designed to evaluate the effectiveness of different flexible pavement preservation treatments (thin overlay, slurry seal, crack seal, and chip seal) on pavement performance under multiple design factors (climatic zone, traffic loading, initial pavement condition, and structural adequacy etc.) (Hall et al., 2002). There are totally 81 SPS-3 sites with 445 sections, while 255 sections have three to seven years of friction data.

Factors influencing pavement friction can be categorized into several groups: highway alignment, environment conditions, traffic characteristics, and driver/vehicle characteristics (Hall and Hanna

2009). In this case study, climate, traffic, pavement surface conditions, and pavement structural adequacy are considered as potential influencing factors for friction model development, as shown in Table 4.1 primarily due to the data availability in the LTPP database. Many climate aspects affect pavement friction based on the previous study. The climate characteristics used in this case study include precipitation, humidity, Freezing Index and temperature. Traffic characteristics include Annual Average Daily Traffic (AADT), Annual Average Daily Truck Traffic (AADTT) and 18-Kip equivalent single axle load (ESAL). Pavement performance indicators include initial friction, pavement age when PM treatment was applied, pavement cracking, rutting, IRI. Falling Weight Deflectometer (FWD) is the most commonly used device to evaluate pavement structural adequacy. In this case study, the average deflection values at the center and farthest sensors of FWD measurements are used to represent pavement structural adequacy.

The parameters and their data source tables in the LTPP database are as follows:

- Friction: MON_FRICTION
- Annual Average Precipitation (AAP): CLM_VWS_PRECIP_ANNUAL
- Annual Average Temperature (AAT): CLM_VWS_TEMP_ANNUAL
- Annual Average Freezing Index (AAFI): CLM_VWS_TEMP_DAILY
- Annual Average Humidity (AAH): CLM_VWS_HUMIDITY_ANNUAL
- Traffic: TRF_HIST_EST_ESAL
- Treatment Age: SECTION_STRUCTURE_HISTORY
- Pavement Cracking: MON_DIS_AC_CRACK_INDEX

- Pavement Rutting: MON_RUT_DEPTH_POINT
- IRI: MON_HSS_PROFILE_SECTION
- FWD: MON_DEFL_DROP_DATA

Table 4.1. Candidate Variables for LTPP SPS-3 Database

Category	Variable		Description
Dependent variable		Friction	Pavement friction
Independent Variables	Age	Age	Pavement Age
	Treatment Type	Treatment	Subject variable describing preventive treatments, (Categorical data with 1 for thin overlay, 2 for slurry seal, 3 for crack seal, 4 for control section, 5 for chip seal)
	Climate	AAT	Annual Average Temperature (deg C)
		AAP	Annual Average Precipitation (mm)
		AAH	Annual Average Humidity (%)
		AAFI	Annual Average Freeze Index (deg C deg days)
	Traffic	AADT	Annual Average Daily Traffic (AADT)
		AADTT	Annual Average Daily Truck Traffic (AADTT)
		ESAL	18-Kip Equivalent Single Axel Load
	Pavement Condition	IF	Pavement Initial Friction Value
		LCWP	Length of Longitudinal Cracking within Wheel Path (m)
		LCNWP	Length of Longitudinal Cracking outside of Wheel Path (m)
		Rutting	Pavement Rutting depth (mm)
		Fatigue	Area of Fatigue Cracking (m2)
		IRI	International Roughness Index (IRI) (m/km)
	Structural Adequacy	ADC	Average FWD Deflection (9-kip) for the Center Sensor(microns)
		ADF	Average FWD Deflection (9-kip) for the Farthest Sensor (microns)

Figure 4.2 shows the distribution of friction of SPS-3 pavement sections during the multiple-year period, while Table 4.2 provides the summary statistics of the selected influencing variables and its correlation to friction value. It is seen that the SPS-3 pavement friction data contains high degrees of freedom and significant variations (or heterogeneity across groups and over time),

while the correlations between the influencing factors and friction are generally weak except initial friction. As a result, using ordinary regression modeling method to develop friction models may be subject to omitted variable bias. In addition, the friction data sets contain both cross-sectional characteristics (various maintenance treatments under different climate conditions, traffic levels and pavement conditions) and time-series characteristics (multiple years of observations). Therefore, Panel Data Analysis (PDA) could be an appropriate method for analysis of friction data for various preventive maintenance treatments. PDA allows the control of variables variance which cannot be observed or measured for pavement preventive maintenance treatments across different sites, or variables that change over time but not across entities (such as climate and traffic variables).

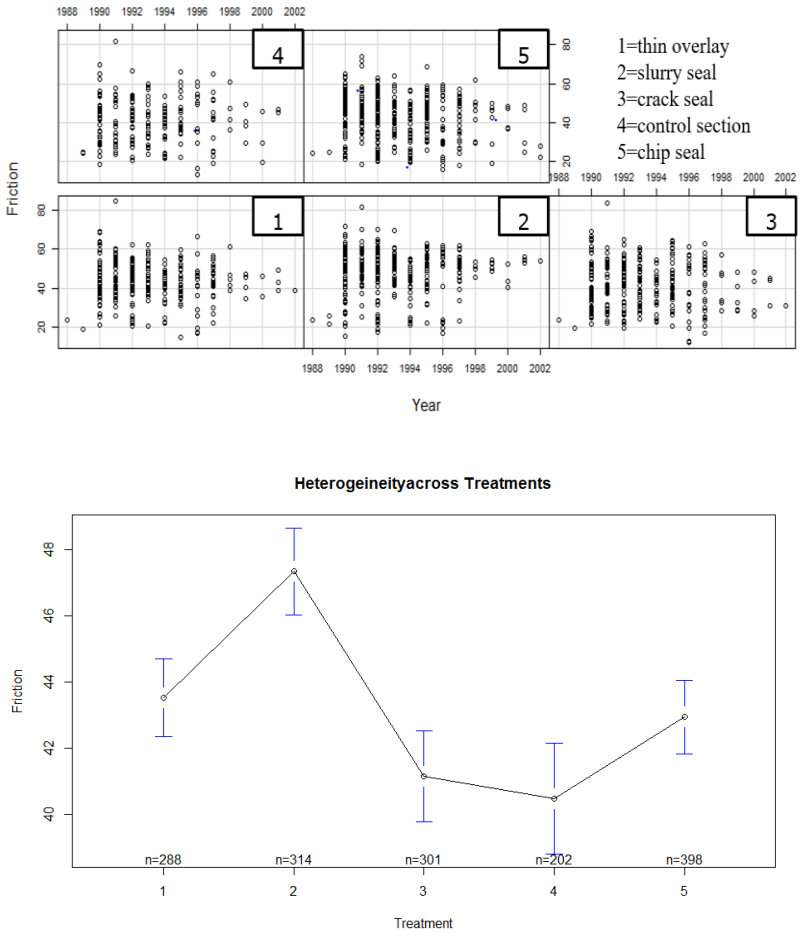

Figure 4.2. Distribution and Heterogeneity of Friction Data in LTPP SPS-3 Sections

Table 4.2. Description of Indicator Variables

Variable	Unit	Mean	Median	Std deviation	Minimum	Maximum	Correlation with Friction
Friction	-	43.28	44.50	11.69	12.00	84.50	1.00
AAT	deg C	14.06	14.20	5.60	0.20	23.40	-0.03
AAP	mm	927.60	945.40	392.04	113.80	1965.80	0.03
AAH	%	67.14	69.00	8.32	34.00	84.50	-0.01
AAFI	deg C deg days	275.37	69.00	430.81	0.00	2448.00	-0.05
AADT	-	2363.59	1927.00	1901.45	146.00	11321.00	-0.16
AADTT	-	371.09	249.00	442.93	35.00	3516.00	-0.11
ESAL	KESAL	138.49	74.00	200.89	5.00	2091.00	-0.06
IF	-	45.97	48.00	11.38	19.00	84.50	0.70
Age	Year	16.65	16.00	7.17	3.00	45.00	-0.02
LCWP	m	50.13	4.10	81.67	0.00	410.50	-0.07
LCNWP	m	76.30	0.00	2333.63	0.00	84146.00	-0.04
Rutting	mm	7.92	7.00	4.26	1.00	29.00	-0.08
Fatigue	m^2	19.05	0.00	57.86	0.00	544.40	0.00
IRI	m/km	1.52	1.32	0.66	0.56	4.51	-0.08
ADC	microns	316.53	275.00	173.40	52.00	1084.00	-0.04
ADF	microns	35.19	33.00	12.95	8.00	82.00	-0.05

4.2.2 Analysis Results and Model Development

The statistical analysis in this chapter is based on the programming language of R. Traditional OLS regression model, which does not consider the heterogeneity across groups or time, is firstly used to model the friction data. Parameter estimates and the corresponding t-statistics for the OLS models are shown in Table 4.3. Subsequently, parameter estimates and the corresponding t-statistics for the fixed-effects and random effects models are shown in Table 4.4 and Table 4.5 respectively.

Table 4.3. Coefficient Estimates and t-Statistics for OLS Model

Variable	Estimate	Std. Error	t-value	Pr(>|t|)	Sig. level
(Intercept)	16.011	5.698	2.810	0.005	**
AAP	0.000	0.002	-0.091	0.927	
AAT	0.628	0.155	4.059	0.000	***
AAFI	0.006	0.002	3.302	0.001	**
AAH	0.017	0.088	0.196	0.845	
AADT	0.001	0.000	2.632	0.009	**
AADTT	-0.007	0.002	-3.249	0.001	**
ESAL	0.005	0.003	1.899	0.058	.
IF	0.510	0.034	15.187	0.000	***
Age	-0.044	0.067	-0.653	0.514	
Fatigue	0.022	0.008	2.918	0.004	**
LCWP	-0.007	0.005	-1.474	0.141	
LCNWP	-0.014	0.020	-0.678	0.498	
Rutting	-0.394	0.124	-3.186	0.002	**
IRI	1.703	0.874	1.948	0.052	.
ADC	-0.008	0.003	-2.692	0.007	**
ADF	-0.012	0.034	-0.352	0.725	
			R-Squared		0.383
			Adj. R-Squared		0.362

Significant level=0.1, * Significant level=0.05, ** Significant level=0.01, ***Significant level=0.001

Table 4.4. Coefficient Estimates and t-Statistics for Fixed-Effects Model

Variable	Estimate	Std. Error	t-value	Pr(>|t|)	Sig. level
AAP	-0.011	0.003	-3.643	0.000	***
AAT	1.933	1.031	1.875	0.062	.
AAFI	0.011	0.005	2.414	0.017	*
AAH	0.618	0.216	2.862	0.005	**
AADT	0.002	0.001	1.788	0.075	.
AADTT	-0.031	0.009	-3.448	0.001	***
ESAL	0.014	0.021	0.686	0.493	
Age	-0.825	0.338	-2.443	0.015	*
Fatigue	0.025	0.011	2.300	0.022	*
LCWP	0.018	0.009	1.896	0.059	.
LCNWP	-0.007	0.045	-0.162	0.871	
Rutting	0.042	0.315	0.133	0.895	
IRI	-0.878	2.431	-0.361	0.718	
ADC	-0.008	0.009	-0.919	0.359	
ADF	0.059	0.148	0.395	0.693	
			R-Squared		0.214
			Adj. R-Squared		0.097
			P-value		0.000

Significant level=0.1, * Significant level=0.05, ** Significant level=0.01, ***Significant level=0.001

Table 4.5. Coefficient Estimates and t-Statistics for Random-Effects Model

Variable	Estimate	Std. Error	t-value	Pr(>|t|)	Sig. level
AAP	-0.003	0.002	-1.377	0.169	
AAT	0.783	0.165	4.732	0.000	***
AAFI	0.007	0.002	3.741	0.000	***
AAH	0.090	0.087	1.029	0.304	
AADT	0.001	0.000	2.185	0.029	*
AADTT	-0.008	0.002	-3.499	0.001	***
ESAL	0.005	0.003	1.814	0.070	.
IF	0.578	0.038	15.100	0.000	***
Age	-0.107	0.077	-1.394	0.164	
Fatigue	0.019	0.007	2.751	0.006	**
LCWP	-0.002	0.005	-0.341	0.733	
LCNWP	-0.010	0.021	-0.452	0.651	
Rutting	-0.344	0.137	-2.510	0.012	*
IRI	1.539	0.888	1.733	0.084	.
ADC	-0.010	0.003	-3.181	0.002	**
ADF	-0.002	0.037	-0.063	0.949	
1 thin overlay	9.105	6.020	1.513	0.131	
2 Slurry seal	13.393	6.143	2.180	0.030	*
3 cracking seal	7.543	6.063	1.244	0.214	
4 control section	8.201	6.231	1.316	0.189	
5 chip seal	8.696	6.064	1.434	0.152	
			R-Squared		0.540
			Adj. R-Squared		0.516
			P-value		0.000

Significant level=0.1, * Significant level=0.05, ** Significant level=0.01, ***Significant level=0.001

To select an appropriate model type for friction prediction model development, F-test, LM test, and Hausman test are performed and the results are shown in Table 4.6. Since p-value of F-Test is approximately 0, which is much smaller than 0.05, the null hypothesis is rejected at 95% confidence level, indicating that not all of the fixed effect intercepts are zeros. As a result, fixed effect panel model should be preferred as compared to the OLS model. For the LM test, the p-value is approximately 0, and thus the null hypothesis is rejected, indicating that there are significant random effects in the panel data, and thus random effects model is preferred over the OLS model to handle heterogeneity within the panel data. Finally, in favor of selecting the fixed-effects rather than the random-effects model is the Hausman test presented in Table 4.6. The p-value of Hausman Test is 0.0006 and the null hypothesis is rejected at 95% confidence level,

indicating that random-effects model is inconsistent and fixed-effects model should be selected as the best fit for the final model development.

Table 4.6. Comparisons of Test Results

Test	F/H Value	df	P-value	Null hypothesis
F-Test	2.7323	248/220	0.0000	Rejected
LM-Test	173410	1	0.0000	Rejected
Hausman Test	39.391	15	0.0006	Rejected

Comparted with cross-sectional or time-series data, panel data raise new specification issues that need to be considered during analysis. The most important of these is cross-sectional bias, which should be the central focus of panel data analysis (Washington et al. 2011, Greene 2012). Statistically, fixed-effects model always provides consistent results but may not be the most efficient solution. On the other hand, random-effects model is generally more efficient (such as better P-values and higher adjusted R-squared value), but may not be consistent. The Hausman Specification Test is one of the most widely used methodologies to determine whether endogeneity bias exists in this model, and select whether the fixed or random effects model should be used. The research question is whether there is significant correlation between the unobserved unit-specific random effects and the regressors. If there is no such correlation, then the random effects model may be more powerful and parsimonious. If there is such a correlation, the random effects model would be inconsistently estimated and the fixed effects model would be the model of choice. In this case study, based on Hausman test results, the random-effects model is inconsistent, and thus the fixed-effect model is selected, which is consistent but not as efficient comparing to the random-effects model. As a result, even though the R-squared value for the random model is higher, fixed-effect model is used due to its consistency which is more important for panel data models. In addition, R-squared value is generally a suitable measure for

prediction, while the major purpose herein is to identify the significant effect of dependent variables.

Fixed-effect panel regression models involve subtracting group means from the regressors. In other words, only time-varying regressors are included in the model. Since IF does not vary with time, the subtraction of the group mean from this variable will result in zero values, and therefore it is excluded from fixed-effect model. As shown in Table 4.4, for fixed-effects model, the significant effect factors include: climate conditions (precipitation, freezing index, and humidity), traffic (AADTT), pavement age, and area of fatigue cracking. As abovementioned, the fixed-effects model is selected based on the Hausman test. Fixed-effects models are designed to study the causes of changes within an entity, while OLS to study the causes of the entirety without time series effects considered. In this case study, both cross-sectional and time-series attributes of the data sets from various PM treatments are considered in the fixed-effects model, the significant variables of fixed- effects model may not be in line with the OLS method.

The impact of one unit change of the significant influencing factors on friction measurement is provided in Table 4.7 and the trend charts of friction to the most significant variables are shown in Figure 4.3 using least square dummy variable model (LSDV), which is the most widely used approach to revealing fixed-effects of the variables. It is observed that the friction is not highly sensitive to the five variables. Other factors, such as the aggregate properties which may have significant impacts on surface friction, are not considered in this paper due to the availability of the data sets in the LTPP database. However, these five charts could clearly demonstrate the trend and relative sensitivity of each variable used in the study. In addition, despite of the data limitations, one important purpose of this case study is to prove the feasibility and capability of PDA methodology for analyzing pavement surface friction data with cross-sectional and time-series characteristics.

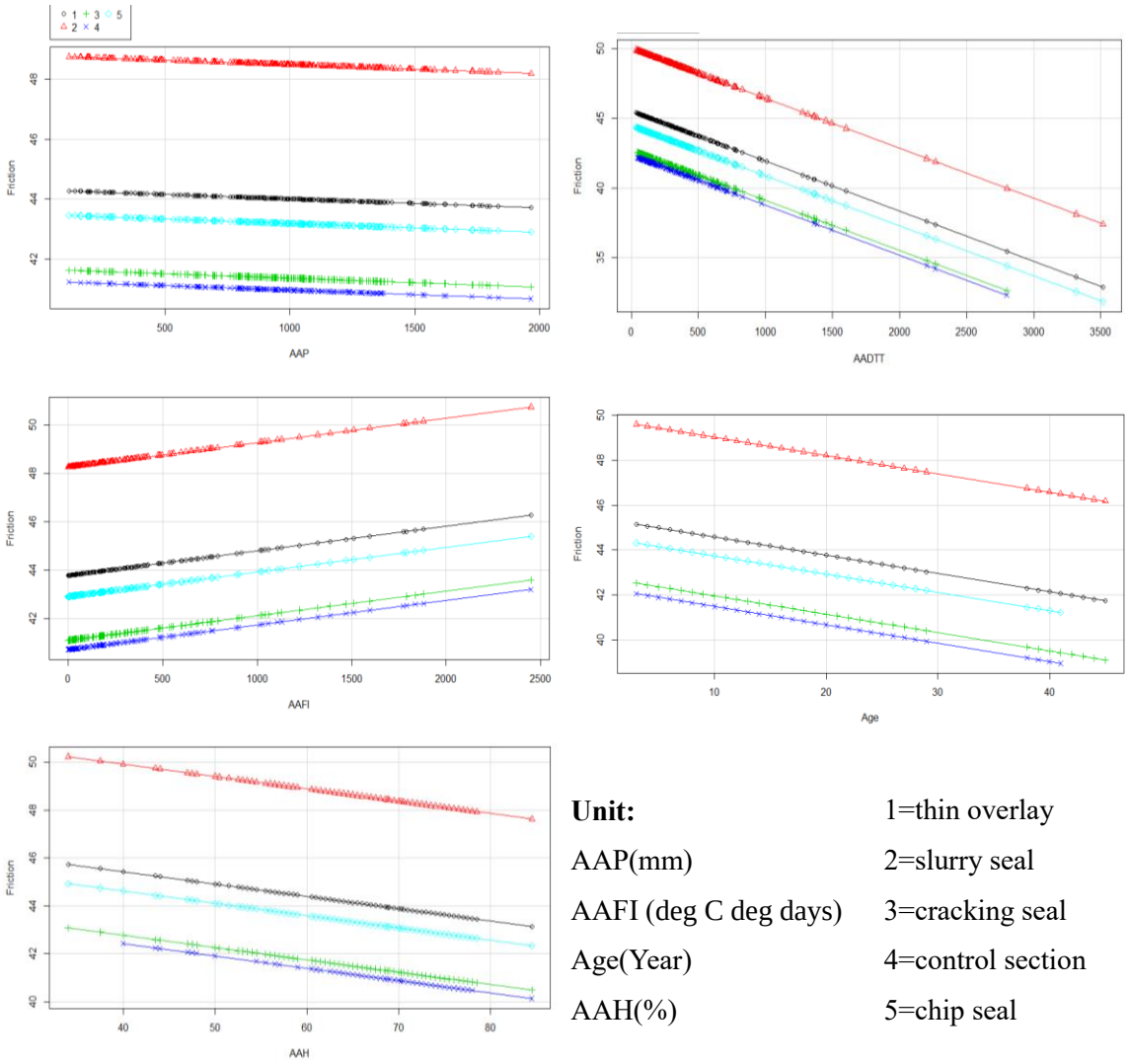

Figure 4.3. Trend Charts of Friction to Significant Influencing Variables

Table 4.7. Sensitivity of Friction to Significant Influencing Factors under Four Treatments

Variable	Coefficient	Intercept				
		Thin overlay	Slurry seal	Cracking seal	Control section	Chip seal
AAP	-0.0003	44.3109	48.7821	41.6692	41.2721	43.4938
AAFI	0.0010	43.7700	48.2500	41.0900	40.7000	42.9000
AAH	-0.0515	47.4923	51.9743	44.8372	44.4903	46.6824
AADTT	-0.004	45.511	50.007	42.701	42.348	44.464
Age	-0.082	45.401	49.851	42.770	42.292	44.562
Fatigue	-0.003	43.898	48.365	41.329	41.153	43.173

Even though different factors impact friction at various levels, the intercepts for each individual variable for the four preventive treatments shows consistent ranking with high to low sequence:

slurry seal > thin overlay > chip seal > cracking seal > control section. Therefore, all the four preservation treatments result in improvements of pavement skid resistance as compared to the control section without any treatment. Slurry seal is the most effective treatment, followed by thin overlay and chip seal. Cracking seal outperforms control section on skid resistance, but the friction improvement is minor.

Table 4.8. Fixed-Effects Model Statistics with the Most Significant Variables

Friction Prediction Model development					
Variable	Estimate	Std. Error	t-value	Pr(>|t|)	Sig. level
AAP	0.003	0.001	2.260	0.024	*
AAFI	0.002	0.001	2.814	0.005	**
AAH	-0.139	0.056	-2.501	0.013	*
AADTT	-0.003	0.001	-5.123	0.000	***
Age	-0.119	0.042	-2.842	0.005	**
1 thin overlay	53.250	2.970	17.928	0.000	***
2 Slurry seal	57.478	2.973	19.333	0.000	***
3 cracking seal	50.677	2.961	17.115	0.000	***
4 control section	50.178	3.036	16.525	0.000	***
5 chip seal	52.476	2.947	17.809	0.000	***
			R-Squared		0.941
			Adj. R-Squared		0.940
			P-value		0.000

Significant level=0.1, * Significant level=0.05, ** Significant level=0.01, ***Significant level=0.001

Subsequently, fixed effects panel model considering only the five most significant influencing factors is developed and the results are shown in Table 4.8. All the five factors remain to be significant for the prediction of friction. The R-squared values of the fixed-effects model is 0.94, indicating that the PDA model could explain most of the variability of the response data around its mean and the model fits the data well.

4.3 Field Data Collection for PM Treatment Sites in Oklahoma

4.3.1 Data Collection Sites

As shown in Figure 4.4, forty-five (45) PM treatment sites have been selected as the testing bed for field data collection, including:

- Six common types of PM treatments in Oklahoma: chip seal, micro-surface, thin overlay (resurface), ultra-thin bounded wearing course (UTBWC, or Nova Chip), High Friction Surface Treatment (HFST), Warm Mix Asphalt (WMA) thin overlay;
- Seven typical aggregates in Oklahoma: granite, limestone, dolomite, rhyolite, sandstone, bauxite, and mine chat;
- Installation ages: average 3.6 years, minimum 0.52 years, and maximum 6.10 years;
- Highway classes: 6 on interstates, 24 State Highways, 12 US Highways, 3 City Streets.

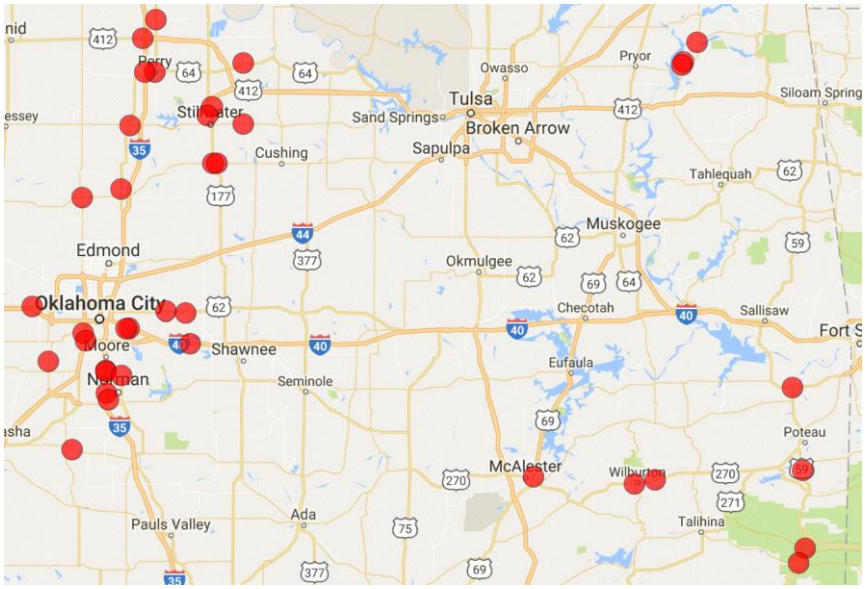

Figure 4.4. Data Collection Sites Map

Seven data collection efforts were made for the HFST sites and the WMA overlay sites, while four collection events were conducted for the other testing sites from 2015 to 2017.

4.3.2 Data Acquisition Systems

The latest 3D laser triangulation based imaging system (Figure 4.5a for the data vehicle and Figure 4.5b for laser triangulation principle) engineered by the research team was used to conduct full lane data collection on roadways at highway speed at 1mm resolution (Wang, 2011). Both 3D

laser imaging intensity and range data from pavement surfaces are acquired through the two sets of sensors. Furthermore, two 3D high resolution digital accelerometers integrated in the system are capable of reporting compensated pavement longitudinal profiles for International Roughness Index (IRI) calculation. The collected data are saved by image frames whose dimensions are 2,048 mm in length and 4,096 mm in width. An example data frame is shown in Figure 4.5c. Distress data are detected and reported for each frame, while IRI and rutting data are reported at an interval of 25 feet. In addition, the AMES 8300 Survey Pro High Speed Profiler, which is introduced in chapter 3, is embedded into data vehicle to collect macro-texture data with 0.5 mm profile wavelength and 0.045mm resolution in vertical direction. Mean profile depth (MPD) is calculated at 3.28 feet interval.

(a) Data Vehicle

(b) PaveVision3D Ultra

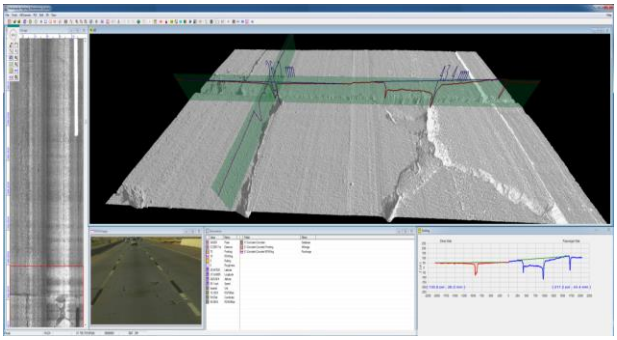

(c) Example Image Frame

Figure 4.5. Data Collection Vehicle

Grip Tester is used to continuously measure the longitudinal friction along the pavement wheel path. The friction data are recorded at 3.28-feet intervals at the speed of 40 mph (64 km/h) using a constant water film thickness of 0.25mm.

4.3.3 Preliminary Analysis Results

Preliminary analysis was conducted on the data sets from the HFST sites to investigate the potential influencing factors of pavement friction. There are six HFST sites in Oklahoma, including two on Interstate 40 (I-40) (eastbound), one on Interstate 44 (I-44) (westbound), and three on State Highway 20 (SH-20) (both directions). Seven data collection efforts were made on HFST sites from November 2015 to December 2017 at approximately every three months. Figure 4.6 (a) shows the development of pavement skid resistance over time. Decreasing tendency of pavement friction is clearly observed for all the HFST sites due to traffic polishing (Figure 4.6b). The average friction values of the six HFST sites from the seven collection events are 0.97, 0.89, 0.79, 0.73, 0.78, 0.69 and 0.61 with an average deterioration rate of 5.46%. Friction numbers on the HFST sites with bauxite aggregates have decreased by 4.49% in rural areas (SH-20 sites 2 & 3) and 6.56% in metropolitan areas with higher traffic volumes (I-40 and I-44 sites). By contrast, the friction numbers on SH-20 Site 1 with mine chat aggregates have decreased by 8.45%, which shares the same traffic and environmental conditions as those for SH-20 sites 2 and 3.

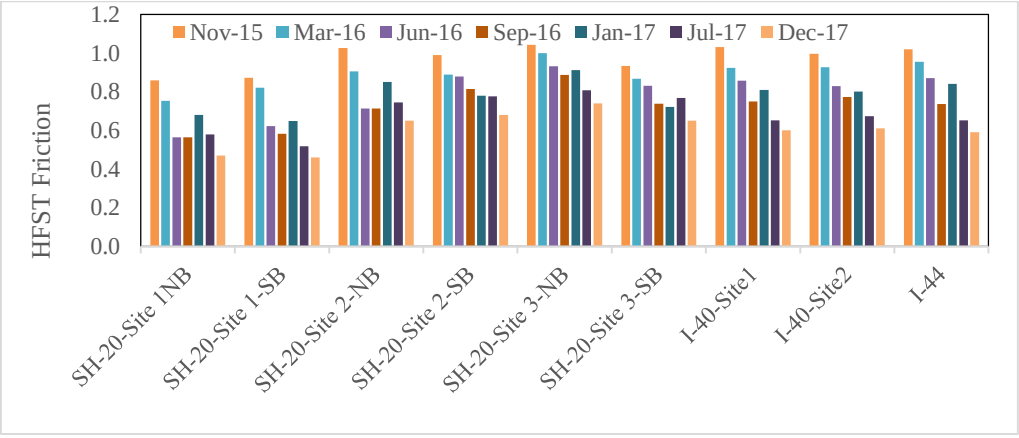

(a) Comparison of HFST Average Friction Number

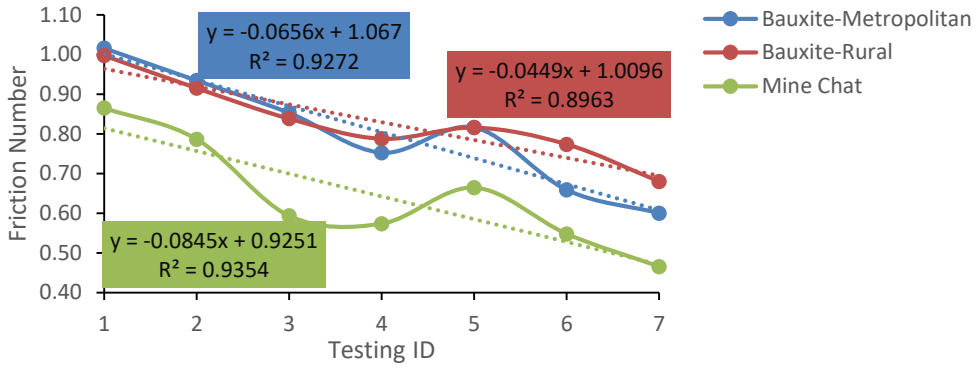

(b) Preliminary Friction Deterioration Model for HFST

Figure 4.6. Preliminary Data Analysis for HFST

Boxplots are provided in Figure 4.7 to compare the friction performance of different PM treatments and different types of aggregate. HFST exhibits the best friction performance over the testing period, which has also been demonstrated in several past studies (Moravec 2013, Bledsoe 2015, Li et al. 2016). Chip seal sites demonstrate a wide variation of friction numbers as compared to other PM treatments, ranging from the lowest friction number of less than 0.2 to highest friction number of more than 0.7. Three of the chip seal testing sites are located on SH-39 built in September 2012 using limestone, while the other two sites on SH-1 and US-259 in southeast Oklahoma built on March 2012 and September 2014, respectively, using limestone but from a different source. The testing sites with the other four treatments show comparable friction numbers.

For aggregates, HFST sites using bauxite and mine chat maintained the highest friction values over the testing period. Testing sites with sandstone as the coarse aggregates produced lower friction numbers than the bauxite and mine chat sections, but better friction numbers than the four other aggregate sources. This result is consistent with several previous studies (Mitchell et al. 2007, Moaveni et al. 2014). Moreover, it is found that the testing sites with limestone show the highest variation of friction measurements. Limestone is one of the most widely used aggregate type for pavement construction in the US due to its availability and high quality of initial

properties (Csathy et al. 1968). However, limestone is generally more prone to polishing under traffic, resulting in poorer long-term skid performance (Smith et al. 2009, Neaylon 2009, Fowler and Rached 2012). Therefore, the friction performance varies considerably among sites with various treatment ages.

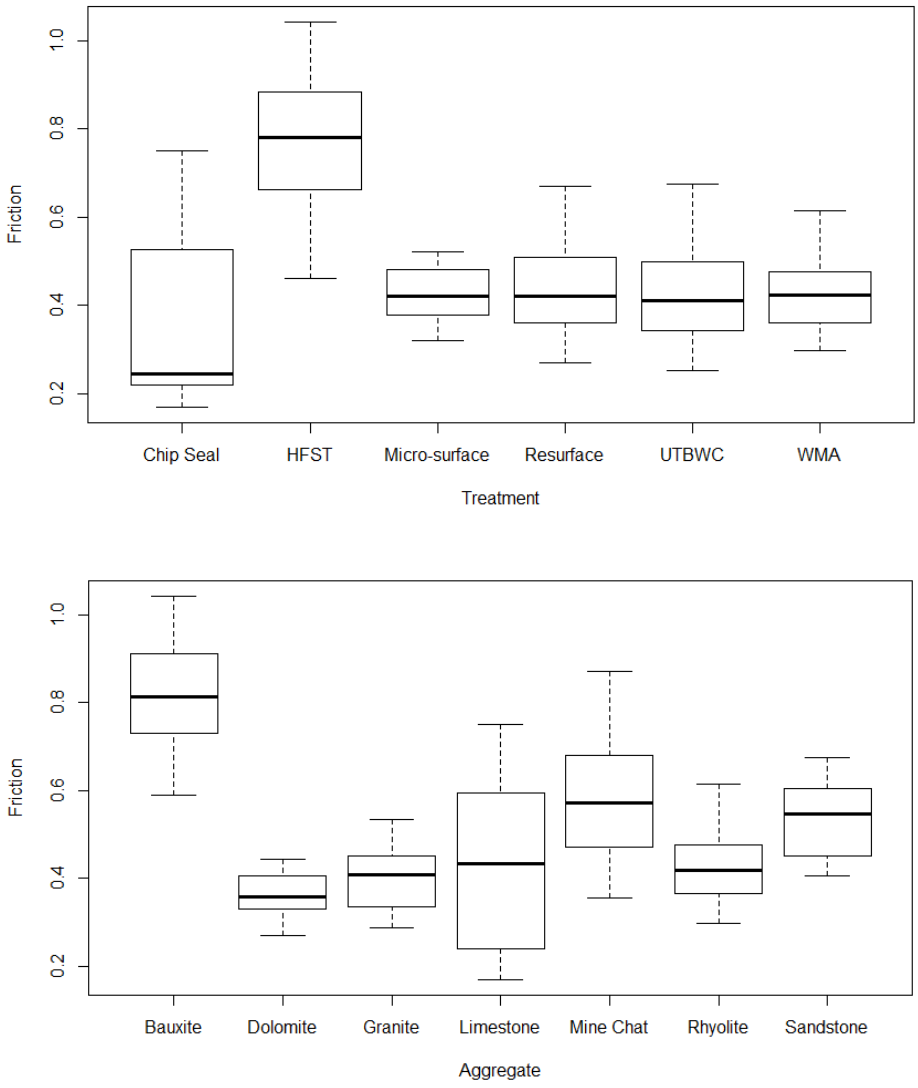

Figure 4.7. Boxplot of Friction for Various Treatments and Aggregates

Figure 4.8 shows the scatterplots of friction numbers by different treatment and aggregate types during the data collection period. Other than sites with HFST and WMA overlay treatments, no clear decreasing trend of surface friction is observed for other PM treatment sites, primarily

because of the short term monitoring and the possible influence of temperature variations. The ambient temperature during data collection in January and December is around 50 ℉, which is much lower than that in July and September with an average temperature of 90 ℉. The friction number tends to increase with decreased ambient or pavement temperature (Luo 2003; Fuents 2009; Jahromi et al. 2011).

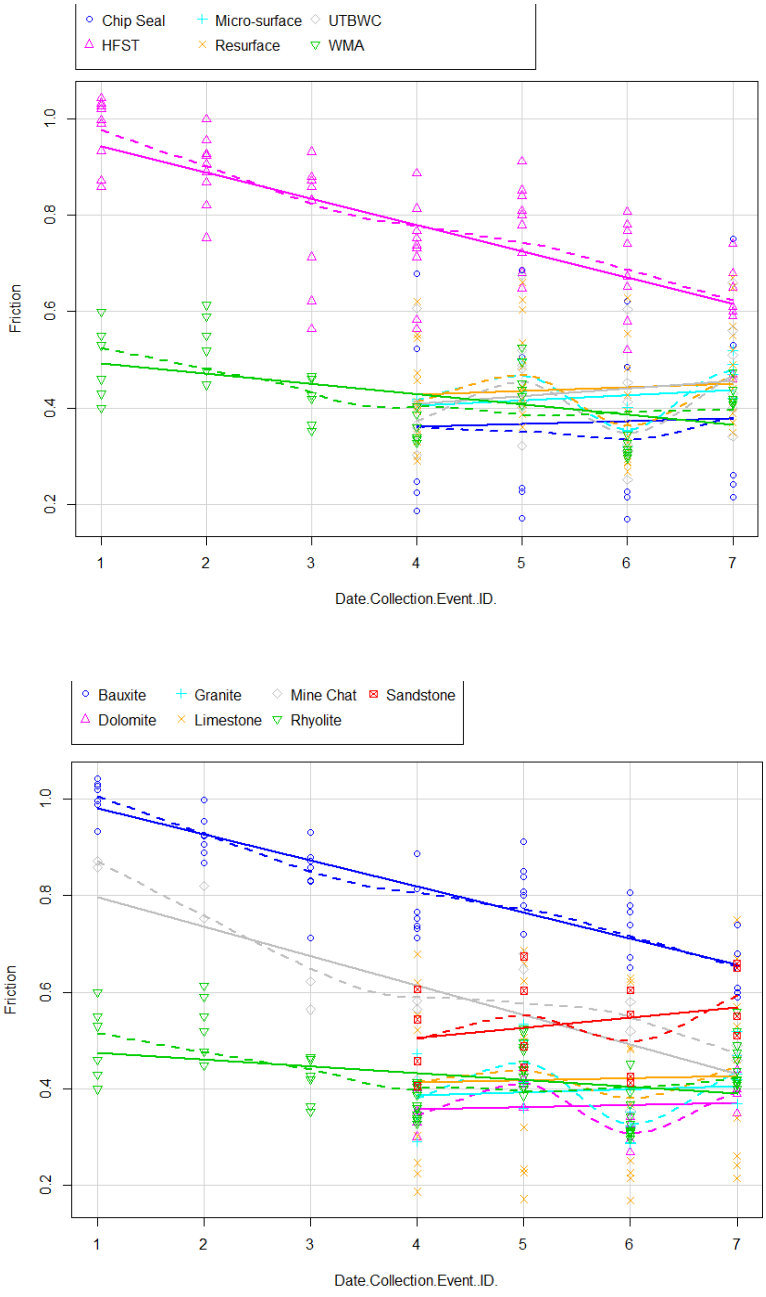

Figure 4.8. Friction Scatterplot Results

The preliminary data analysis results demonstrate that both cross-sectional characteristics (various PM treatments under different temperature, traffic levels, and pavement conditions) and time-series characteristics (multiple times of observations) could affect pavement friction performance. Again, it is found that the friction data sets contain significant variations, or heterogeneity, across groups and over time, and high degrees of freedom (DOF). Therefore, PDA should be used for friction data analysis.

4.4 Laboratory Aggregate Characterization

It is well documented in past studies (Bloem 1971, Mahmoud 2005) that the properties of aggregates in asphalt mixtures have distinct influences on pavement performance including surface friction. Angular and rough-surfaced aggregates are normally recommended in asphalt mixture design for better skid resistance. In this paper, aggregates' resistance to abrasion and polishing are measured according to the Micro-Deval test and the Aggregate Imaging System (AIMS). The aggregates are subjected to breakage, abrasion and polishing processes during the Micro-Deval test, as described in the ASTM D6928 "Standard Test Method for Resistance of Coarse Aggregate to Degradation by Abrasion in the Micro-Deval Apparatus" and ASTM D7428 "Standard Test Method for Resistance of Fine Aggregate to Degradation by Abrasion in the Micro-Deval Apparatus". The aggregate materials used in this study are selected from a wide range of mineralogical properties and sampled from quarries in various geographical regions in the state of Oklahoma. Eleven sources of aggregates: dolomite, rhyolite, sandstone, bauxite, mine chat, granite from two sources and limestone from four sources, are identified for all the 45 field testing sites. The lab testing of aggregate properties consisted of the following three processes:

- Measuring the original aggregate properties (before the Micro-Deval process) using AIMS;
- Polishing and abrading aggregates following the Micro-Deval process;

- Measuring the degraded aggregate properties, after the Micro-Deval process, using AIMS.

4.4.1 Micro-Deval Test

Micro-Deval (MD) tests (Figure 4.9) are conducted on three replicates of each aggregate source. MD testing provides insight about the polishing and abrasion resistance, as well as the durability of coarse aggregates by evaluating the percentage of aggregate weight loss subsequent to rotation in a jar with an abrasion charge (steel balls). A lower percentage of weight loss indicates that aggregate is more durable and resistant to polishing and abrasion. In this study, sandstone presents the most percentage of weight loss, while mine chat used on one HFST site has the least aggregate loss. Specifications generally limit loss to less than 25%, while literature shows good friction performance correlating with losses of less than 15%.

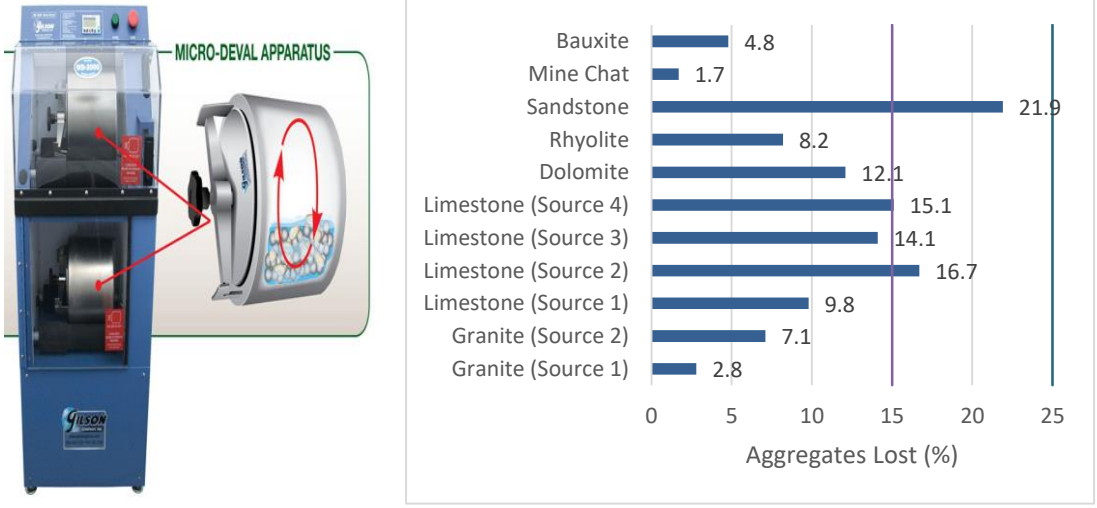

(a) MD Appearance (b) MD Testing Results

Figure 4.9. Micro-Deval Testing

4.4.2 Aggregate Imaging System (AIMS)

As shown in Figure 4.10 (a), the AIMS system consists of a computer-automated system unit, which utilizes a closed-loop DC servo control unit of the x, y, and z axles for precise positioning and highly repeatable focusing. Two separate lighting schemes and a camera are equipped to

capture three-dimensions of aggregates at varying resolutions, upon which aggregate characteristics can be measured (Masad 2005). The software component of AIMS includes an image processing algorithm that can compute the angularity, surface texture, as well as the sphericity of aggregate particles. AIMS data is used to evaluate an aggregate's ability to maintain a PM treatment's frictional properties (Gudimettla et al. 2006). Angularity and surface texture are directly related to the MD degradation and polishing process. Sphericity is included as an additional characteristic to evaluate the aggregates' resistance to breakage.

Angularity is an indicator of the level of sharpness of the aggregate particle corners, which can be measured based on the gradient image processing technique. The average change in the inclination of the gradient vectors is adopted as the indicator for angularity. As shown in Figure 4.10 (b), aggregates below the equality line present loss of angularity due to the aggressive MD abrasion and degradation processes. However, granite, rhyolite, mine chat, and bauxite show good resistance to abrasion with respect to angularity, since they are close to the equality line.

Surface texture describes the surface roughness of aggregate particles and is defined as the average and variation of the pixel levels within an image using the wavelet technique. Figure 4.10 (c) presents the scatter plot of surface texture before and after the MD test. All the aggregates presented loss of surface texture property due to the aggressive MD polishing processes. The results suggest that the granite from source 2 tends to be less resistant to polishing, due to the significant loss of surface texture. The sandstone and mine chat presented a lower loss of surface texture as compared to the other aggregates.

Sphericity describes the three-dimensional form of an aggregate particle, ranging from 0 to 1. A 1.0 sphericity represents a cubic-shaped particle. Since most aggregates lost their angularity after the Micro-Deval test, they lost their sharp edges. Figure 4.10 (d) shows that the change in sphericity varies greatly among different types of aggregates and quarries.

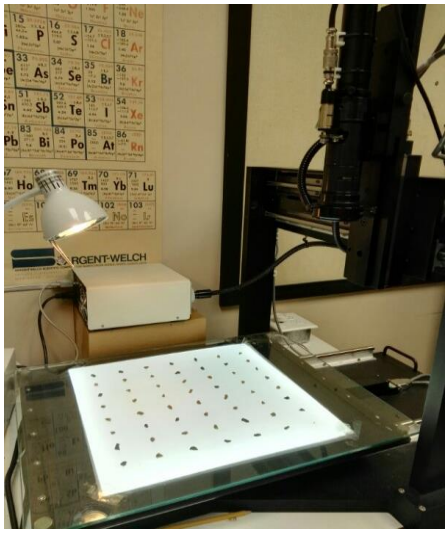

(a) AIMS Appearance

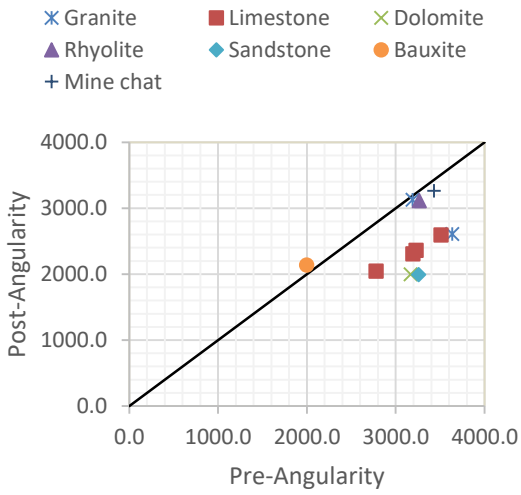

(b) Angularity

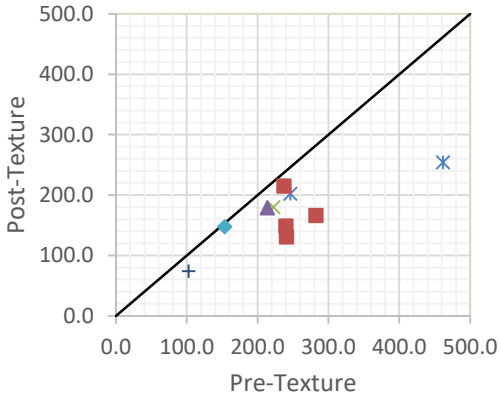

(c) Surface Texture

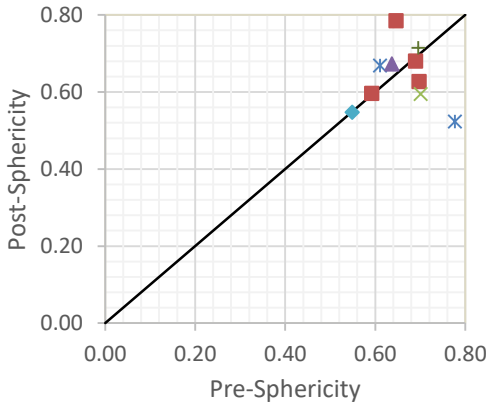

(d) Sphericity

Figure 4.10. Scatter Chart of AIMS Measurement Results before and after MD Test

4.5 Friction Panel Model Development

4.5.1 Candidate Variables

Based on preliminary case study for LTPP SPS-3 data, temperature, traffic volume, pavement age, pavement surface characteristics, and aggregate characteristics are considered as the potential influencing factors for friction model development for PM treatment sites in Oklahoma. The temperature data are recorded during the field data collection events. Traffic characteristics include Annual Average Daily Traffic (AADT) and total traffic volume, which are acquired from the Oklahoma Department of Transportation (ODOT) SAFE-T database. Pavement ages since the

PM treatments were applied are obtained from the ODOT's SiteManager database. Pavement surface condition data are acquired using the PaveVision3D laser imaging system (Wang 2014), which are subsequently analyzed in terms of mean profile depth (MPD) for macrotexture, IRI for longitudinal roughness and rutting for transverse profiling. Aggregate characteristics in terms of angularity, surface texture and sphericity are measured using the Aggregate Imaging Measurement System (AIMS) before and after the Micro-Deval (MD) testing. Cadidate variables are presented in Table 4.9.

Table 4.9. Candidate Variables for PM Treatment Sites in Oklahoma

Category	Variable		Description
Dependent variable	Skid Resistance	FN	Pavement friction
Independent variables	PM Treatment	Treatment	Chip seal, Micro-surface, Resurface, UTBWC, HFST, WMA overlay
	Climate	Temperature	Air Temperature
	Traffic	AADT	Annual Average Daily Traffic
		Total Traffic Volume	Accumulative Traffic volume (AADT * Age)
	Pavement Age	Age	Since PM treatment applied date
	Pavement surface characteristics	MPD	Mean Profile Depth
		IRI	International Roughness Index
		Rutting	Rutting depth in wheelpath
	Aggregate characteristics	NMAS	Nominal Maximum Aggregate Size
		MD	Micro Deval Loss % (avg)
		Angularity	Aggregate initial Angularity
		Texture	Aggregate initial Surface Texture
		Sphericity	Aggregate initial shape
		Loss of angularity	Change of Angularity due to MD Polishing
		Loss of texture	Change of Surface Texture due to MD Polishing
		Loss of sphericity	Change of Sphericity due to MD Polishing

4.5.2 Panel Data Modeling Process

Traditional ordinary least squares (OLS) regression model is developed to model pavement friction data, whose statistical analysis results are shown in Table 4.10. Subsequently, parameter estimates and the corresponding t-statistics for the FE and RE models are shown in Table 4.11 and Table 4.12, respectively.

Table 4.10. Coefficient Estimates and t-Statistics for OLS Model

Variable	Estimate	Std. Error	t-value	Pr(>|t|)	Sig. level
(Intercept)	3.3700	0.7788	4.327	2.73e-05	***
HFST	-0.0746	0.0810	-0.921	0.3585	
Micro-surface	0.0013	0.0507	0.025	0.9799	
Resurface	-0.0402	0.0435	-0.924	0.3568	
UTBWC	-0.0317	0.0504	-0.628	0.5309	
WMA Overlay	-0.0888	0.0521	-1.703	0.0907	.
AADT	-4.2e-06	2.9e-06	-1.452	0.1487	
Total Traffic Volume	1.7e-07	9.3e-07	0.179	0.8585	
Age	-0.0170	0.0059	-2.868	0.0047	**
Temperature	-0.0030	0.0003	-8.707	0.0000	***
MPD	-0.6327	0.5661	-1.118	0.2655	
IRI	-0.0003	0.0002	-1.698	0.0916	.
Rutting	-0.0396	0.0971	-0.408	0.6838	
MD	-0.0087	0.0030	-2.946	0.0037	**
NMAS	-0.0426	0.0109	-3.921	0.0001	***
Texture	-0.0002	0.0002	-0.879	0.3809	
Angularity	-0.0004	0.0001	-6.231	0.0000	***
Sphericity	-0.6791	0.8650	-0.785	0.4336	
Loss of texture	0.0052	0.0014	3.677	0.0003	***
Loss of angularity	-0.0037	0.0021	-1.788	0.0757	.
Loss of sphericity	0.0094	0.0034	2.746	0.0068	**
			R-Squared		0.7805
			Adj. R-Squared		0.7541
			P-value		< 2.2e-16

. Significant level=0.1, * Significant level=0.05, ** Significant level=0.01, ***Significant level=0.001

Table 4.11. Coefficient Estimates and t-Statistics for Fixed-Effects Model

Variable	Estimate	Std. Error	t-value	Pr(>|t|)	Sig. level
Total Traffic Volume	4.7e-06	0.0000	2.8517	0.005	**
Age	-0.0516	0.0090	-5.7498	6.22E-08	***
Temperature	-0.0032	0.0003	-12.3071	< 2.2e-16	***
MPD	-0.1467	0.5800	-0.253	0.8007	
IRI	-0.0003	0.0001	-1.7952	0.0750	.
Rutting	0.0675	0.0824	0.8196	0.4140	
			R-Squared		0.6091
			Adj. R-Squared		0.4778
			P-value		< 2.2e-16

. Significant level=0.1, * Significant level=0.05, ** Significant level=0.01, ***Significant level=0.001

Table 4.12. Coefficient Estimates and t-Statistics for Random-Effects Model

Variable	Estimate	Std. Error	t-value	Pr(>|t|)	Sig. level
(Intercept)	2.8859	1.2638	2.284	0.024	*
HFST	-0.2277	0.1361	-1.674	0.096	.
Micro-surface	0.0418	0.0924	0.453	0.651	
Resurface	-0.0053	0.0762	-0.070	0.944	
UTBWC	-0.0094	0.0849	-0.111	0.912	
WMA Overlay	-0.0838	0.0889	-0.943	0.347	
AADT	-1.05e-05	4.47e-06	-2.356	0.020	*
Total Traffic Volume	2.21e-06	1.25e-06	1.773	0.078	.
Age	-0.0353	0.0073	-4.807	0.000	***
Temperature	-0.0031	0.0003	-11.906	< 2.2e-16	***
MPD	-0.1690	0.5539	-0.305	0.761	
IRI	-0.0003	0.0001	-1.886	0.061	.
Rutting	0.0187	0.0809	0.231	0.818	
MD	-0.0135	0.0053	-2.555	0.012	*
NMAS	-0.0380	0.0176	-2.163	0.032	*
Texture	-0.0005	0.0003	-1.615	0.108	
Angularity	-0.0005	0.0001	-3.598	0.000	***
Sphericity	0.3405	1.3287	0.256	0.798	
Loss of texture	0.0038	0.0023	1.603	0.111	
Loss of angularity	-0.0022	0.0034	-0.642	0.522	
Loss of sphericity	0.0135	0.0054	2.475	0.014	*
			R-Squared		0.6566
			Adj. R-Squared		0.6111
			P-value		< 2.2e-16

. Significant level=0.1, * Significant level=0.05, ** Significant level=0.01, ***Significant level=0.001

With three friction prediction models developed, the next step is to select the most appropriate model. The selection process is closely related to the characteristics of the friction and corresponding data under investigation. The flow chart for the model selection is illustrated in Figure 4.1. The testing results is shown in Table 4.13.

As shown in Table 4.13, since the p-value of F-Test is much smaller than 0.05, the null hypothesis should be rejected at 95% confidence level, indicating that the fixed-effects are non-zero. As a result, FE model should be selected instead of the OLS model.

The p-value of LM test is much smaller than 0.05, and the null hypothesis is rejected at 95% confidence level, indicating significant random-effects exist in the panel data. Therefore, RE model can better handle the heterogeneity in the panel data than the OLS model.

Finally, the Hausman test results are shown in Table 4.13. Because the p-value is 0.062, the null hypothesis should be accepted at 95% confidence level, indicating that RE model should be selected according to the Hausman test because of its efficiency.

Table 4.13. Comparisons of Test Results

Test	F/H Value	df	P-value	Null hypothesis
F-Test	7.2325	23/128	3.85e-14	Rejected
LM-Test	29.856	1	4.65e-8	Rejected
Hausman Test	11.991	6	0.062	Accepted

In addition, the FE model is inappropriate in this case study since the FE model requires the calculation of within-group variation for model estimation (Qi et al. 2007). FE model involves subtracting group means from the regressors, and thus, only time-varying regressors are included in the model. Since the aggregate characteristics and AADT volume are constant for some testing sites and do not vary with time, the effects of these parameters are absorbed by the FE model.

Therefore, RE model should be selected as the best fit for the final model development in this case study.

4.5.3 Final Friction Panel Model

Subsequently, RE panel model considering only the nine most significant influencing factors is developed and the results are shown in Table 4.14. The p-values of roughness (IRI) and Micro Deval Loss (MD) are 0.0668 and 0.0563 individually, which are slightly larger than 0.05, suggesting that they might be variables of interest. The p-value of AADT is 0.1879, however, many past studies indicated that traffic volume could affect the deterioration rate of pavement friction (Cenek 2004, Rezaei et al. 2011, Kotek and Florkova 2014). Therefore, variables with $p < 0.2$ are retained for future study. The R-squared value of the final RE model is 0.63 and the p-value of the final RE model is very close to 0, indicating that the model explains most of the variability of the response data around its mean and the model fits the data well.

As shown in Table 4.14, pavement age (Age), temperature (Temperature), Nominal Maximum Aggregate Size (NMAS), angularity, loss of texture, loss of sphericity are six significant effect factors for friction prediction at 95% confidence level. AADT, Age, Temperature, IRI, MD and NMAS demonstrate negative correlations with friction number, which generally agrees with those from previous studies (Noyce 2005, Anupam 2013, Kassem et al. 2013, Wang and Wang 2013, Susanna et al. 2017). Unexpectedly, angularity also shows negative correlation to friction, which seems to be against engineering wisdom. A study by National Center for Asphalt Technology (NCAT, 2017) also found that “although an aggregate might be initially characterized by a high level of angularity and measure good friction values, it may not be suitable for a pavement surface layer if the aggregate cannot maintain a sufficient level of friction due to polishing under traffic”. Change of texture and sphericity due to MD polishing are positively correlated to friction, which seems to be plausible. Since the loss of texture (sphericity) equal to texture (sphericity) value after MD polishing minus the value before MD test, which is supposed to be

negative. Greater negative value of texture (sphericity) loss means higher texture (sphericity) value after MD polishing, indicating the aggregate is more durable and resistant to polishing and abrasion, resulting in higher friction value.

Table 4.14. Final RE Model

Variable	Estimate	Std. Error	t-value	Pr(>|t|)	Sig. level
(Intercept)	2.4743	0.2395	10.3298	< 2.2e-16	***
AADT	-2.62e-06	0.0000	-1.3225	0.1879	
Age	-0.0161	0.0037	-4.3998	0.0000	***
Temperature	-0.0030	0.0003	-11.5990	< 2.2e-16	***
IRI	-0.0003	0.0001	-1.8452	0.0668	.
MD	-0.0043	0.0022	-1.9222	0.0563	.
NMAS	-0.0401	0.0051	-7.9436	0.0000	***
Angularity	-0.0004	0.0001	-5.4965	0.0000	***
Loss of texture	0.0049	0.0011	4.4739	0.0000	***
Loss of sphericity	0.0113	0.0019	5.8289	0.0000	***
			R-Squared		0.6321
			Adj. R-Squared		0.6116
			P-value		< 2.2e-16

. Significant level=0.1, * Significant level=0.05, ** Significant level=0.01, ***Significant level=0.001

It is worth noting that from this case study, aggregate properties have more significant effects on pavement friction than the type of PM treatment. When both PM treatments and aggregate properties are considered as the influencing factors for the friction prediction model development, PM treatments do not statistically show a significant influence on friction. To demonstrate the impacts of pavement friction, another RE friction prediction model is developed only considering PM treatments and several other external parameters as the influencing factors, while excluding aggregate characteristics from the model. Although MPD, IRI, Rutting, NMAS and MD are considered in the initial model development, they do not show significant influence on friction in this model since the p-value is much greater than 0.05. The refined RE results for this model is shown in Table 4.15. Total traffic volume, pavement age and temperature are also negatively correlated to pavement friction. All the PM treatment types show significant influence on pavement friction except for WMA overlay and chip seal. The intercepts of the model for the PM

treatments shows the following sequence from high to low: HFST > Micro-surface > UTBWC > Resurface > Chip seal > WMA overlay. Such result is consistent to those from several previous studies (Moravec 2013, Ji et al. 2015, Li et al. 2016). The R-squared value of this model is 0.51, which is smaller than the final RE model developed in this study based on aggregate characteristics.

Table 4.15. RE Model with Treatment Types but not Aggregate Characteristics as the Influencing Factors

Variable	Estimate	Std. Error	t-value	Pr(>|t|)	Sig. level
(Intercept)	0.7118	0.0557	12.7684	< 2.2e-16	***
HFST	0.3521	0.0581	6.0614	0.0000	***
Micro-surface	0.2021	0.0708	2.8537	0.0048	**
Resurface	0.1117	0.0535	2.0886	0.0379	*
UTBWC	0.1450	0.0642	2.2586	0.0249	*
WMA overlay	-0.0059	0.0633	-0.0931	0.9259	
Chip seal	0	-	-	-	
Total Traffic Volume	-2.31e-06	0.0000	-3.2463	0.0014	**
Age	-0.0266	0.0064	-4.1755	0.0000	***
Temperature	-0.0031	0.0003	-10.4869	< 2.2e-16	***
			R-Squared		0.5143
			Adj. R-Squared		0.5000
			P-value		< 2.2e-16

. Significant level=0.1, * Significant level=0.05, ** Significant level=0.01, ***Significant level=0.001

Based on the developed coefficients of the final RE model, the predicted and measured frictions for all the seven data collection efforts for the testing sites are plotted in Figure 4.11 with the R-squared value being 0.74. The final RE model developed in this study could clearly demonstrate the trend of friction deterioration and capture the relative sensitivity of each variable, which may assist highway agencies better understanding the friction performance of different PM treatments and aggregates to improve skid resistance performance in the field. In addition, this paper also proves the capability and feasibility of PDA methodology for the analysis of pavement friction data with both cross-sectional and time-series characteristics.

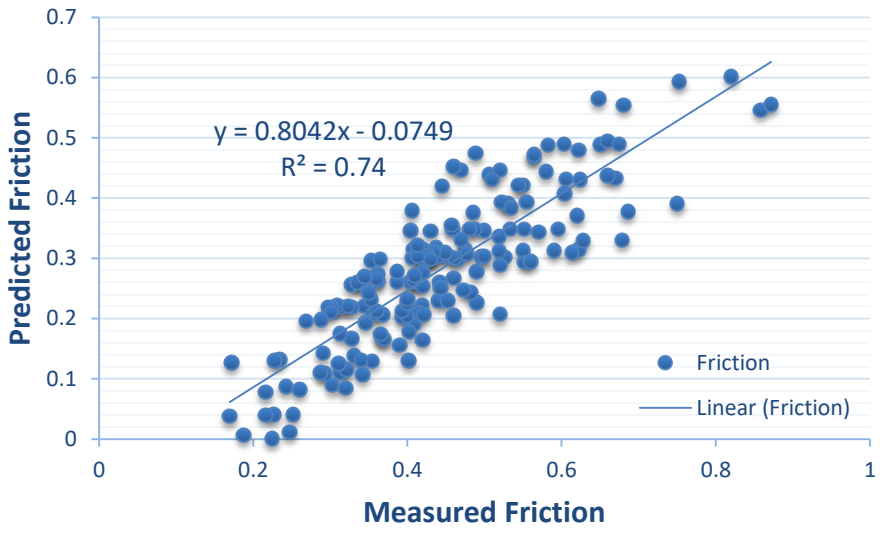

Figure 4.11. Friction Prediction Using the Final RE Model

4.6 Summary

Panel data analysis (PDA), which is able to investigate the differences of cross-sectional information, but also the time-series changes over time, is conducted in this chapter to identify the most significant influencing factors for pavement friction prediction model development. Results from the PDA models are compared to those from traditional ordinary regression models.

In LTPP SPS-3 case study, slurry seal is demonstrated to be the most effective treatment. Five factors (precipitation, freezing index, and humidity, traffic, pavement age) are identified to be significant for pavement friction. Fixed-effects panel model is identified to be the appropriate model.

Then, filed data collection are conducted for Forty-five pavement sites, including six major preventive maintenance (PM) treatments and seven typical types of aggregates in Oklahoma. Multiple field data collection events have been performed from 2015 to 2017. The state-of-the-art 3D laser imaging technology and the Grip Tester, which is a continuous friction measurement equipment (CFME), are used to collect 1-mm 3D pavement surface data and friction data, respectively, at highway speed in the field, while the Aggregate Imaging System (AIMS) is

utilized in the laboratory to analyze the surface characteristics of aggregates. Statistical analyses indicate that random-effects panel model outperforms the fixed-effects and the traditional ordinary least squares regression model for the field data. The final results demonstrate that PM Treatment age, temperature and aggregate characteristics significantly affect pavement friction.

This chapter not only demonstrates the capability of PDA for analyzing friction data with cross-sectional and time-series characteristics, but also can assist decision makers in the selection of PM treatments and aggregates for optimized skid resistance performance.

Chapter 5 DEEP RESIDUAL NETWORK ARCHITECTURE FOR PAVEMENT SKID RESISTANCE PREDICTION

As one of the newest trends in Artificial Intelligence, deep learning (DL) methods have brought revolutionary advances in computer vision and machine learning. Especially in the recent years, state-of-the-art DL techniques have been proposed with great success in various applications, such as ImageNet 2013 winner Zeiler-Fergus (ZF)-Net (Zeiler and Fergus 2014), 2014 winner VGG-Net (Simonyan and Zisserman 2014), 2015 winner ResNet (He et al. 2016). However, such architectures cannot be directly applied to friction prediction.

This work is inspired by a Deep Residual Networks (ResNets) with demonstrated accuracy for ImageNet and challenging recognition tasks (Russakovsky et al. 2015, He et al. 2016, Ledig et al. 2017, Li and Shen 2017). A Friction-ResNets architecture is tailored for friction prediction and validation, whose input are pavement macro-texture feature vectors while output are friction levels ranging from 0.2 to 0.9 measured by Grip Tester. Friction-ResNets has the ability to learn and extract pavement surface macro-textural features and classification boundaries for direct friction evaluation. This network has shown the capability to solve the problem of "degradation", and increase the prediction accuracy by adding eleven convolution layers through an extensive training and validation process using 63651 pairs of texture and friction data sets collected in the field.

5.1 Deep Residual Network (ResNets)

Network depth is very important, and top-ranked teams on ImageNet challenging all exploit "very deep" models. A lot of visual recognition tasks benefited from very deep models (Zeiler and Fergus 2014, Simonyan and Zisserman 2014, He et al. 2015). However, as the example shown in Figure 5.1, a degradation problem always exposes with the deeper networks start converging. This phenomenon means that deeper network depth causes degradation problem, leading to a higher training error. However, the reason for the degradation problem is not overfitting.

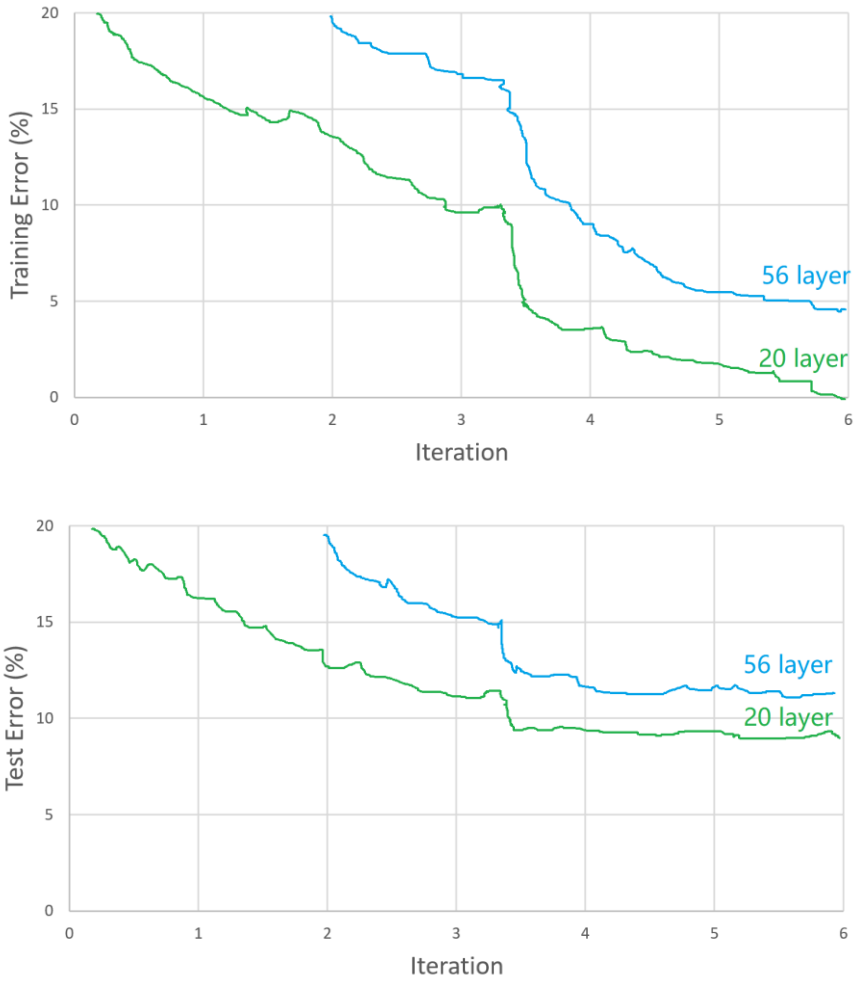

Figure 5.1. Training error (top) and test error (bottom) on CIFAR-10 with 20-layer and 56-layer networks (He et al. 2016)

He et al. (2016) proposed a Deep Residual Networks (ResNets) for image classification. In machine learning, the vanishing gradient problem is a difficulty found in training artificial neural networks with gradient-based learning methods and backpropagation (Bengio et al. 1994, Glorot and Bengio 2010). ResNets have significantly lower gradients and thus can circumvent the exploding gradient problem, enabling the effective training of much deeper networks. By noticing that any neural network is a residual network, ResNets devise the residual trick by introducing skip connections, which simplifies the network mathematically and results in success of prediction (Philipp et al. 2018). Figure 5.2 presents the fundamental concept of ResNets to solve degradation problem by stacking residual unit of the same connecting shape.

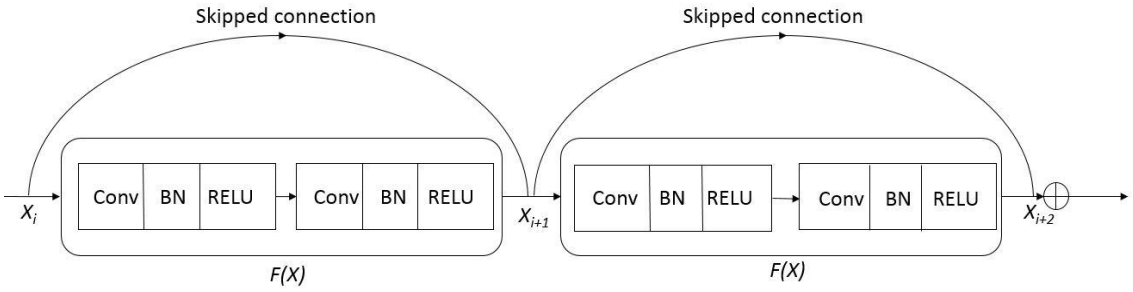

Figure 5.2. Fundamental Concept of ResNets

The residual unit performs the following computation (He et al. 2016):

$$X_{i+1} = X_i + F(X_i, W_i) \tag{5.1}$$

Where X_i is the input feature to the i^{th} residual unit. $W_i = \{W_{i,k} | 1 \leq k \leq K\}$ is a set of weights (and biases) associated with the i^{th} residual unit, and K is the number of layers in a residual unit. Function F denotes the type of residual work in each unit, such as convolutional (Conv) layers, batch norm (BN) layer (Ioffe and Szegedy 2015) and rectified linear unit (RELU) layer. This process can be repeated recursively.

$$X_{i+2} = X_{i+1} + F(X_{i+1}, W_{i+1}) \tag{5.2}$$

$$_{i+2} = X_i + F(X_i, W_i) + F(X_{i+1}, W_{i+1}) \quad (5.3)$$

For any deeper unit *I* and any shallower unit *i*, the equation could be generalized as follows:

$$X_I = X_i + \sum_{k=i}^{I-1} F(X_k, W_k) \quad (5.4)$$

The deeper feature (X_I) of any deeper unit *I* can be expressed as the summation of shallower feature (X_i) of any shallower unit *i* and a residual function ($\sum_{k=i}^{I-1} F$), meaning that the model is in a residual pattern between any units *I* and *i*. ResNets is different from plain convolution neuron networks, where a feature (X_I) is a series of matrix-vector products, resulting in vanishing/exploding problem (He et al. 2016). ResNets solves the degradation problem because Equation 5 also generates optimal backward propagation properties. Assigning the loss function *e*, according to the chain rule of backpropagation (LeCun et al. 1989), the following equation could be produced:

$$\frac{\partial e}{\partial X_i} = \frac{\partial e}{\partial X_I}\frac{\partial X_I}{\partial X_i} = \frac{\partial e}{\partial X_I}\left(1 + \frac{\partial}{\partial X_i}\sum_{k=i}^{I-1} F(X_k, W_k)\right) \quad (5.5)$$

Where, $\frac{\partial e}{\partial X_I}$ propagates information backward directly without any weight layer within a unit, ensuring that the information arrives at any shallower unit *i*, while the term $\frac{\partial e}{\partial X_I}\frac{\partial}{\partial X_i}\sum_{k=i}^{I-1} F$ propagates through the weight layers within a unit. As a result, the gradient of a stage can't vanish, since $\frac{\partial}{\partial X_i}\sum_{k=i}^{I-1} F$ cannot always equal to -1 for all samples in a mini-batch.

In summary, the "convolutional unit" and "skipped connection" helps avoid the "gradient vanishing" problem by enabling information or signal to directly propagate forward or backward from one group to another.

5.2 Data Collection and Preparation

5.2.1 Field Testing Sites

The testing bed of this study includes 49 High Friction Surfacing Treatments (HFST) sites located in 12 states (Figure 5.3 and 5.4) for a three-year research project sponsored by the Federal Highway Administration (FHWA). HFST sites are installed at horizontal curves or high friction demanding sites to reduce fatalities and injuries from crashes. Both pavement surface texture and friction characteristics data are collected simultaneously at highway speed both on HFST and the abutting untreated sections, with multiple pavement surface types such as asphalt pavements (AC), concrete pavements (PCC), grooved AC and PCC pavements and bridge decks.

Figure 5.3. Map of Data Collection Sites

(a) HFST from WV-I77

(b) AC from KY-605

(c) PCC from OK-I44

(d) Grooved AC from MO-I44

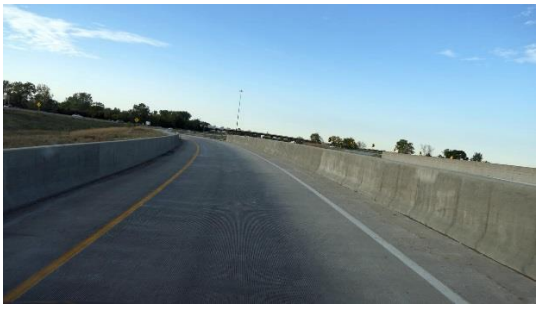

(e) Grooved PCC from IA-I80-Ramp

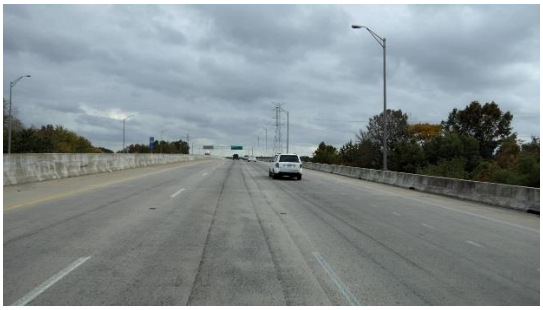

(f) Bridge Deck from TN-SR385

Figure 5.4. Example of Different Types of Pavement Surface

5.2.2 Data Collection Devices

Pavement surface texture data is collected using the AMES 8300 Survey Pro High Speed Profiler that meets the ASTM E950 (2018) Class 1 profiler specification requirements. Pavement friction data is measured by a Grip Tester at an interval of 1-meter (3.28 feet) at 40 mph testing speed with 0.25mm of water film depth. Grip tester and AMES 8300 Survey Pro High Speed Profiler have been introduced in chapter 3.

5.2.3 Data Preparation

Firstly, the acquired surface texture profiles and their corresponding friction numbers are paired by location for every 1-meter (3.28 ft) segment of the testing site. 63,651 pairs of data sets are prepared for training, validation and test in this study. Secondly as shown in Figure 5.5, the 1-dimensional (1D) surface texture data (2,000 points for the 1-meter texture profile) are transformed to 2-dimension (2D) spectrograms (51×48), which are then fed into the various machine learning (ML) models and Friction-ResNets. The transformation of 1D profile into spectrogram has gained success in information retrieval and audio signal processing (Deng et al.

2010, Wulfing and Riedmiller 2012, Dieleman and Schrauwen 2013, Abdel-Hamid et al. 2014, Dieleman and Schrauwen 2014, Huang et al. 2015).

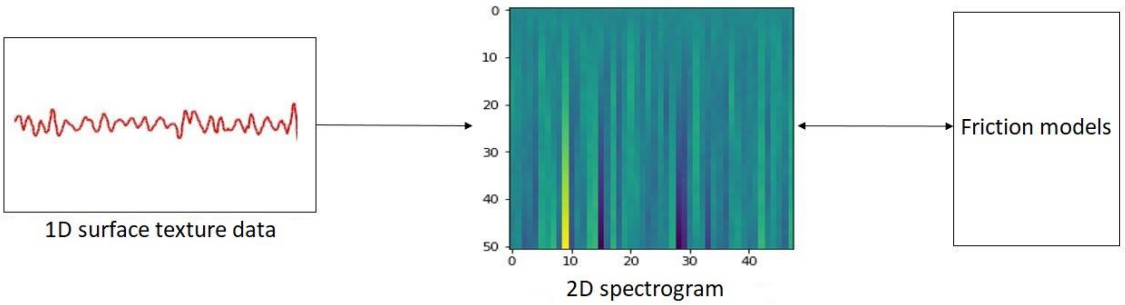

Figure 5.5. Data Preparation

The friction numbers are grouped into eight bins at every 0.1 interval ranging from 0.2 to 1.0 (<0.2, 0.3, 0.4, 0.5, 0.6, 0.7, 0.8, >0.9). 4,200 pairs of surface texture and friction data are randomly selected from each bin of friction level. In total, 33,600 pairs are prepared for the friction prediction model development. 70%, 15%, and 15% of the prepared data sets are then randomly used for each bin for training, validation, and testing, respectively.

5.3 Proposed Friction-ResNets for Friction Prediction

In Friction-ResNets, several convolutional and batch normalization (BN) operations are used together to form a computational unit, also called “convolutional group”. In general, Friction-ResNets is composed of 10 convolutional layers within convolutional groups (2 convolutional layers for each convolutional group) and 1 additional convolution layer. Convolution is the most important and fundamental concept in deep learning. The output for any arbitrary input can be constructed using a convolution operation. One example of convolution is shown in Figure 5.6. It is the process of adding each element of the 2D matrix to its local neighbors, weighted by the 3*3 kernel.

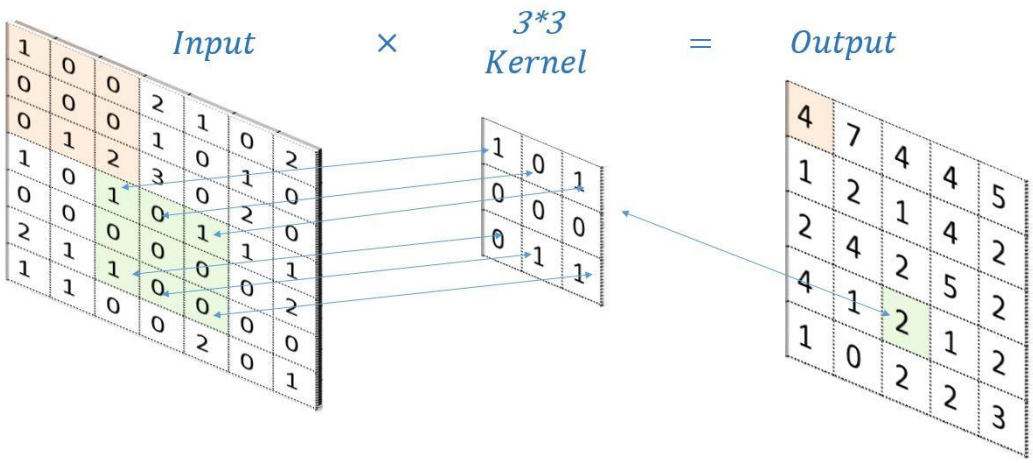

Figure 5.6. One Example of Convolution

Convolutional group is depicted in Figure 5.7. Each convolutional group consists of two primary convolutional layers and each is followed by a BN layer and ReLU activation function (references). BN makes normalization a part of the model architecture and performs the normalization for each training mini-batch. A higher testing accuracy can be achieved by using much higher learning rates and ignoring the initialization (Ioffe and Szegedy 2015). ReLU is the most commonly used activation function in deep learning models, which helps a network account for interaction effects and capture non-linearity's characteristics so as to improve discriminative performance (Nair and Hinton 2010).

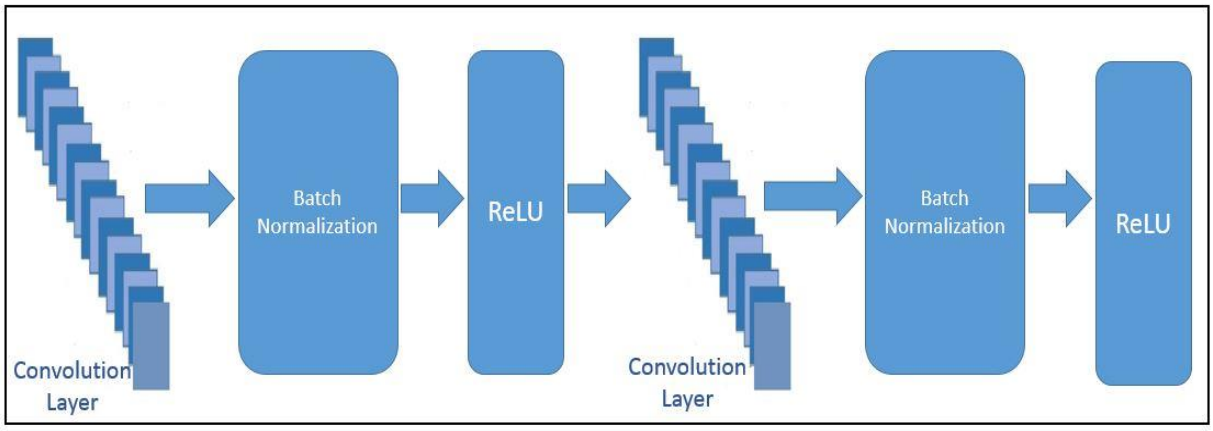

Figure 5.7. Convolutional Group

The overall Friction-ResNets architecture is designed as shown in Figure 5.8 and Table 5.1. In the beginning, the input layer of the proposed network accepts the spectrogram of raw texture profile with the dimension of 51 $\times$ 48. Subsequently, one convolutional layer and a stack of convolutional groups are applied in the network to extract representative and useful features. The output shape keeps the same for the same stage, while reduced to half in the following stage (stage 2 to stage 4). Sixteen 3 by 3 kernels contain in the first convolutional layer. There are 16, 32, 64, and 96 3 by 3 kernels for the convolutional layers from stage 1 to stage 4 respectively. Average pooling operation is used to remove redundant information. Finally, the output layer produces the probability distribution of the predicted 8 friction levels based on numerous types of neurons and Softmax activation function. To reduce the testing error and overcome the overfitting problem, two dropout layers (Krizhevsky et al. 2012 and Srivastava et al. 2014) and average pooling layer with the probability of 0.25 and 0.6 are included after stage 3. In addition, convolutional groups combined with skipped connections are used in this network to avoid any "gradient vanishing" and degradation problems.

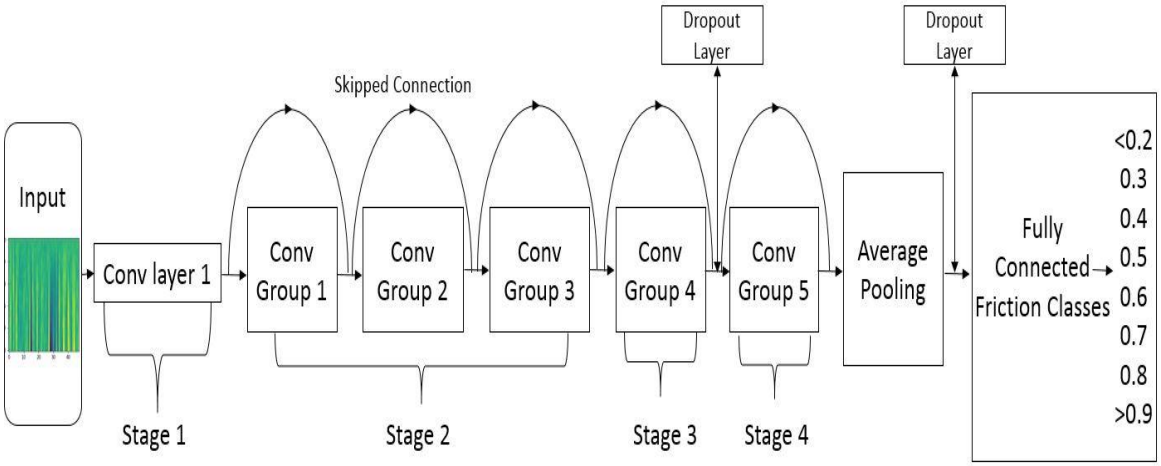

Figure 5.8. Friction- ResNets Overall Architecture

Table 5.1. Architecture for Each Stage of Friction- ResNets

Stage Name	Stage 1	Stage 2	Stage 3	Stage 4	Average pooling
Output Size	51*48	51*48	25*24	12*12	1*1
Number of kernels (3*3)	16	32	64	96	-
Number of Conv Units	1 conv layer	3 conv groups	1 conv group	1 conv group	-

The network is trained using 23,520 pairs of pavement texture spectrogram and their corresponding friction data sets. Pytorch (https://pytorch.org/), a sophisticated python library, is used for the Friction-ResNets development. Employing tensor computation with strong GPU acceleration allows PyTorch to implement the Reverse-mode auto-differentiation technique which changes the way the network behaves arbitrarily without significant overhead or lag.

5.4 Results and Discussions

5.4.1 Learning Curve

23,520 and 5,040 pairs of pavement texture spectrogram and friction data sets are randomly selected for the training and validation of Friction-ResNets. Learning curves, one of the most commonly used evaluation measures for deep learning or machine learning algorithms, are used to evaluate the training and validation process of Friction-ResNets. With a processor of Intel (R) Core (TM) i7-4702HQ CPU @ 2.20 GHz and 0.0005 learning rate, the training process takes 9.2 hours with 8000 iterations (65 epochs) to reach the maximum training and validation accuracy. As shown in Figure 5.9, training loss continue to decrease as the number of iterations increases. The accuracy curve is presented in Figure 5.10, it can be seen that the training and validation

accuracy continuously improved as the number of training epochs increases. The accuracy of training data achieves at 99.85% while 91.95% for validation data, and no "underfitting" or "overfitting" phenomenon is overserved during the training process.

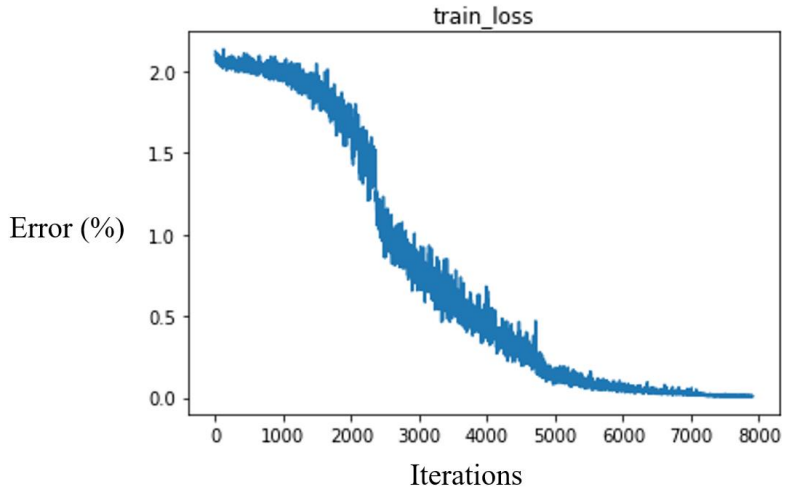

Figure 5.9. Train Loss Summary

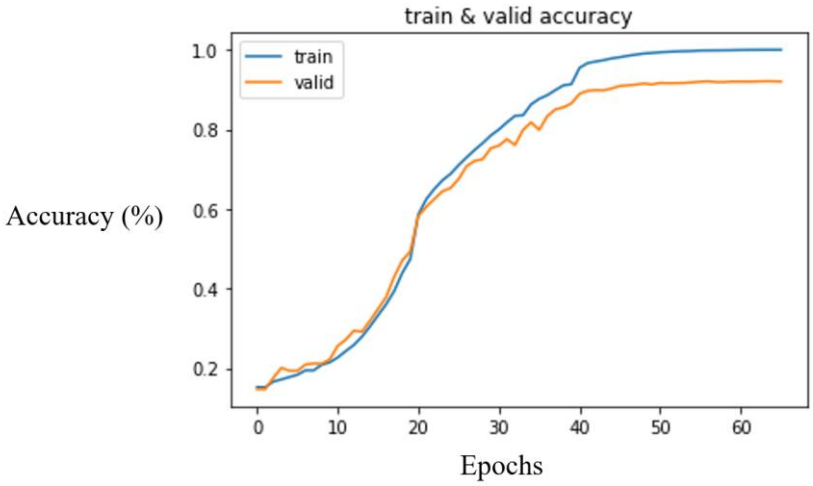

Figure 5.10. Accuracy Curve

5.4.2 Testing Results Evaluation

Finally, 5,040 pairs of untrained data sets collected from the feild on various pavement sufaces are used to test the performance of Friction-ResNets. Classification accuracy is the number of correctly recognized data sets divide by the total number of testing examples. The detailed testing

results are summarized in Table 5.2. The numbers located along the diagonal direction represent the correct predictions. The classification accuracy of testing data set is 91.3% using the predefined parameters from the network training process.

Table 5.2. Friction-ResNets Testing Results

Testing Distribution		*Predicted Friction Level*							
		<0.2	0.3	0.4	0.5	0.6	0.7	0.8	>0.9
Actual Friction Level	<0.2	579	11	10	9	12	3	2	4
	0.3	11	565	10	12	11	9	8	4
	0.4	10	17	568	8	7	4	8	8
	0.5	11	5	9	582	7	5	7	4
	0.6	1	8	7	8	590	9	6	1
	0.7	2	2	11	3	12	588	7	5
	0.8	3	10	15	10	6	16	551	19
	>0.9	3	6	5	5	4	9	19	579

5.4.3 Comparisons with Tradition Machine Learning Algorithms

Friction-ResNets is compared with the other four Machine Learning (ML) algorithms. As mentioned in the preceding section, ML approaches to classification problems had limitations (LeCun et al. 2015). However, before the widespread adoption of deep learning in recent years, machine learning was the most effective classification tool. SVM and Random Forest have been dominant ML algorithms for pattern recognition and classification in past ten years. (Luo 2014, Lentka et al. 2015, Misumi et al. 2016, Liu and Xiong 2012, Saki and Kehtarnavaz 2014).

Gaussian Naive Bayes (GNB) and K-Nearest Neighbor (KNN) has been successfully applied in many classification implementations (Moraes and Machado 2015, Guney and Cakar 2016, Imandoust and Bolandraftar 2013, Venkatalakshmi and Prabakaran 2014). Thus, these four methods are selected for comparison in this study.

Naive Bayes Classifier technique is based on the Bayesian theorem (Friedman and Goldazmidt 1997):

$$P(F|t) = \frac{P(F)\times P(t|F)}{P(t)} \tag{5.6}$$

In this work *F* is defined as the friction level and *t* as the input texture data or measurement. $P(F)$, the fraction of the probability of class *F* without considering the input observations *t*, is called the "prior probability." $P(t|F)$, the class likelihood, is the probability that an observation belonging to *F* with the associated observation value of *t*. In Gaussian Naive Bayes, the likelihood is assumed to follow Gaussian distribution. $P(F|t)$, the posterior probability, is the probability of class *F* with the given the observation *t*. Based on the given posterior probability of all classes, the most likely class of friction is determined.

The K-Nearest Neighbor (KNN) approach is a widely used nonparametric technique for classification (Cohen 1996, Cover and Hart 1967, Imandoust and Bolandraftar 2013, Venkatalakshmi and Prabakaran 2014). In KNN classification, the output is the class membership, the friction level in this study. An observation, the surface texture in this study, is assigned into the class that obtained the most votes from its *k* nearest neighbors.

With given labeled training data, Support Vector Machines (SVM) algorithm outputs an optimal hyperplane to categorize new classifiers. In this study, Support Vector Classifier (SVC) is used with the radial basis function kernel (RBF). The main parameters of RBF are *Gamma* and *C (provide references)*. The *Gamma* parameter defines how far the influence of a single training

example reaches (Pedregosa et al. 2011). The *C* parameter trades off misclassification of training samples against simplicity of the decision surface (Pedregosa et al. 2011). The *Gamma* and *C* parameters in this paper are chosen by performing a comprehensive grid search.

Decision trees is a widely used non-parametric supervised learning method used for classification (Pedregosa et al. 2011). Random Forest (RF) is an ensemble of decision tree classifiers, with increasing classification accuracy (Breiman 1999, Pal 2005, Liu and Xiong 2012, Saki and Kehtarnavaz 2014). *N-estimators*, *max-features*, *max-depth* and *min-samples-split* are four important parameters in RF classifier. *N-estimators* and *max-features* are main parameters needed to be adjusted. *N-estimators* is the number of trees in the forest, while *Max-features* is the size of the random subsets of features to consider when splitting a node. Good testing results are often achieved when trees are fully developed (*max-depth*=None, *min-samples-split*=2) (Pedregosa et al. 2011). In this paper, grid search algorithm (Pedregosa et al. 2011) is implemented to determine the most appropriate parameters for RF.

Comparison results are summarized in Figure 11. SVM and random forest (RF) outperform Gaussian Naive Bayes (GNB) and KNN, while the proposed Friction-ResNets excels all the four ML algorithms by a wide margin.

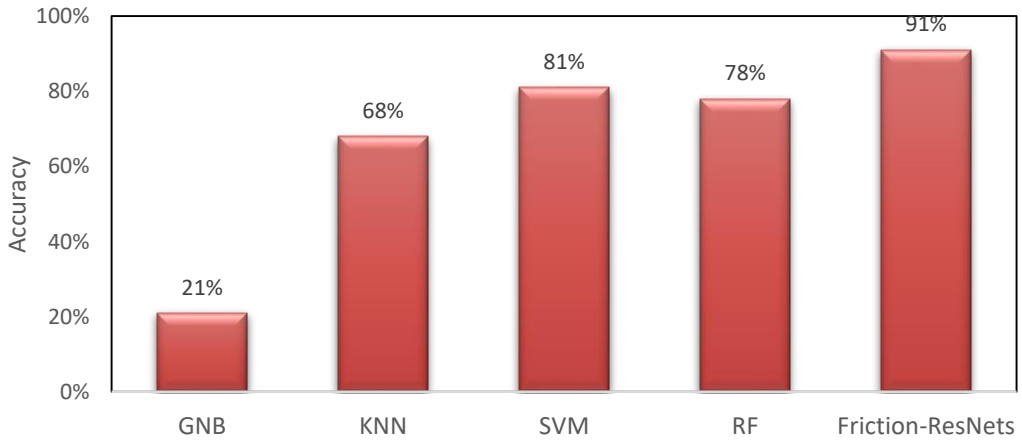

Figure 5.11. Algorithm Comparison

5.4 Summary

Acknowledging the gaps in understanding the relationship between pavement surface friction and texture, this paper designs and implements a novel Deep Residual Network (ResNets), named Friction-ResNets, tailored for pavement friction prediction based on surface texture data sets. The Friction-ResNets architecture consists of eleven convolution layers, one average pooling layer, and one fully-connected layer with millions of neurons. Different from Deep Convolutional Neural Networks, Friction-ResNets used a residual learning framework with skip connections to significantly lower gradients and enable the effective training of much deeper networks for improved classification accuracy. 33,600 pairs of friction and their corresponding texture data are collected and prepared from multiple pavement surface types distributed in 12 states for training, validating and testing of Friction-ResNets. The testing results show that Friction-ResNets can achieve a classification accuracy of 91.3%, outperforming the four conventional machine learning methods (Naïve Bayes, K-Nearest Neighbors, Support Vector Machines, and Random Forests) investigated in this study by a wide margin. The application of ResNets in this study demonstrates the potential of using highway speed non-contact texture measurements for pavement friction evaluation using deep leaning algorithms.

Chapter 6 CONCLUSIONS AND FUTURE WORK

6.1 Conclusions

The limitations of existing pavement friction testing instruments motivates the study to use non-contact measurements for friction evaluation from a comprehensive perspective. This study examines four categories of novel 3D parameters for pavement aggregate characterization: textural, feature, height, and volume parameters, and two state-of-the-art methodologies: Panel Data Analysis and Deep Residual Network tailored for pavement friction prediction, so as to address various needs in non-contact levels and friction prediction accuracies on different types of pavement surfaces. 1mm 3D pavement surface data, texture data and friction data are collected at highway speeds using the latest 3D laser triangulation imaging technology, High Speed Profiler and Grip Tester. Aggregate characteristics are measured and analyzed in the laboratory using the ultra-high resolution 3D surface scanner and Aggregate Imaging System (AIMS). The testing beds in this study include 255 LTPP SPS-3 testing sections, two years of field data collected from 45 PM treatment sites in Oklahoma, and 49 HFST sites distributed in 23 states. The contributions of this dissertation can be summarized as follows:

- The comprehensive analysis of the aggregate properties on pavement friction could help researchers and practitioners better understand how aggregates should be measured and which indicators should be used for aggregate characterization to directly result in improved field performance.

- This study demonstrates the potential of using non-contact texture measurements for pavement skid resistance evaluation and prediction.
- Per the author's knowledge, this work is the first attempt to exploit the "deep" residual network to evaluate pavement surface friction using highway speed non-contact texture measurements.

6.2 Key Findings

The key findings from this study are summarized in the following:

(1) Based on Pearson correlation analysis and multivariate analysis, MPD, T_{etp}, S_{tr}, S_{pd}, S_{pc}, S_{dv}, S_{sk} and S_{mr} have significant influences on pavement friction. Among them, MPD demonstrates the least influence, while T_{etp} (textural parameter) and S_{pc} (feature parameter) are the strongest influencing 3D aggregate texture parameters.

(2) Several climate characteristics, including temperature, precipitation, freezing index, and humidity, have shown to significantly affect pavement friction.

(3) Traffic volume in terms of AADTT shows strong correlation with pavement friction, while AADT does not present significant impact on friction possibly due to the incompleteness of AADT data.

(4) Pavement age and pavement surface characteristics including MPD, IRI and rutting are evaluated in the initial friction prediction model development. Pavement age is among the most influential factors on pavement friction. However, pavement roughness (IRI) doesn't show consistent correlation with friction, MPD and rutting don't have significant influence on friction.

(5) Aggregate properties have more significant effects on pavement friction than the type of PM treatment. If both treatment type and aggregate parameters are considered in the PDA model developments, PM treatment type is not a significant factor, while several aggregate parameters, including Nominal Maximum Aggregate Size (NMAS), angularity,

change of texture and sphericity after MD Polishing, have been determined to significantly affect pavement friction.

(6) Slurry seal is the most effective friction improvement among the four preservation treatments in LTPP SPS-3 database. Thin overlay and chip seal shows improvements of friction, while cracking seal doesn't cause apparent friction improvement as compared to performance of the control section.

(7) Among the field testing sites in Oklahoma, HFST is ranked as the most effective friction improvement among the six PM treatments under study, followed by micro-surfacing, UTBWC and HMA resurfacing.

(8) Statistics of OLS model, fixed-effects and random-effects panel models are developed and compared. Fixed-effect panel model is identified to be the most suitable for the LTPP SPS-3 data sets, while random-effect panel model outperforms other models for the field data sites in Oklahoma.

(9) The proposed Friction-ResNets has a classification accuracy of 91.3%, outperforming the four conventional machine learning methods (Na ïve Bayes, KNN, SVM, and Random Forest) investigated in this study by a wide margin.

6.3 Future Work

It should be acknowledged that both the field and laboratory testing take significant amount of time and labor to acquire necessary data sets for this dissertation. However, for wide implementation of the proposed friction models, further studies are still needed in several aspects, such as collecting more data sets with various levels of surface texture and friction properties for training and testing, model architecture fine-tuning and enhancements, software algorithm upgrading and optimization:

Firstly, additional data collection sites should be performed with more parameters. For example, in Chapter 3, forty-four pairs of data sets from the selected testing sites are very limited.

Additional areal pavement surface indicators should be explored to better characterize pavement surface frictional properties. In Chapter 4, It should be recognized that the data used in the LTPP SPS-3 database are extensive but many important factors such as aggregate properties are not directly considered due to the unavailability of the data. Some external factors, climate parameters and structural parameters are not fully considered in the friction panel model for Oklahoma. In Chapter 5, including a broader scope of time series testing sites with multiple observations, various treatment types and aggregate sources is anticipated for the validation of the developed Friction-ResNets model.

Secondly, a robust adaptive algorithm is desired. This dissertation uses linear regression, Panel Data Analysis and Deep Residual Network for friction model development. The proposed Friction-ResNets is promising for pavement friction prediction using non-contact texture measurements. However, a robust adaptive algorithm deserves further research for automated friction prediction considering comprehensive pavement surface data (time series data, different PM treatments and various aggregate types), structural indicators, aggregate characteristics, temperature etc. as training data set. Furthermore, mechanical friction model using finite element analysis and other techniques should be embedded into the Friction-ResNets if possible.

ACKNOWLEDGEMENTS

This dissertation is under research projects, “Long Term Performance Monitoring of High Friction Surfacing Treatment (HFST) Sites”, sponsored by the Federal Highway Administration (FHWA), and “Development of Aggregate Characteristics-Based Preventive Maintenance Treatments Using 3D Laser Imaging and Aggregate Imaging Technology for Optimized Skid Resistance of Pavements” supported by Oklahoma Department of Transportation (ODOT). The opinions expressed in the dissertation is author, who is responsible for the accuracy of the facts and data herein, and do not necessarily reflect the official policies of the sponsoring agency. This dissertation does not constitute a standard, regulation, or specification.

REFERENCES

Abdel-Aal, H. (2005). The relation between wear and irreversible entropy generation in the dry sliding metals.

Abdel-Hamid, O., Mohamed, A., Jiang, H., Deng, L., Penn, G., Yu, D. (2014). "Convolutional neural networks for speech recognition," IEEE Transactions on Audio, Speech, and Language Processing, vol.22, no.1, pp.1533-1545.

Adelle W. (2006). Quantitative characterisation of surface finishes on stainless steel sheet using 3D surface topography analysis. Doctoral thesis, University of Huddersfield.

Ahammed, M. A., & Tighe, S. L. (2008). Concrete pavement surface textures and multivariables frictional performance analysis: A North American case study. Canadian Journal of Civil Engineering Can. J. Civ. Eng., 35(7), 727-738. Doi: 10.1139/l08-025

Ahammed, M. A., & Tighe, S. L. (2012). Asphalt pavements surface texture and skid resistance — exploring the reality. Canadian Journal of Civil Engineering, 39(1), 1-9. doi:10.1139/l11-109

Al-Rousan, T.M. et al. (2007). Evaluation of Image Analysis Techniques for Quantifying Aggregate Shape Characteristics. Construction and Building Materials, Vol. 21, 978-990.

Anupam, K., Srirangam, S. K., Scarpas, A., and Kasbergen, C. (2013). Influence of Temperature on Tire-Pavement Friction: Analyses. accepted for Transprtation Research Board.

Arambula E. et al. (2013). Performance and Cost Effectiveness of Permeable Friction Course (PFC) Pavements. FHWA/TX-12/0-5836-2. FHWA, U.S. Department of Transportation.

Artyushkova, K., Cornejo, J. A., Ista, L. K., Babanova, S., Santoro, C., & Atanassov, P. (2015). Relationship between surface chemistry, biofilm structure, and electron transfer in Shewanella anodes. American Vacuum Society, 10, 019013th ser., 57-64. doi:10.1116/1.4913783

Asi, I. M. (2007). Evaluating skid resistance of different asphalt concrete mixes. Building and Environment, 42(1), 325-329.

ASTM E1845-15 (2015) Standard Practice for Calculating Pavement Macrotexture Mean Profile Depth, ASTM International, West Conshohocken, PA, https://doi.org/10.1520/E1845-15

ASTM E1859/E1859M-11(2015) Standard Test Method for Friction Coefficient Measurements Between Tire and Pavement Using a Variable Slip Technique, ASTM International, West Conshohocken, PA, 2015, https://doi.org/10.1520/E1859_E1859M-11R15

ASTM E950/E950M-09 (2018) Standard Test Method for Measuring the Longitudinal Profile of Traveled Surfaces with an Accelerometer-Established Inertial Profiling Reference, ASTM International, West Conshohocken, PA, https://doi.org/10.1520/E0950_E0950M-09R18

ASTM Standard D6928-17 (2017). Standard Test Method for Resistance of Coarse Aggregate to Degradation by Abrasion in the Micro-Deval Apparatus, ASTM International, West Conshohocken, PA, https://doi.org/10.1520/D6928-17

ASTM Standard D7428-15 (2015). Standard Test Method for Resistance of Fine Aggregate to Degradation by Abrasion in the Micro-Deval Apparatus. ASTM International, West Conshohocken, PA, 2015, DOI: 10.1520/D7428-15.

ASTM Standard E1911-09a (2009). Standard Test Method for Measuring Paved Surface Frictional Properties Using the Dynamic Friction Tester. ASTM International, West Conshohocken, PA, 2009, DOI: 10.1520/E1911-09AE01.

ASTM Standard E2157-15 (2015). Standard Test Method for Measuring Pavement Macro-texture Properties Using the Circular Track Meter. ASTM International, West Conshohocken, PA, 2015, DOI: 10.1520/E2157-15.

ASTM Standard E274/E274M-11 (2011). Standard Test Method for Skid Resistance of Paved Surfaces Using a Full-Scale Tire. ASTM International, West Conshohocken, PA, 2008, DOI: 10.1520/E0274_E0274M-11.

ASTM Standard E303-93 (2013). Standard Test Method for Measuring Surface Friction Properties Using the British Pendulum Tester. ASTM International, West Conshohocken, PA, 2013, DOI: 10.1520/E0303-93R13.

ASTM Standard E670-09 (2009). Standard Test Method for Testing Side Force Friction on Paved Surfaces Using the Mu-Meter. ASTM International, West Conshohocken, PA, 2008, DOI: 10.1520/E0670- 09.

ASTM Standard E965-15 (2015). Standard Test Method for Measuring Pavement Macro-texture Using a Volumetric Technique. ASTM International, West Conshohocken, PA, 2015, DOI: 10.1520/E0965-15.

Aydogan, D. B., & Hyttinen, J. (2014). Characterization of microstructures using contour tree connectivity for fluid flow analysis. Journal of the Royal Society Interface, 11(95), 20131042. http://doi.org/10.1098/rsif.2013.1042

Bazlamit, S. M., & Reza, F. (2005). Changes in Asphalt Pavement Friction Components and Adjustment of Skid Number for Temperature. *Journal of Transportation Engineering,131*(6), 470-476. doi:10.1061/(asce)0733-947x(2005)131:6(470)

Bell, A., & Jones, K. (2015). Explaining Fixed Effects: Random Effects Modeling of Time-Series Cross-Sectional and Panel Data. *Political Science Research and Methods, 3*(1), 133-153. doi:10.1017/psrm.2014.7

Bengio, Y., Simard, P. and Frasconi, P. (1994). Learning long-term dependencies with gradient descent is difficult. IEEE Transactions on Neural Networks, 5(2):157 – 166.

Bessa, I. S., Branco, V. T., & Soares, J. B. (2014). Evaluation of polishing and degradation resistance of natural aggregates and steel slag using the aggregate image measurement system. Road Materials and Pavement Design, 15(2), 385-405. doi:10.1080/14680629.2014.883323

Beyenal, H., Donovan, C., Lewandowski, Z., & Harkin, G. (2004). Three-dimensional biofilm structure quantification. Journal of Microbiological Methods, 59(3), 395-413. doi: 10.1016/j.mimet.2004.08.003.

Beyenal, H., Lewandowski, Z., & Harkin, G. (2004). Quantifying Biofilm Structure: Facts and Fiction. Biofouling, 20(1), 1-23. doi:10.1080/0892701042000191628.

Bijsterveld W. and Val, M. (2016). Towards Quantification of Seasonal Variations in Skid Resistance Measurements. Road Materials and Pavement Design, 17:2, pp. 477-486, DOI: 10.1080/14680629.2015.1090909.

Bischoff, D. (2008). Investigative Study of the Italgrip TM System. WI-04-08. Wisconsin Department of Transportation, Madison, WI.

Bitelli, G., Simone, A., Girardi, F., & Lantieri, C. (2012). Laser Scanning on Road Pavements: A New Approach for Characterizing Surface Texture. *Sensors, 12*(7), 9110-9128. doi:10.3390/s120709110

Bledsoe J. (2015). Missouri Demonstration Project: The Use of High-Friction Surface Treatments on Missouri Highways. FHWA, U.S. Department of Transportation. Available from http://plan4operations.dot.gov/hfl/summary/pdf_2/Missouri%20High%20Friction%20Report%20draft%20Final.pdf.

Bloem, D. (1971). Skid resistance – The role of aggregates and other factors (pp. 1–30). Silver Spring, MD: National Sand and Gravel Association Circular 109.

Brandes, H.G. and Robinson, C.E. (2006). "Correlation of Aggregate Test Parameters to Hot Mix Asphalt Pavement Performance in Hawaii." Journal of Transportation Engineering, Vol 132, Issue 1.

Breiman, L. (1999). Random forests—random features. Technical Report 567, Statistics Department, University of California, Berkeley, ftp://ftp.stat.berkeley.edu/pub/users/ breiman.

Breusch, T. and Pagan, A. (1980). "The LM Test and Its Applications to Model Specification in Econometrics," Review of Economic Studies, 47, 239-254.

Burchett, J. L. (1978). Seasonal variations in the skid resistance of pavements in Kentucky: Final report. Lexington, KY: Division of Research, Bureau of Highways, Dept. of Transportation.

Cenek, P. D. (2004). Prediction of skid resistance performance of chipseal roads in New Zealand. Wellington, N.Z.: Transfund New Zealand.

Chen X.H. and Wang D.W. (2011). Fractal and Spectral Analysis of Aggregate Surface Profile in Polishing Process. Wear, Vol. 271, 2746-2750.

Chen, G. M., Tan, Y. Q., Wang, Z. R., Liu, L. H., Ma, H. P. (2006). Experimental design for measurement on aggregates surface texture. China Journal of Highway & Transport, 19(2): 36–41 (in Chinese).

Chen, P. C., & Pavlidis, T. (1979). Segmentation by texture using a co-occurrence matrix and a split-and-merge algorithm. *Computer Graphics and Image Processing, 10*(2), 172-182. doi:10.1016/0146-664x(79)90049-2

Cohen, H. (n.d.). Image restoration via N-nearest neighbour classification. *Proceedings of 3rd IEEE International Conference on Image Processing*. doi:10.1109/icip.1996.559671

Cover, T. M. and Hart, P. E. (1967). "Nearest Neighbor Pattern Classification", IEEE Transactions on Information Theory, vol. 13, No. 1, pp. 21-27.

Croissant, Y., and Millo, G. (2008). Panel data econometrics in R: The plm package. Journal of Statistical Software, **27**(2). doi:10.18637/jss.v027.i02.

Csathy, T.I., Burnett, W.C., and Armstrong, M.D. (1968). *State-of-the-Art of Skid Resistance Research*, Highway Research Board Special Report 95, Highway Research Board, National Research Council, Washington, D.C.

Davis, L. S., Johns, S. A., & Aggarwal, J. K. (1979). Texture Analysis Using Generalized Co-Occurrence Matrices. *IEEE Transactions on Pattern Analysis and Machine Intelligence, PAMI-1*(3), 251-259. doi:10.1109/tpami.1979.4766921.

Davis, R.M. (2001). Comparison of surface characteristics of hot-mix asphalt pavement surfaces at the virginia smart road. Thesis submitted to the Faculty of Virginia Polytechnic Institute and State University.

Deltombe R., Kubiak K.J., Bigerelle M. (2011). How to select the most relevant 3D roughness parameters of a surface. *Scanning*, Vol. 36, No. 1, pp. 150-160, DOI: 10.1002/sca.21113.

Deng, L., Seltzer, M., Yu, D., Acero, A., Mohamed, A. and Hinton, G. (2010). "Binary coding of speech spectrograms using a deep auto-encoder," in Proc. Interspeech.

Dieleman S. and Schrauwen, B., (2014). End-to-End Learning for Music Audio. 2014 IEEE International Conference on Acoustics, Speech and Signal Processing (ICASSP), pp. 6964-6968.

Dieleman, S. and Schrauwen, B. (2013). "Multiscale approaches to music audio feature learning," in Proceedings of the 14th International Conference on Music Information Retrieval (ISMIR).

Do M. et al. (2009). Evolution of Road-Surface Skid-Resistance and Texture Due to Polishing. Wear, Vol. 266, 574-577.

Dunford, A. (2013). Friction and the Texture of Aggregate Particles Used in the Road Surface Course. Ph.D. Dissertation, University of Nottingham, United Kingdom.

Dunford, A. M., Parry, A. R., Shipway, P. H., and Viner, H. E. (2012). Three- Dimensional Characterization of Surface Texture for Road Stones Undergoing Simulated Traffic Wear. *Wear*, Vol. 292 – 293, pp. 188 – 196. https://doi.org/10.1016/j.wear.2012.05.010.

Flintsch, G., Huang, M., & Mcghee, K. (2005). Harmonization of Macrotexture Measuring Devices. *Journal of ASTM International*, *2*(9), 13043. doi:10.1520/jai1304

Flintsch, G.W., De Leon, E., McGhee, K.K., Al-Qadi, I.L. (2003). *Pavement Surface Macro-Texture Measurement and Application*; Transportation Research Board: Washington, DC, USA; pp. 168–177.

Florková, Z., & Jambor, M. (2017). Quantification of Aggregate Surface Texture Based on Three Dimensional Microscope Measurement. Procedia Engineering, 192, 195-200. doi: 10.1016/j.proeng.2017.06.034

Fowler, D.W. and Rached, M. M. (2012). *Polish Resistance of Fine Aggregates in Portland Cement Concrete Pavements*, Transportation Research Record: Journal of the Transportation Research Board, No. 2267, Transportation Research Board of the National Academies, Washington, D.C., pp. 29–36.

Friedman, N. & Goldszmidt, M. (1996). Learning Bayesian networks with local structure. In E. Horvits & F. Jensen (Eds.), Proceedings of the Twelfth Conference on Uncertainty in Artificial Intelligence (pp. 252-262). San Francisco, CA: Morgan Kaufmann.

Friel S. et al. 2013. Use of Wehner Schulze to Predict Skid Resistance of Irish Surfacing Materials. Airfield and Highway Pavement, France, 12 p.

Fuentes, L., Gunaratne, M., and Hess, D. (2010). Evaluation of the effect of pavement roughness on skid resistance. Journal of Transportation Engineering, **136**(7): 640 – 653. doi:10.1061/(ASCE)TE.1943-5436.0000118.

Fuents L.G. (2009). Investigation of the Factors Influencing Skid Resistance and the International Friction Index. Ph.D. Dissertation, University of South Florida, Tampa, FL.

Glorot, X. and Bengio, Y. (2010). Understanding the difficulty of training deep feedforward neural networks. AISTATS.

Gong, H., Dong, Q., Huang, B., & Jia, X. (2016). Effectiveness Analyses of Flexible Pavement Preventive Maintenance Treatments with LTPP SPS-3 Experiment Data. Journal of Transportation Engineering J. Transp. Eng., 142(2), 04015045. Doi: 10.1061/ (asce) te.1943-5436.0000818

Greene, William H. (2012). Econometric Analysis (7th ed.). Pearson. p. 420. ISBN 978-0-273-75356-8

Gudimettla, J., Myers, L.A., and Paugh, C. (2006). *AIMS: The Future in Rapid, Automated Aggregate Shape and Texture Measurement*, US Department of Transportation, Federal Highway Administration, Washington, DC

Guney, S., & Cakar, C. (2016). Comparison of expectation maximization and Naïve Bayes algorithms in character recognition. *2016 24th Signal Processing and Communication Application Conference (SIU)*. doi:10.1109/siu.2016.7496100

Hall J.W. et al. (2009). NCHRP Web Document 108: Guide for Pavement Friction. Transportation Research Board, National Research Council, Washington, D.C.

Hall, J. W., & Hanna, A. N. (2009). Guide for pavement friction: Background and research. Washington, DC: Transportation Research Board.

Hall, K. T., Correa, C. E., & Simpson, A. L. (2002). LTPP data analysis: Effectiveness of pavement maintenance and rehabilitation options. Washington, D.C.: National Academy Press.

Haralick, R. M., Shanmugan, K. and Dinstein, I. H. (1973). "Textural features for image classification," IEEE Trans. Syst., Man, Cybern., vol. SMC-3, pp. 610–621.

Hartikainen, L., Petry, F. and Westermann, S. (2014). Frequency-wise Correlation of the Power Spectral Density of Asphalt Surface Roughness and Tire Wet Friction. Wear, Vol. 317, pp. 111-119.

He, K., Zhang, X., Ren, S. & Sun, J. (2016). Deep residual learning for image recognition. In *Proc. 29th IEEE Conf. Comput. Vis. Pattern Recognit.* 770 – 778.

He, K., Zhang, X., Ren, S., & Sun, J. (2016). Identity Mappings in Deep Residual Networks. *Computer Vision – ECCV 2016 Lecture Notes in Computer Science*, 630-645. doi:10.1007/978-3-319-46493-0_38

Henry, J. J. (2000). NCHRP Synthesis of Highway Practice 291: Evaluation of Pavement Friction Characteristics. TRB, National Research Council, Washington, D.C.

Hicks, R., Dunn, K., & Moulthrop, J. (1997). Framework for Selecting Effective Preventive Maintenance Treatments for Flexible Pavements. Transportation Research Record: Journal of the Transportation Research Board, 1597, 1-10. doi:10.3141/1597-01

Hotař, V. (2017). Application of Fractal Dimension in Industry Practice. Fractal Analysis - Applications in Physics, Engineering and Technology. doi:10.5772/intechopen.68276

Hsiao, C. (2006). Panel Data Analysis - advantages and challenges. SSRN. [Electronic Journal.] doi:10.2139/ssrn.902657.

Hsiao, C., Lahiri, K., Lee, L., and Pesaran, M.H. (*Editors*). (1999). Analysis of panels and limited dependent variable models. Cambridge University Press, Cambridge.

Huang, J.T., Li, J., and Gong, Y. (2015). An Analysis of Convolutional Neural Networks for Speech Recognition. 2015 IEEE International Conference on Acoustics, Speech and Signal Processing (ICASSP), pp. 4989-4993.

Imandoust, S.B., Bolandraftar, M. (2013). Application of K-Nearest Neighbor (KNN) approach for predicting economic events: theoretical background. Int J Eng Res Appl 2013;3(5):605–10

Ioffe, S.; Szegedy, C. (2015). Batch normalization: Accelerating deep network training by reducing internal covariate shift. In Proceedings of the 32nd International Conference on Machine Learning, ICML, Lille, France, 6–11 July 2015; pp. 448–456

ISO/TS CD 25178-2 (2012). Geometrical Product Specification (GPS) – Surface Texture: Areal – Part 2. Terms, Definitions and Surface Texture Parameters.

Izeppi, E., Flintsch, G., and McGhee, K. (2010). Field Performance of High Friction Surfaces. FHWA/VTRC 10-CR6. FHWA, U.S. Department of Transportation. http://www.virginiadot.org/vtrc/main/online_reports/pdf/10-cr6.pdf. Accessed May 15, 2016.

Wulfing, J. and Riedmiller, M. (2012). "Unsupervised learning of local features for music classification," in Proceedings of the 13th International Society for Music Information Retrieval Conference (ISMIR).

Jahromi S.G. et al. (2011). Evaluation of Pavement Temperature on Skid Frictional of Asphalt Concrete Surface. International Journal of Pavement Engineering, 12:1, 47-58, DOI: 10.1080/10298436.2010.501864.

Jayawickrama, P., & Thomas, B. (1998). Correction of Field Skid Measurements for Seasonal Variations in Texas. Transportation Research Record: Journal of the Transportation Research Board, 1639, 147-154. doi:10.3141/1639-16

Ji, Y., Nantung, T., & Tompkins, B. (2015). Evaluation for UTBWC on SR-11 as Pavement Preservation Treatment: A Case Study. *International Journal of Pavement Research and Technology, 8*(4), 267-275. doi:10.6135/ijprt.org.tw/2015.8(4).267

Kanafi, M. M., Kuosmanen, A., Pellinen, T. K., & Tuononen, A. J. (2014). Macro- and micro-texture evolution of road pavements and correlation with friction. International Journal of Pavement Engineering, 16(2), 168-179. Doi:10.1080/10298436.2014.937715

Kane, M., Do, M.T. and Piau, J.M. (2010). On the Study of Polishing of Road Surface under Traffic Load. Journal of Transportation Engineering, Vol. 136, No. 1, 45-51.

Kane, M., Rado, Z., & Timmons, A. (2014). Exploring the texture–friction relationship: From texture empirical decomposition to pavement friction. International Journal of Pavement Engineering, 16(10), 919-928. Doi:10.1080/10298436.2014.972956

Kangkhajitre, C. and Kanitpong, K. (2011). Effect of aggregate characteristics on texture and skid resistance of asphalt pavement surface. Eastern Asia Soc Transp Stud 8: 247.

Kargah-Ostadi, N., & Howard, A. (2015). Monitoring Pavement Surface Macrotexture and Friction. *Transportation Research Record: Journal of the Transportation Research Board, 2525*, 111-117. doi:10.3141/2525-12

Kassem, E., Ahwed, A., Masad, E.A., and Little, D.N. (2013). *Development of Predictive Model for Skid Loss of Asphalt Pavements,* Transportation Research Record, Journal of the Transportation Research Board, No 2372, Transportation Research Board of the National Academies, pp: 83-96.

Kline, S.W., Phiukhao, W., Griffin, M.L., and Miller, J.W. (2007). Evaluation of the sodium sulfate soundness test for qualifying dolomites of northern Arkansas for construction aggregate. In Shaffer, N.R., and DeChurch, D.A., eds, Proceedings of the 40th Forum on the Geology of Industrial Minerals, 2004: Indiana Geological Survey Occasional Paper 67.

Kokkalis, A. G., & Panagouli, O. K. (1998). Fractal Evaluation of Pavement Skid Resistance Variations. I: Surface Wetting. *Chaos, Solitons & Fractals, 9*(11), 1875-1890. doi:10.1016/s0960-0779(97)00138-0

Komas, T., (2011). Advanced Surface Preparation and Preservation Treatments for Concrete Pavements, CP2 Center News, Newsletter of the California Pavement Preservation Center, No. 20, December.

Kong, T.Y., and Rosenfeld, A. (1989). Digital Topology: Introduction and Survey, CVGIP, vol.48, pp.357-393

Kotek, P., and Florková, Z. (2014). Comparison of the skid resistance at different asphalt pavement surfaces over time. Procedia Engineering, **91**: 459 – 463 doi: 10.1016/j.proeng.2014.12.026.

Kowalski, K.J. et al. (2009). Long-Term Monitoring of Noise and Frictional Properties of Three Pavements: Dense-Graded Asphalt, Stone Matrix Asphalt, and Porous Friction Course. In *Transportation Research Record: Journal of the Transportation Research Board, N0. 2127,* Transportation Research Board of the National Academies, Washington, D.C., 12-19.

Krizhevsky, A., Sutskever, I., and Hinton, G. (2012). ImageNet classification with deep convolutional neural networks. In NIPS.

Kummer, H. and Meyer, W. (1963) Penn State Road Surface Friction Tester as Adapted to Routine Measurement of Pavement Skid Resistance. Road Surface Properties, 42nd Annual Meeting, 7-11 January 1963, 1-31.

Kummer, H. and Meyer, W. (1967). Tentative Skid-Resistance Requirements for Main Rural Highways (Vol. 37, 0077-5614, NCHRP Report). Transportation Research Board.

Lancieri, F., Losa, M. and Marradi, A. (2005). Resistance to polishing and mechanical properties of aggregates for asphalt concrete wearing courses, Italian Society for Road Infrastructures (SIIV), SSD ICAR 04. Retrieved from http://siiv.scelta.com/bari2005/162.pdf

Leach R. (2012). Characterisation of Areal Surface Texture. Springer-Verlag Berlin Heidelberg, DOI: 10.1007/978-3-642-36458-7.

LeCun, Y., Bengio, Y. and Hinton, G. (2015). Deep learning. Nature, 521:436–444. doi:10.1038/nature14539

LeCun, Y., Boser, B., Denker, J.S., Henderson, D., Howard, R.E., Hubbard, W., Jackel, L.D. (1989). Backpropagation applied to handwritten zip code recognition. Neural computation.

Ledig, C., Theis, L., Huszar, F., Caballero, J., Cunningham, A., Acosta, A., Shi, W. (2017). Photo-Realistic Single Image Super-Resolution Using a Generative Adversarial Network. *2017 IEEE Conference on Computer Vision and Pattern Recognition (CVPR).* doi:10.1109/cvpr.2017.19

Lee, D. G., & Kim, S. (2005). Impacts of geographical location and construction type on as-built roughness in highway pavement construction. KSCE Journal of Civil Engineering KSCE J Civ Eng, 9(6), 447-452. Doi: 10.1007/bf02831483

Lentka, Ł.; Smulko, J.M.; Ionescu, R.; Granqvist, C.G.; Kish, L.B. (2015). Determination of gas mixture components using fluctuation enhanced sensing and the LS-SVM regression algorithm. Metrol. Meas. Syst. **2015**, 3, 341–350.

Li S., Zhu K. and Noureldin S. (2007). Evaluation of Friction Performance of Coarse Aggregates and Hot-Mix Asphalt Pavements. Journal of Testing and Evaluation, Vol. 35, No. 6, 1-7.

Li, Q. J., Yang, G., Wang, K. C., Zhan, Y., Merritt, D., & Wang, C. (2016). Effectiveness and performance of high friction surface treatments at a national scale. Canadian Journal of Civil Engineering, 43(9), 812-821. doi:10.1139/cjce-2016-0132

Li, Q., Yang, G., Wang, K. C., Zhan, Y., & Wang, C. (2017). Novel Macro- and Micro-texture Indicators for Pavement Friction by Using High-Resolution Three-Dimensional Surface Data. *Transportation Research Record: Journal of the Transportation Research Board, 2641*, 164-176. doi:10.3141/2641-19

Li, S., Noureldin, S., Jiang, Y., Sun, Y. (2012). Evaluation of Pavement Surface Friction Treatments. Publication FHWA/IN/JTRP- 2012/04. Joint Transportation Research Program, Indiana Department of Transportation and Purdue University, West Lafayette, Indiana. DOI: 10.5703/1288284314663

Li, Y., & Shen, L. (2017). A Deep Residual Inception Network for HEp-2 Cell Classification. *Deep Learning in Medical Image Analysis and Multimodal Learning for Clinical Decision Support Lecture Notes in Computer Science*, 12-20. doi:10.1007/978-3-319-67558-9_2

Liu, Z., & Xiong, H. (2012). Object Detection and Localization Using Random Forest. *2012 Second International Conference on Intelligent System Design and Engineering Application*. doi:10.1109/isdea.2012.669

Luo Y. (2003). Effect of Pavement Temperature on Frictional Properties of Hot-Mix-Asphalt Pavement Surfaces at the Virginia Smart Road. Master Dissertation, Virginia Polytechnic Institute and State University, Blacksburg, Va.

Luo, Z. (2014). A new SVM algorithm and selected application in sequence analysis. *Future Information Engineering*. doi:10.2495/icie20130892

Madanat, S. M., Karlaftis, M. G., & Mccarthy, P. S. (1997). Probabilistic Infrastructure Deterioration Models with Panel Data. J. Infrastruct. Syst. Journal of Infrastructure Systems, 3(1), 4-9. Doi: 10.1061/ (asce) 1076-0342(1997)3:1(4)

Maerz, N. H. (1998). Aggregate sizing and shape determination using digital image processing. Center For Aggregates Research (ICAR) Sixth Annual Symposium Proceedings, St. Louis, Missouri, April 19-20, pp. 195-203.

Mahmoud, E. (2005). Development of experimental methods for the evaluation of aggregate resistance to polishing, abrasion, and breakage (M.Sc. thesis). Texas A&M University, College Station, TX.

Mahmoud, E., and Masad, E. (2007). Experimental Methods for the Evaluation of Aggregate Resistance to Polishing, Abrasion and Breakage, Journal of Materials in Civil Engineering, ASCE, Vol. 19, No. 11, pp. 977-985.

Marcelino, P., Antunes, M. D., Fortunato, E., & Gomes, M. C. (2017). Machine Learning for Pavement Friction Prediction Using Scikit-Learn. *Progress in Artificial Intelligence Lecture Notes in Computer Science*, 331-342. doi:10.1007/978-3-319-65340-2_28

Masad E. (2003). Final Report for Highway-IDEA Project 77: The Development of a Computer Controlled lmage Analysis System for Measuring Aggregate Shape Properties. Transportation Research Board, National Research Council, Washington, D.C.

Masad E. (2007). Relationship of Aggregate Texture to Asphalt Pavement Skid Resistance Using Image Analysis of Aggregate Shape. Final Report for Highway IDEA Project 114.

Masad E. et al. (2005). Computations of Particle Surface Characteristics Using Optical and X-ray CT Images. Computational Materials Science, Vol. 34, 406-424.

Masad, E. (2005). Aggregate Imaging System (AIMS) basics and applications, Report no. FHWA/TX-05/5-1707-01-1, Texas Department of Transportation and Federal Highway Administration, Washington, D.C.

Masad, E., Al-Rousan, T., Button, J., Little, D., and Tutumluer, E. (2007). NCHRP Report 555: Test Methods for Characterizing Aggregate Shape, Texture, and Angularity. Transportation Research Board of the National Academies, Washington, D.C..

Masad, E., Muhunthan, B., Shashidhar, N., & Harman, T. (1999). Internal Structure Characterization of Asphalt Concrete Using Image Analysis. Journal of Computing in Civil Engineering, 13(2), 88-95. doi:10.1061/(asce)0887-3801(1999)13:2(88)

Mataei, B., Zakeri, H., Zahedi, M., & Nejad, F. M. (2016). Pavement Friction and Skid Resistance Measurement Methods: A Literature Review. *Open Journal of Civil Engineering, 06*(04), 537-565. doi:10.4236/ojce.2016.64046

Matuszewski, M., Mikolajczyk, T., Pimenov, D. Y., & Styp-Rekowski, M. (2016). Influence of structure isotropy of machined surface on the wear process. The International Journal of Advanced Manufacturing Technology, 88(9-12), 2477-2483. doi:10.1007/s00170-016-8963-z

Meegoda, J. N., and Gao, S. (2015). Evaluation of pavement skid resistance using high speed texture measurement. Journal of Traffic and Transportation Engineering (English Edition), 2 (6), 382–390.10.1016/j.jtte.2015.09.001

Michigan Metrology Surface Texture Parameters Glossary. (2014). Michigan Metrology, LLC, MI.

Misumi, M., Orii, H., Sharmin, T., Mishima, K., & Tsuruoka, T. (2016). Image Classification for the Painting Style with SVM. *The Proceedings of the 4th International Conference on Industrial Application Engineering 2016*. doi:10.12792/iciae2016.046

Mitchell, M. R., Link, R. E., Luce, A., Mahmoud, E., Masad, E., & Chowdhury, A. (2007). Relationship of Aggregate Microtexture to Asphalt Pavement Skid Resistance. *Journal of Testing and Evaluation, 35*(6), 101080. doi:10.1520/jte101080

Moaveni, M., Mahmoud, E., Ortiz, E. M., Tutumluer, E., and Beshears, S. (2014). Evaluation of Aggregate Resistance to Breakage, Abrasion, and Polishing Using Advanced Aggregate Imaging Systems, Transportation Research Record: Transportation Research Board, Washington, D.C.

Moaveni, M., Mahmoud, E., Ortiz, E., Tutumluer, E., & Beshears, S. (2014). Use of Advanced Aggregate Imaging Systems to Evaluate Aggregate Resistance to Breakage, Abrasion, and Polishing. Transportation Research Record: Journal of the Transportation Research Board, 2401, 1-10. doi:10.3141/2401-01

Moraes, R. M., & Machado, L. S. (2015). A Fuzzy Poisson Naive Bayes Classifier for Epidemiological Purposes. *Proceedings of the 7th International Joint Conference on Computational Intelligence*. doi:10.5220/0005642801930198

Moravec M. (2013). High Friction Surface Treatments at High-Crash Horizontal Curves. Arizona Pavements/Materials Conference, Phoenix, AZ. Available from http://www.intrans.iastate.edu/events/midcon2013/documents/presentation-submissions/3-C_61_08142013.pdf.

Mustafa, M., Taib, M. N., Murat, Z. H., & Lias, S. (2010). GLCM texture feature reduction for EEG spectrogram image using PCA. 2010 IEEE Student Conference on Research and Development (SCOReD). doi:10.1109/scored.2010.5704047

Nair,V.; Hinton, G.E. (2010) "Rectified Linear Units Improve Restricted Boltzmann Machines", *Proc. Int'l Conf. Machine Learning*.

Najafi, S., Flintsch, G. W., & Khaleghian, S. (2016). Pavement friction management – artificial neural network approach. *International Journal of Pavement Engineering,* 1-11. doi:10.1080/10298436.2016.1264221

Najman, L. and Schmitt, M. (1994). Watershed of a continuous function. In Signal Processing (Special issue on Mathematical Morphology.), Vol. 38, pages 99–112

Nataadmadja, A. D., Do, M. T., Wilson, D. J., and Costello, S. B. (2012). Quantifying Aggregate Micro-texture with Respect to Wear-Case of New Zealand Aggregates. Wear, Vol. 332–333, pp. 907–917. https://doi.org/10.1016/j.wear.2014.11.028.

NCAT (2017). "Evaluation of the AIMS2 and Micro-Deval to Characterize Aggregate Friction Properties," NCAT Report 17-02, Auburn, AL.

Neaylon, K. (2009). The PAFV Test and Road Friction, AAPA 13th International Flexible Pavements Conference.

Noyce, D., A. (2005). "Incorporating Road Safety Into Pavement Management : Maximizing Asphalt Pavement Surface Friction For Road Safety Improvements," Midwest Regional University Transportation Center Traffic Operations and Safety (TOPS) Laboratory.

NSP. (2010). Aggregate Classification Map of the United States, accessed July 16, 2014 from: http://nationalequipment.com/assets/documents/National_Aggregate_Hardness_US.pdf

Oczeretko, E., Jurgilewicz, D., & Rogowski, F. (2002). Some Remarks on the Fractal Dimension Applications in Nuclear Medicine. Fractals in Biology and Medicine, 207-217. doi:10.1007/978-3-0348-8119-7_22

Olaniyi, E. O., Adekunle, A. A., Odekuoye, T., & Khashman, A. (2017). Automatic system for grading banana using GLCM texture feature extraction and neural network arbitrations. Journal of Food Process Engineering, 40(6). doi:10.1111/jfpe.12575

Otsu, N. (1979). "A Threshold Selection Method from Gray-Level Histograms," IEEE Transactions on Systems, Man, and Cybernetics, Vol. 9, No. 1, 1979, pp. 62-66.

Ouadfeul, S., Aliouane, L., & Boudell, A. (2012). Fractal and Chaos in Exploration Geophysics. Fractal Analysis and Chaos in Geosciences. doi:10.5772/53560

Pal, M. (2005). Random forest classifier for remote sensing classification. *International Journal of Remote Sensing, 26*(1), 217-222. doi:10.1080/01431160412331269698

Panahandeh, G., Ek, E., & Mohammadiha, N. (2017). Road friction estimation for connected vehicles using supervised machine learning. *2017 IEEE Intelligent Vehicles Symposium (IV)*. doi:10.1109/ivs.2017.7995885

Park, Hun Myoung. (2011). Practical Guides to Panel Data Modeling: A Step-by-step Analysis Using Stata. Tutorial Working Paper. Graduate School of International Relations, International University of Japan.

Paulus, S., Eichert, T., Goldbach, H., & Kuhlmann, H. (2014). Limits of Active Laser Triangulation as an Instrument for High Precision Plant Imaging. Sensors, 14(12), 2489-2509. doi:10.3390/s140202489

Pawlus, P., Reizer, R., & Wieczorowski, M. (2017). Problem of Non-Measured Points in Surface Texture Measurements. *Metrology and Measurement Systems, 24*(3). doi:10.1515/mms-2017-0046

Philipp, G., Song, D., Carbonell, J. G. (2018). Gradients explode - Deep Networks are shallow - ResNet explained. *ICLR 2018 Conference.*

Pradhan, M. (2016). Evaluate The Use of Fpga Soc for Real Time Data Acquisition and Aggregate Micro-Texture Measurement Using Laser Sensors. University of Texas at Arlington.

Prapaitrakul, N., Freeman, T., and Glover, C. J. (2005). Analyze Existing Fog Seal Asphalts and Additives: Literature Review. Texas Transportation Institute, Research and Technology Implementation Office, Report No. FHWA/TX-06/0-5091-1.

Prowell B.D., Zhang J. and Brown E.R. (2005). NCHRP Report 539: Aggregate Properties and the Performance of Superpave-Designed Hot Mix Asphalt. TRB, National Research Council, Washington, D.C.

Puccinelli J. et al. (2014). Long-Term Pavement Performance Warm Mix Asphalt Study. FHWA, VA.

Qi, Y., Smith, B. L., & Guo, J. (2007). Freeway Accident Likelihood Prediction Using a Panel Data Analysis Approach. *Journal of Transportation Engineering, 133*(3), 149-156. doi:10.1061/(asce)0733-947x(2007)133:3(149)

Rado, Z. and Kane, M. (2014). An Initial Attempt to Develop an Empirical Relation between Texture and Pavement Friction Using the HHT Approach. Wear, Vol. 309, 233-236.

Rezaei, A., Masad, E., and Chowdhury, A. (2011). Development of a model for asphalt pavement skid resistance based on aggregate characteristics and gradation. Journal of Transportation Engineering, **137**(12): 863 – 873. doi:10. 1061/(ASCE)TE.1943-5436.0000280.

Rezaei, A., Masad, E., Chowdhury, A., and Harris, P. (2009). Predicting Asphalt Mixture Skid Resistance by Aggregate Characteristics and Gradation. In Transportation Research Record: Journal of the Transportation Research Board, No. 2104, Transportation Research Board of the National Academies, Washington, D.C., 24–33.

Roberts, D., & Roberts, F. (2012). Correlation Coefficients - MathBitsNotebook(A2 - CCSS Math). Retrieved from https://mathbitsnotebook.com/Algebra2/Statistics/STCorrelationCoefficients.html

Roe, P., Parry, A. and Viner, H. (1998). High and Low Speed Skidding Resistance: The Influence of Texture Depth.

Russakovsky, O., Deng, J., Su, H., Krause, J., Satheesh, S., Ma, S., Huang, Z., Karpathy, A., Khosla, A., Bernstein, M. et al. (2014) ImageNet large scale visual recognition challenge. arXiv:1409.0575.

Russakovsky, O., Deng, J., Su, H., Krause, J., Satheesh, S., Ma, S., Huang, Z., Karpathy, A., Khosla, A., Bernstein, M., Berg, A.C., Fei-Fei, L. (2015): ImageNet Large Scale Visual Recognition Challenge. IJCV

Saito, K., et al. (1996) Development of Portable Tester for Measuring Skid Resistance and Its Speed Dependency on Pavement Surfaces. Transportation Research Record: Journal of the Transportation Research Board, 1536, 45-51.

Saki, F., & Kehtarnavaz, N. (2014). Background noise classification using random forest tree classifier for cochlear implant applications. *2014 IEEE International Conference on Acoustics, Speech and Signal Processing (ICASSP)*. doi:10.1109/icassp.2014.6854270

Scikit-learn: Machine Learning in Python, Pedregosa *et al.*, JMLR 12, pp. 2825-2830, 2011.

Sedlaček, M., Gregorčič, P., & Podgornik, B. (2016). Use of the Roughness Parameters Ssk and Sku to Control Friction—A Method for Designing Surface Texturing. *Tribology Transactions*,*60*(2), 260-266. doi:10.1080/10402004.2016.1159358

Sengoz, B., Onsori, A., & Topal, A. (2014). Effect of aggregate shape on the surface properties of flexible pavement. KSCE Journal of Civil Engineering KSCE J Civ Eng, 18(5), 1364-1371. Doi: 10.1007/s12205-014-0516-0

Shah, M. and Abdullah, M. E. (2010) Effect of aggregate shape on skid resistance of compacted Hot Mix Asphalt (HMA). 2nd International Conference on Computer and Network Technology, ICCNT 2010, 421-425.

Shanmugavadivu, P., Sivakumar, V. (2012) Fractal Dimension Based Texture Analysis of Digital Images, In Procedia Engineering, Volume 38, Pages 2981-2986, ISSN 1877-7058.

Simonyan, K.; Zisserman, A. (2014). Very deep convolutional networks for large-scale image recognition. arXiv:1409.1556v6.

Smith, A. M., Wooster, M. J., Powell, A. K., & Usher, D. (2002). Texture based feature extraction: Application to burn scar detection in Earth observation satellite sensor imagery. International Journal of Remote Sensing, 23(8), 1733-1739. doi:10.1080/0143116011010610

Smith, K.L., Hall, J.W., and Littleton, P., (2009). *NCHRP Report 634: Texturing of Concrete Pavements*. Transportation Research Board, National Cooperative Highway Research Program, Washington DC.

Song, W., Smith, X., Chen, T. and Hedfi A. (2006). Investigation of hot mix asphalt surfaced pavements skid resistance in Maryland state highway network system. In: Proceeding of TRB 85th Annual Meeting, Transportation Research Board, Washington, DC.

Srivastava N., Hinton, G., Krizhevsky, A., Sutskever, I., and Salakhutdinov, R. (2014). Dropout: A Simple Way to Prevent Neural Networks from Overfitting. Journal of Machine Learning Research, 15, pp. 1929–1958.

Srivastava, R. K., Greff, K. and Schmidhuber, J. (2015). Training very deep networks. 1507.06228.

Steven, B.D. (2009). Friction Testing of Pavement Preservation Treatments: Temperature Correlations and Operator/Machine Variability. CA11-1200 C. State of California Department of Transportation.

Sthitpattanapongsa, P., Srinark, T. (2011). An equivalent 3D Otsu's thresholding method, in: Advances in Image and Video Technology: 5th Pacific Rim Symposium, Gwangju, South Korea, pp. 358–369.

Susanna, A., Crispino, M., Giustozzi, F., & Toraldo, E. (2017). Deterioration trends of asphalt pavement friction and roughness from medium-term surveys on major Italian roads. *International Journal of Pavement Research and Technology*, *10*(5), 421-433. doi:10.1016/j.ijprt.2017.07.002

Szegedy, C., Liu, W., Jia, Y., Sermanet, P., Reed, S., Anguelov, D., Erhan, D., Vanhoucke, V., and Rabinovich, A. (2015). Going deeper with convolutions. In CVPR.

Tarefder, R.A., Zaman, M. and Hobson, K. (2003). "Micro-Deval Test for Evaluating Properties of Roadway Aggregate." International Journal of Pavements: maintenance and rehabilitation of pavements and technological control, Vol. 2, Issue 1-2.

Ueckermann et al. (2015). Calculation of Skid Resistance from Texture Measurements. Journal of Traffic and Transportation Engineering, Vol. 2, No. 1, 3-16.

Venkatalakshmi, S., & Prabakaran, T. E. (2014). Application of k-Nearest Neighbour Classification Method for Intrusion Detection in Network Data. *International Journal of Computer Applications*,*97*(7), 34-37. doi:10.5120/17021-7306

Villani M. M., Scarpas, A., Bondt, A., Khedoe, R., and Artamendi, I. (2014). Application of Fractal Analysis for Measuring the Effects of Rubber Polishing on the Friction of Asphalt Concrete Mixtures. Wear, Vol. 320, pp. 179-188.

Wang Kelvin C. P. (2011). Elements of Automated Survey of Pavements and a 3D Methodology. Journal of Modern Transportation, Volume 19, Number 1, pp: 51-57.

Wang, H., and Wang, Z. (2013). Evaluation of pavement surface friction subject to various pavement preservation treatments. Construction and Building Materials, 48: 194–202. doi: 10.1016/j.conbuildmat.2013.06.048.

Washington Simon P., Matthew G. Karlaftis, Fred L. Mannering (2011). Statistical and Econometric Methods for Transportation Data Analysis (2nd Edition). CRC Press, Taylor & Francis Group.

Watson, M. et al. (2011). Hot Mixed Asphalt Pavement Surface Characteristics Related to: Ride, Texture, Friction, Noise and Durability. Minnesota Department of Transportation, Maplewood, MN.

White, T.D., Haddock, J.E., and Rismantojo, E. (2006). Aggregate Tests for Hot-Mix Asphalt Mixtures Used in Pavements. NCHRP Report No. 557, Transportation Research Board, Washington, D.C.

Wojciechowski, L., Majchrowski, R., & Mathia, T. G. (2017). Contribution of roughness parameters in the scuffing performance of metallic surfaces. *Industrial Lubrication and Tribology, 69*(4), 507-515. doi:10.1108/ilt-05-2016-0116

Wu, Y., Parker, F. and Kandhal, K. (1998). "Aggregate Toughness/Abrasion Resistance and Durability/Soundness Tests Related to Asphalt Concrete Performance in Pavements." NCAT Report N. 98-4, National Center for Asphalt Technology, Auburn University, Auburn, Alabama.

Xiao, H. (2009). An Improved Fractal Dimension Algorithm and its Application on Gear Fault Recognition. 2009 Sixth International Conference on Fuzzy Systems and Knowledge Discovery. doi:10.1109/fskd.2009.508

Yang, G., Li, Q. J., Zhan, Y. J., Wang, K. C., & Wang, C. (2017). Wavelet based macro-texture analysis for pavement friction prediction. KSCE Journal of Civil Engineering, 22(1), 117-124. doi:10.1007/s12205-017-1165-x

Yang, X., Tridandapani, S., Beitler, J. J., Yu, D. S., Yoshida, E. J., Curran, W. J., & Liu, T. (2012). Ultrasound GLCM texture analysis of radiation-induced parotid-gland injury in head-and-neck cancer radiotherapy: An in vivo study of late toxicity. Medical Physics, 39(9), 5732-5739. doi:10.1118/1.4747526

Zaman, M., Gransberg, D., Riemer, C., Pittenger, D. and Aktas, B. (2010). "Quantifying the Costs and Benefits of Pavement Retexturing as a Pavement Preservation Tool – Phases 1 & 2," Final Report, Oklahoma Transportation Center, Oklahoma City, Oklahoma.

Zeiler, D. and Fergus, R. (2014). Visualizing and understanding convolutional networks, in: Computer Vision. In Proceedings of the 13th European Conference in Computer Vision, Zurich, Switzerland, 6–12 September 2014; pp. 818–833.

VITA

YOU ZHAN

Candidate for the Degree of

Doctor of Philosophy

Dissertation: EVALUATION OF PAVEMENT SKID RESISTANCE USING COMPUTATIONAL INTELLIGENCE

Major Field: Civil Engineering

Biographical:

Education:

Completed the requirements for the Doctor of Philosophy in Civil Engineering at Oklahoma State University, Stillwater, Oklahoma in August, 2018.
Completed the requirements for the Master of Science in Civil Engineering at Southwest Jiaotong University, Chengdu, China in 2014.
Completed the requirements for the Bachelor of Science in Surveying and Mapping Engineering at Southwest Jiaotong University, Chengdu, China in 2012.

Experience:
August, 2014-August, 2018: Research Assistant, Oklahoma State University